MODELING CHEMOTHERAPY- AND RADIOTHERAPY-INDUCED HEMATOLOGICAL TOXICITY

by

Christine Carcillo

B.S., Chemical Engineering, North Carolina State University, 2012

Submitted to the Graduate Faculty of

the Swanson School of Engineering in partial fulfillment

of the requirements for the degree of

Doctor of Philosophy

University of Pittsburgh

2017

UNIVERSITY OF PITTSBURGH

SWANSON SCHOOL OF ENGINEERING

This dissertation was presented

by

Christine Carcillo

It was defended on

July 26, 2017

and approved by

Robert S. Parker, Ph.D., Professor, Swanson School of Engineering

Eugene Koay, MD, Ph.D., Professor, Department of Radiation Oncology, University of Texas MD Anderson Cancer Center

Joseph J. McCarthy, Ph.D., Professor, Swanson School of Engineering

Jason Shoemaker, Ph.D., Professor, Swanson School of Engineering

Dissertation Director: Robert S. Parker, Ph.D., Professor, Swanson School of Engineering

MODELING CHEMOTHERAPY- AND RADIOTHERAPY-INDUCED HEMATOLOGICAL TOXICITY

Christine Carcillo, PhD

University of Pittsburgh, 2017

Chemotherapy and radiation are common treatments for cancer patients. Their mechanism of action is not targeted to cancerous cells specifically, and non-cancerous cells can suffer the consequences. Too much therapy can induce hematological toxicities. When cell counts dip too low, bleeding and infection can reduce and delay treatment. The use of mathematical models to understand these toxic events is a starting point for avoiding high-grade toxicity. If patients can be flagged as sensitive to a given therapy early on in their treatment, adjustments can be implemented in real-time.

A biologically-motivated model of chemotherapy-induced thrombocytopenia is developed. Platinum compounds such as carboplatin, oxaliplatin, and cisplatin can significantly lower platelet counts. These chemotherapeutics kill stem and progenitor cells in the bone marrow, which ultimately leads to a decrease in the circulating platelet count. The model parameters are able to identify which patients will react strongly to the chemotherapy, as characterized by a rapid decline in cell count followed by a low-magnitude rebound. This model was then expanded to include neutropenia, a separate toxicity common to systemic chemotherapeutics. Clinical outcomes based on survival (good vs. poor) and tumor differentiation from healthy tissue (denoted as high or low delta), were used to bin patients. This model simultaneously captures thrombocytopenia and neutropenia in pancreatic cancer patients and predicts which patients will have a better or worse overall survival time.

While chemotherapy toxicity often affects rapidly dividing cells in the bone marrow, radiation can be toxic whether bone marrow is in the beam path or not. Lymphopenia

occurs as a result of the cells circulating through blood vessels in the beam path while the patient is being irradiated. An algorithm was developed to track the amount of integrated damage taken by circulating lymphocytes, and as the damage accumulates which cells die. Lymphocyte death and replenishment occurs at biological rates taken from the literature. This model predicts the depth of lymphopenia after each fraction of radiation and can be combined with a chemotherapy-induced lymphosuppression model to predict cell counts after combination therapy.

TABLE OF CONTENTS

LIST OF TABLES

LIST OF FIGURES

PREFACE

There are many people to thank for my time at NCSU and Pitt. First, I want to thank my family. My mom and dad for their support, advice, and love. You guys were there when things got challenging and always gave me encouragement to keep going. I want to thank my sister and best friend Cathy who made countless trips to visit me and even lived with me in Boston. Thanks for keeping me normal. And of course Charlie, Rose, Lexi, Bailey, Andie and Humphrey. Next I would like to thank Kevin for taking a risk and moving to Pittsburgh. I could not have done it without you. Who would have thought that you and I would live in Pittsburgh. Clair, thank you for being a great friend and for going on so many fun trips with me. I want to thank Uncle Joe, Aunt Joan and Ruth for all the Sunday dinners and great times.

I want to express my gratitude to my advisor Bob. You took a chance on me despite me not knowing any coding. I thank you for opening the door to this field and teaching me along the way. I also appreciate that you were an involved advisor because it made the friendships in our lab that much stronger like all the times following gravity. Which leads me to thank all great friends I have met along the way including Sharlee, Amey, Melissa, Matt, Li Ang, Tim, Ari, Natania, Thang, Megan, Flo, and Michelle. I would also like to thank Eugene for coming to our rescue with data but also for being so positive about saving lives. Lastly, I want to thank all the great mentors I have had including Dean, Greg, Lisa, and Joe. Your help and advice over the years is greatly appreciated, and who knows where I would have ended up if you hadn't been there.

This material is based upon work supported by the National Science Foundation under Grant No. 1235182.

1.0 INTRODUCTION

Cancer is a devastating disease characterized by abnormal cell growth and unparalleled heterogeneity. Cytotoxic chemotherapy is able to overcome some of the heterogeneity by targeting functions common in all dividing cells. This is positive since it is inclusive of cancer cells, but negative because healthy cells are dying in the process. This results in direct medical costs upwards of $87.8 billion in 2014. Even with treatment options, over 600,000 Americans are expected to die from cancer in 2017 [12].

Patients can develop severe treatment-induced toxicities, which can lead to dose reductions and delays, negatively impacting efficacy and outcome. Hematological dose-limiting toxicities that can arise include thrombocytopenia (low platelet count), neutropenia (low neutrophil count), erythropenia (low red blood cell count), and leukopenia (low white blood cell count). Modeling and simulating the mechanisms behind cytotoxicity can provide insights into: cell death and subsequent rebound; treatment options; prognostic indicators; and cost effective next steps [13].

However, mathematical approaches to systems medicine often result in mathematical elegance but are not practical in the clinic [14]. Incorporating clinically relevant measurements and biological mechanisms into pharmacokinetic and pharmacodynamic models can sometimes bolster their predictive capabilities. Additionally, a biological underpinning will make the model translatable for other diseases and disorders. Modeling the behavior of hematocytes in response to therapy can yield patient subpopulations with varying degrees of cytotoxicity and/or overall survival. Patients predicted to respond better and tolerate the drug for the whole course of treatment could remain on one regimen, while those predicted to underperform could try alternative therapies. This type of analysis that cannot be captured by sparse data alone can be predictive of overall survival and guide personalized medicine.

Cancer occurs when cell growth is uncontrolled and cell proliferation rates exceed apoptosis rates. As the cells grow and divide, a mass known as a tumor forms. Once the tumor is large enough to be detected, there is a good chance that the cancer has spread or metastasized to other areas of the body [12]. Surgery can remove most of the primary tumor when it is in an accessible and operable area but does not always get all of the cells in that region. Radiation, while still a localized option, can be used to shrink the tumor prior to surgery or reach the cancer cells surrounding the tumor that escaped surgery. Alternatively, immunotherapy, or targeted therapies can have more widespread kill, but they are still specific to a certain mechanism that may or may not be present in all cancerous cells. The only systemic treatment currently available to infiltrate metastases is chemotherapy [12].

Cytotoxic chemotherapies target mechanisms found in all cells and can therefore kill cancerous and healthy cells. The mechanisms of action tend to involve the cell cycle, to take advantage of cancerous cells rapid cell division [12]. Bone marrow cells also rapidly divide and are a prime target for chemotherapy. These stem and progenitor cells in the bone marrow differentiate into circulating cells such as platelets, neutrophils, and lymphocytes. These mature cells play important roles in the clotting process, and innate and adaptive immunity [15, 16, 17]. When these processes are impaired by low cell counts, bleeding and infection can occur. This is why a balance between efficacy and toxicity is of such importance in cancer treatment plans. Even if more chemotherapy reduces tumor growth, the limiting factor is toxicity.

Any drug, including chemotherapy, has an associated patient-specific pharmacokinetic (PK) profile of absorption, distribution, elimination and metabolism that can be quantified with a variety of bodily measurements including drug concentrations in the blood plasma, urine, and tumor. Using PK models that are drug specific is important, because even within chemotherapy, drugs have different residence times and mechanisms of action. Different cell types have varying sensitivities to different chemotherapies. For instance, doxorubicin has a high rate of neutropenia associated with it, and carboplatin has a high rate of thrombocytopenia [18]. The magnitude and duration of drug are often inputs into the PK model, and the output profile drives drug effects on the body referred to as pharmacodynamics (PD) [19, 20].

As with any drug, the desired effects need to outweigh the side effects. Both desired PD (tumor suppression) and undesired PD (toxicity) result from a given dose (Figure 1.1). Toxicities arise when the patient is highly sensitive to a dose, or the patient does not have sufficient time to recover from the toxic side effects before the next dose. Toxicities can halt or reduce scheduled chemotherapy doses. Modeling the hematological toxicities can provide keys to understand why some patients can tolerate chemotherapy, while others require lower, less frequent or alternative treatments.

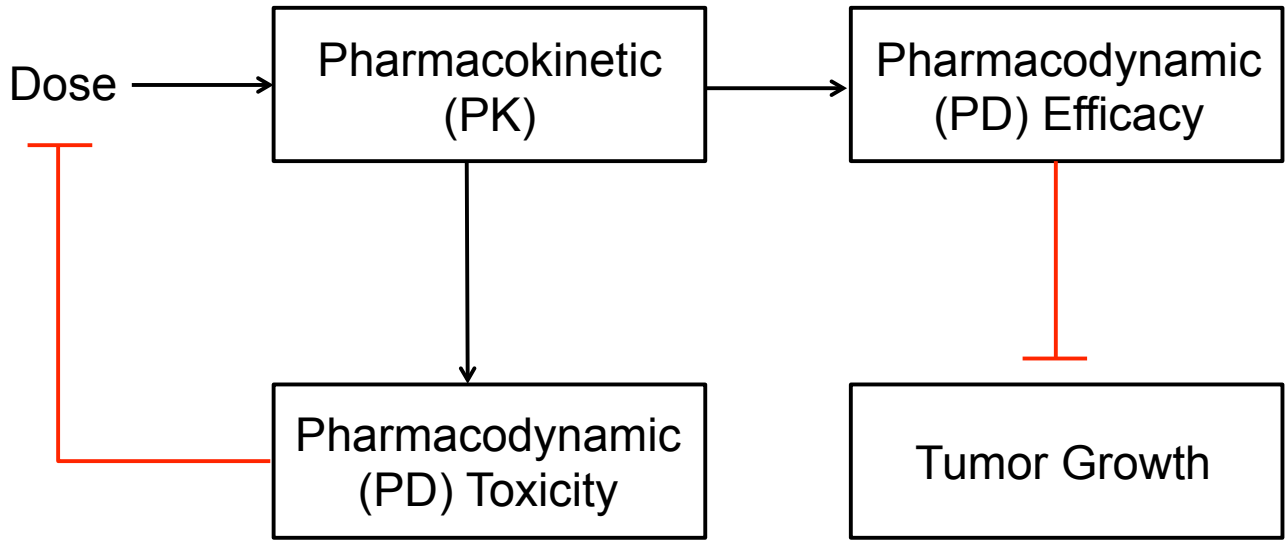

Figure 1.1: Models of cancer, chemotherapy, and their interactions. A scheduled dose of chemotherapy has drug pharmacokinetics that drive pharmacodynamics. Desired pharmacodynamics suppress tumor growth by killing cancerous cells, while undesired pharmacodynamics lead to toxicities that can reduce or delay subsequent doses.

1.1 LINEAGE TREE

Stem cells are undifferentiated cells that can proliferate and mature into specific cell types (Figure 1.2). They are similar to cancerous cells, since they are rapidly dividing. This makes them susceptible to chemotherapy with mechanisms of action involving the cell cycle. Progenitor cells also proliferate but have signals from the body to become certain cell types.

Therefore, in a thrombocytopenic model, the thrombocyte progenitor cells are also at risk of cell death due to chemotherapy. However, a common progenitor cell population can give rise to more than one cell type. Therefore, eliminating progenitors can result in downstream effects of multiple cell types.

The time it takes from the patient receiving the drug to the observable decline in progenitor cells has been modeled a number of ways. A step function or switch turns on and off drug effects, in a binary way, indicating a rapid effect time. This is not always biological but easy to start with, if no other information is available [21]. Another option is to use the entire PK profile to cause a PD effect. The PK and PD models can be joined directly, or additional states can be added if a time delay is observed from plasma to bone marrow concentrations.

After appropriate equations are set for the drug entering the bone marrow from the blood stream, the elimination term is introduced on stem and progenitor cells in the bone marrow. Starting simple, a linear elimination term has been used to remove cells through direct cell death (Eqn. 1.1). This term has been modified by some to mimic saturating drug pharmacokinetics using the hill equation (Eqn. 1.2). For instance, cycle specific drugs can only impact cells in a certain stage of the cell cycle. Therefore, the drug may be eliminated as cells are in other stages of the cycle.

$$Linear \quad = \quad -Slope \times Drug(t)Cell(t) \tag{1.1}$$

$$Hill \quad = \quad \frac{-Emax \times Drug(t)^n Cell(t)}{EC_{50}^n + Drug(t)^n} \tag{1.2}$$

This toxic effect in the progenitor populations produces dynamic behaviors that propagate down to mature circulating cells, the clinically measurable data. Two main modeling methods are used including a lag time, that delays the onset of effects by a given time, and transit compartments, that reduce the early time effects. Lag time models introduce numerical issues and completely ignore any initial effects. Meanwhile, adding or subtracting the number of transit compartments adds flexibility in the output profile. This is why transit

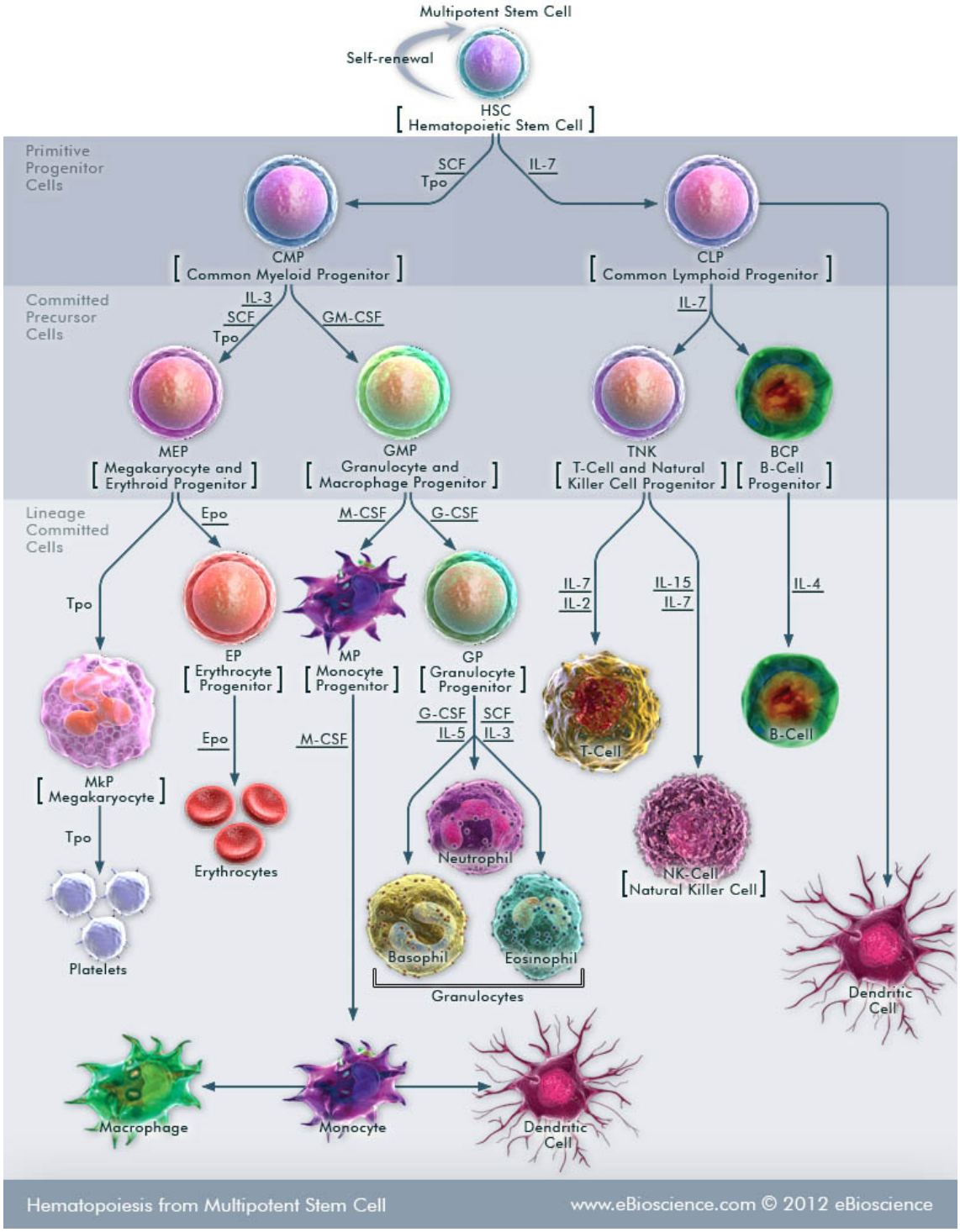

Figure 1.2: Hematopoiesis lineage. Figure obtained at affymetrix eBioscience [2]. Multipotent stem cells can differentiate into different cell types including platelets, neutrophils and lymphocytes such as T- and B-cells. Various cytokines impact specific steps in the transition from stem cell to fated cell type.

Table 1.1: Platelet, neutrophil and lymphocyte grades of toxicity. Toxicity is graded from 1 to 4 with 4 being the most severe. Often grades 3 and 4 warrant dose reductions or delays, while grade 2 will be monitored. LLN is the lower limit of normal [1].

Grade	**Platelets (cells/L)**	**Neutrophils (cells/L)**	**Lymphocytes (cells/L)**
1	$75\times10^9<Pc<LLN$	$1.5\times10^9<Nc(t)<LLN$	$0.8\times10^9<Lc(t)<LLN$
2	$50\times10^9<Pc<75\times10^9$	$1.0\times10^9<Nc(t)<1.5\times10^9$	$0.5\times10^9<Lc(t)<0.8\times10^9$
3	$25\times10^9<Pc<50\times10^9$	$0.5\times10^9<Nc(t)<1.0\times10^9$	$0.2\times10^9<Lc(t)<0.5\times10^9$
4	$Pc<25\times10^9$	$Nc(t)<0.5\times10^9$	$Lc(t)<0.2\times10^9$

compartments are used more often [22]. The maturation cascade used with transit compartments typically uses an average maturation time between each state within a given cell type. However, when switching from a neutrophil to a thrombocyte, the maturation time must be adjusted because each cell type has its own unique range of maturation. Thrombocytes have a longer time to mature thrombocyte than neutrophils. Even though an average maturation time is used in population analysis, letting this parameter be patient specific could shed light on individual variability.

The toxicity in the clinically observable cell types are graded on a scale from 1 to 4, with 4 being the most severe (See Table 1.1) [1]. When the cells nadir in the grade 3 or 4 toxicity range, dose reductions and delays occur. This reduction or delay of future doses can greatly impact the effectiveness of chemotherapy on tumor reduction. If the severity of toxicity can be predicted, drug schedules can be optimized to avoid toxicity.

When the cells begin to decline in number, the body sends feedback signals to stem and progenitor cells through cytokines and other regulatory molecules, to increase cell division and regain homeostasis. The feedback response typically produces some overshoot. The rebound is commonly represented as a power function of the ratio between the individuals baseline cell count and the current cell count with time (Eqn. 1.3).

$$Rebound \quad = \quad (\frac{C_0}{C_c(t)})^{\gamma} \tag{1.3}$$

Care must be taken so that oscillations dampen and are not sustained well after treatment ends. Additionally, rescues, often a recombinant version of the cytokine responsible for proliferation, can be exogenously administered to speed up recovery and prevent grade 3 and 4 toxicity.

The following sections will provide characteristics specific to white blood cells, red blood cells, and platelets, as well as, common connections in the hematopoietic lineage tree (Figure 1.2) and available rescues. Also, models in the literature that address chemotherapy-induced hematological toxicity will be reviewed as they apply to specific cell types.

1.2 LEUKOPENIA

White blood cells (WBC), also known as leukocytes, make up the cells in the immune system and are derived from stem cells in the bone marrow. WBC are broken down into five main types: (1) neutrophils (60 %) (2) lymphocytes (30 %) (3) monocytes (4) eosinophils and (5) basophils [23]. Many models lump all white blood cells together and track the total WBC count over the course of treatment. Minami *et al.* [24, 25] used an indirect-response approach to account for leukopenia in patients receiving a 3-hour infusion of paclitaxel. They incorporated a sensitivity factor of the myeloid cells, to account for variable cell death over time, and a lag time for peripheral leukocyte decline. The data provided was captured by the model with nadirs ranging from 12 to 16 days, but feedback regulation was neglected, and an overshoot is not possible by using this model.

Soon after that, a model was published studying leukopenia in rats, after the administration of 5-Fluorouracil [26]. This model has a feedback function from the circulating leukocytes back to the production rate of the first set of sensitive proliferating cells. The feedback is the fraction of leukocytes at baseline over the leukocytes in circulation.

Using a similar model with human patient data, Friberg *et al.* tested a single model independently on leukocytes and neutrophils under six different chemotherapies [3]. The structure of the model has one proliferating compartment sensitive to chemotherapy that is regulated by a feedback term of the baseline circulating cell type over the current circulating cell concentration. Unlike their rat model, it is raised to a power, γ. The proliferating cells mature at a mean transition time (MTT), that is broken up into mean transit rates (ktr), until they mature and enter circulation in the blood stream (Figure 1.4).

The circulating cells have a natural cell death to maintain steady state. By changing only the MTT, gamma, and drug elimination terms, (slope for linear and Emax and EC50 for Emax model), the underlying model can separately capture neutrophils and leukocytes throughout treatment. This model is a hallmark model in the pharmacometric literature and the basis of most chemotherapy-induced hematological toxicity models. The simple structure captures the basic understanding of biology and uses only a few parameters to capture multiple cell types and drugs. The power lies in the simplicity, but when a deeper understanding is desired, additional biology must be incorporated.

Kobuchi *et al.* took Friberg's human model with the gamma term and separately applied it to 5-Fluorouracil in rat neutrophil, leukocyte, and lymphocyte counts [27]. The model structure inherently can produce sustained oscillations, if the gamma term is too high, as can be seen in their simulations of lymphocytes. This model artifact is not necessarily biological and could warrant a new feedback response function. This model, on top of tracking leukocytes, also tracks lymphocytes, which are a subset of leukocytes. This is important because lymphocytes are the main cell type of the immune system and are a separate branch of the hematopoietic lineage tree. The mechanisms behind proliferation and maturation could be vastly different.

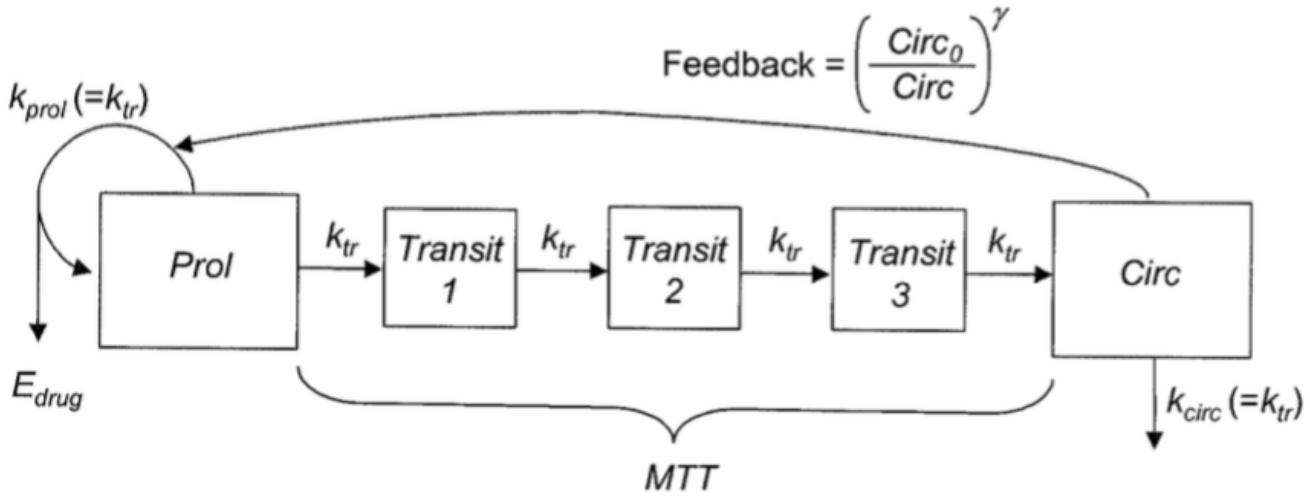

Figure 1.3: Seminal model describing cell maturation with feedback of chemotherapy-induced myelosuppression [3].

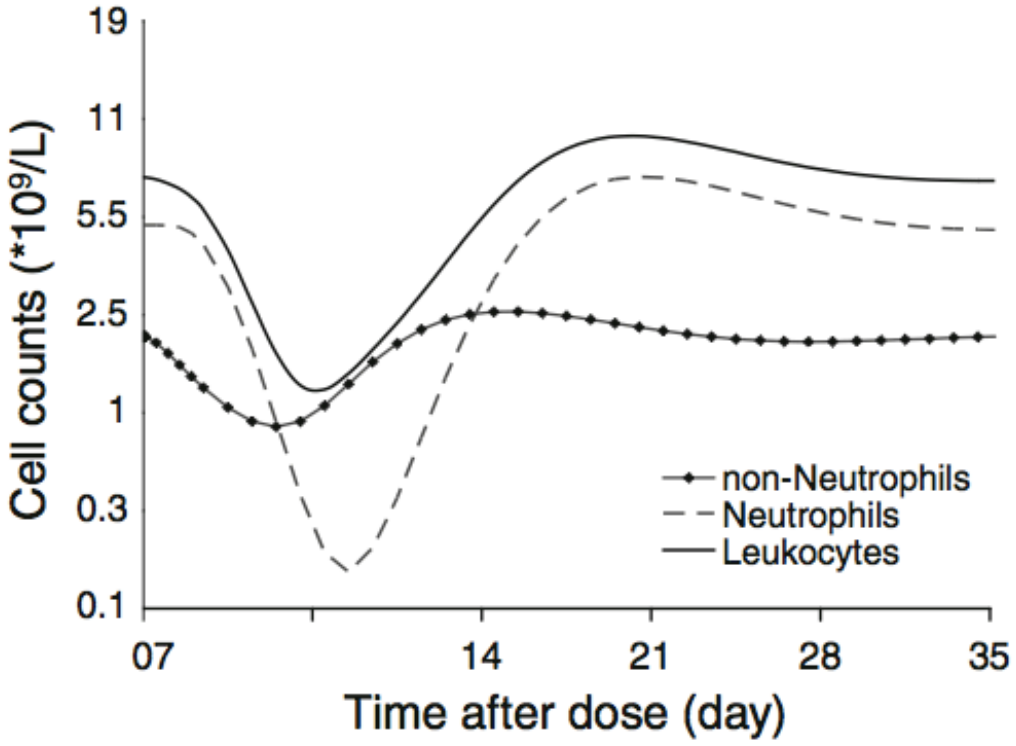

Figure 1.4: Typical time-series profile for different cell types after single dose treatment [4].

1.3 LYMPHOPENIA

All WBCs come from a common myeloid progenitor, with the exception of lymphocytes. McCune *et al.* was able to model lymphopenia through the nadir and approaching baseline levels in the recovery phase [28]. Their Friberg-inspired model should be expanded to include feedback for biology, but the data presented did not require it. This is fine for a single dose but future doses will need to include long term dynamics.

Lymphocytes are further broken down into three types: (1) T cells (2) B cells and (3) natural killer cells. T and B cells account for the vast majority of lymphocytes [23]. Even though T cells develop in the thymus, and B cells develop in the bone marrow, all cell types start out in the bone marrow [23]. One model that delves into the distinctions among lymphocytes was made by Velez de Mendizabal *et al.* By observing rat B cells at different stages of maturity, two subpopulations with different dynamics emerged [29]. If the standard Friberg model was used, then both immature and mature B cells would appear to have similar dynamics. To account for the discrepancy, they added a second maturation chain, that a fraction of the differentiated cells enter, and a second feedback response.

Thus far, models have been reviewed that capture the dynamics of a single cell type. Looking back at the hematopoietic lineage tree (Figure 1.2), many interdependencies are present. Quartino *et al.* do not combine models, but they at least try to account for tracking all WBCs by the summation of neutrophils and non-neutrophils [4].

One possible motivation for exploring combined models is the neutrophil to lymphocyte ratio (NLR) [30, 31, 32]. The ratio is a hypothesized marker of inflammation, and it is also used in cardiovascular mortality and fatty liver disease [33, 34, 35, 36]. Currently the NLR is only looked at as a pretreatment ratio and not dynamically throughout the course of treatment. Many studies have found that patients coming in with a high NLR will have a poor prognosis((>4) [30], high mean (6.02) [31], review article [32]). Another motivation for combined models is overlapping regulation, stemming from a common progenitor state, such as the common myeloid progenitor. The common myeloid progenitor state is responsible for the next three cell types discussed.

1.4 NEUTROPENIA

Compared to other cell types, neutrophil production and regulation are well studied and understood. They make up the majority of white blood cells, play a major role in inflammation and immunity, and neutropenia is a common dose limiting toxicity. Neutrophils have high mobility and can rapidly be recruited in large numbers. The main feedback molecule for stimulating more neutrophils is granulocyte-colony stimulating factor (G-CSF). There are numerous articles and reviews for neutrophils, so the focus of this will be on the most recent of those.

In 2012 Hansson *et al.* modeled patients who had grade IV neutropenia after docetaxel administration [37]. They found that patients with neutropenic fever had a faster time to nadir (MTT) and higher drug sensitivity (EC50). Meanwhile Zhuge *et al.* expanded the average transit rate to be more mechanistic with specific rate constants for proliferation, maturation and apoptosis [38]. This model was extended further to include G-CSF binding and internalization kinetics, and a neutrophil reservoir [39].

A biologically-motivated model with average maturation kinetics by Ho *et al.* not only captures cancer chemotherapy dynamics with G-CSF rescue, but also captures the inflammatory kinetics that occur on a much faster time scale [40]. A marginal pool in the vascular space is in rapid equilibrium with the circulating neutrophils. The circulating neutrophils can enter the extravascular space and be taken up by macrophages, thus activating T cells in the spleen and lymph nodes. This model has many cytokines that have nonlinear feedback relationships to capture both slow and fast dynamics.

A few other recent models include a model with the Friberg base, but a more detailed feedback loop including endogenous G-CSF [41], with additional cell cycle dynamics in the proliferating compartment [42], and with exogenous G-CSF [43].

1.5 THROMBOCYTOPENIA

Neutrophils and thrombocytes share the common myeloid progenitor state, in addition to the key regulatory molecule thrombopoietin (TPO). TPO plays a lesser role in neutrophil production by providing feedback on the common myeloid progenitor cells, but it plays a major role through the lifecycle of platelets. Platelet production is critical in hemostasis, coagulation, and inflammation and is regulated by many types of feedback [15]. For platelets, the maturation path starts with a colony-forming unit megakaryocyte (CFU-Mk), that turns into a megakaryoblast, matures to a promegakaryocyte, and finally into a megakaryocyte. Megakaryocytes are large cells with lobulated nuclei and are the last step before platelet production. Megakaryocytes migrate and localize to the endothelial border where fragments break off into the blood stream. These fragments are the platelets and each megakaryocyte produces 1000-3000 platelets [44, 45]. Once in circulation, one-third of the thrombocytes will sequester in the spleen [46, 47, 48].

The first key regulator of thrombopoiesis is thrombopoietin (TPO). TPO is constitutively produced in the liver and kidneys and inducibly produced in the liver [47]. It is a ligand molecule with a corresponding receptor found on both megakaryocytes and platelets. As platelet production increases, more TPO is taken up by the receptors and out of circulation [49]. Therefore, the platelet/megakaryocyte count and TPO count have an inverse relationship. TPO plays such a major role in feedback regulation, that in TPO deficient mice, a 90% reduction in platelet count was observed [50]. The ligand/receptor relationship relays feedback to achieve homeostasis through signals to the stem and progenitor cells [48].

A second regulatory feedback in platelet production is through stromal cell-derived factor 1 (SDF-1) produced by stromal cells. This chemokine is involved in the chemotaxis of the megakaryocyte to the endothelial border [51]. In response to low platelet counts, SDF-1 helps localize the megakaryocyte and increases the likelihood that it will release platelets into the bloodstream [52].

Bernstein and colleagues used a pharmacodynamic model, to separate good responders from poor responders, by plotting the TPO concentration as a function of platelet count [53]. TPO binds to platelets and megakaryocytes in a ligand receptor fashion, giving TPO

and platelet count have an inverse relationship. Their correlation found it beneficial to have a strong inverse relationship, compared to a weak one.

In addition to including TPO (relative not absolute) into their mechanistic model of thrombocytopenia, Scholz *et al.* added an age structure to platelets [21]. Newly formed platelets tended to sequester in the spleen and are released from the spleen after a function of time. Moreover, they use a complex self-renewal function for stem cells but account for chemotherapy as a simple step function. In another paper with patients receiving an antibody-drug conjugate, two patient subpopulations emerged from their data [54]. Some patients returned to baseline before the subsequent cycle, while others returned to a new and lower baseline, producing a downward drift. The final model was based off the classic Friberg model, but it had a depletion rate on the baseline proliferating compartment.

Of course there are many Friberg-inspired models without additional mechanistic insights, that for reference include one of neutrophils, leukocytes and platelets in response to 2α-deoxy-2α-mehtylidenecytidine [55], and three of neutrophils and platelets in response to indisulam [56, 20] or carboplatin plus paclitaxel [8].

More recently, the TPO receptor ligand relationship was modeled in depth using data from mice receiving chemotherapy and radiation [57]. The model captured the endogenous TPO levels, along with platelet counts over time. However, in their simulated time courses of platelets, the rebound effect is not present in the recovery phase of thrombocytopenia, as seen in humans. This leads back to the controversy of scaling non-human models in humans.

Since TPO is the main regulator of platelet production, recombinant human TPO and TPO receptor agonists have been studied to boost platelet levels, so more drug can be administered. Hayes *et al.* modeled patients getting carboplatin with and without eltrombopag, a TPO receptor agonist [58]. The pharmacodynamic model is simple and uses a linear addition term for the positive effects of eltrombopag. Rescues for thrombocytopenia are still not used widely, unlike G-CSF for neutropenia, so dose reductions and delays must be avoided by choosing appropriate doses.

1.6 ERYTHROPENIA

Platelets are actively involved in the clotting process, and when platelet counts get too low, spontaneous bleeding can occur. Anemia is a condition when red blood cells get too low, due to the chemotherapy itself and as a byproduct of thrombocytopenia. Woo *et al.* modeled chemotherapy-induced anemia in rats that were administered carboplatin [59]. Akin to TPO, erythropoietin, EPO, was the molecule in the feedback loop that stimulates erythropoiesis. Carboplatin killed cells in the proliferating compartment, but it also had a secondary impact due to cell elimination of mature red blood cells from internal hemorrhage associated with thrombocytopenia.

Schirm *et al.* built a more mechanistic model of human anemia, with chemotherapy and exogenous EPO administration [60]. This model was later added to their granulopoiesis model to create one of the first combined hematological toxicity models with overlapping feedback response [61].

In addition to EPO, Jayachandran *et al.* added red blood cell mean corpuscular volume, as a marker for efficacy, in patients with childhood Acute Lymphoblastic Leukemia, who were administered 6-Mercaptopurine [62]. In another study, a very simple pharmacodynamic model of 5-FU-induced erythropenia in rats was built with only two compartments [27]. One compartment was for precursor production, and the other was for circulating blood cells. Again, with no feedback term, this model is incapable of the overshoot in the rebound phase, so all simulations just approach baseline levels.

Few studies have shown the effectiveness of recombinant TPO, but recombinant EPO has been implemented for many years. Ramakrishnan *et al.* modeled recombinant human EPO in healthy patients [63], and more information including cytotoxic chemotherapy and EPO can be found in a review of erythropoiesis-stimulating agents [64].

1.7 NON-HEMATOLOGICAL AND OVERLAPPING TOXICITIES

While the focus of this research tracks hematological toxicity, patients often experience non-hematological toxicities. Dynamic analysis becomes more difficult, since there isn't always a measurable data point to track severity. One patient's level of tolerance may exceed another patient. The side effects range from fatigue and hair loss, to nausea, rash, vomiting, diarrhea, nerve pain and kidney problems, to name a few. For instance, drugs in the taxane and platinum families, at certain cumulative doses, produce peripheral neuropathy. Unlike hematocytes, nerve cells don't always regenerate, resulting in permanent damage [65].

However, even if a side effect is not life threatening or create a permanent problem, the patient may wish to delay future treatments, or try a new therapy, to improve quality of life. Any deviations from the planned treatment course could impact efficacy. This makes modeling and simulation a valuable approach, by limiting the number of toxicities that arise.

Modeling becomes more difficult when multiple drugs are given at the same time. Combination therapy is almost always prescribed, and it has proven successful by attacking the cells at multiple stages of the cell cycle. If the toxicities of the drugs don't overlap, then a boost in efficacy could be achieved. When the toxicities overlap, or drug-drug interactions occur, it is difficult to determine which drugs contribute which percentage of the toxicities. Even though carboplatin and paclitaxel is a combination that is still used for ovarian and lung cancers, thrombocytopenia, anemia, and nausea are common grade 3 and 4 toxicities for both as monotherapies [66]. The overlapping toxicities could be additive or synergistic and result in dose limiting toxicity. Therefore, the dose magnitudes and frequencies must be carefully chosen.

1.8 RADIATION

In addition to chemotherapy, about 50% of cancer patients receive radiation therapy [67]. Radiation is mainly a localized treatment option, although whole body irradiation can be used. Radiation uses targeted high energy waves to damage DNA. The four main types of

radiotherapy are 3D conformal, intensity modulated, image-guided, and stereotactic body [67]. They differ in precision of tumor margins and intensity of beam.

The damage inflicted by radiation can be enough to kill the cell abruptly, in a linear fashion, but also quadratically, as damage accumulates with fractionated radiation [68]. This is because DNA is double stranded, and acute damage to one strand can sometimes be repaired before the next fraction of radiation. Cancerous cells go through cell division at a faster rate than normal cells, and they will have likely divided with damage. Entire fields of study are dedicated to radiation dosimetry, but little is out there regarding the lymphopenia commonly associated with it.

It is generally accepted that lymphocytes are more sensitive to the effects of radiation than other cell types, and in some cancers, the degree of lymphopenia correlates to overall survival [69]. For instance one model concluded this using multivariate regression in non-small cell lung cancer patients [70]. Their explanation is that after enough fractions of radiation, a large percentage of lymphocytes will pass through the field of radiation so that lymphopenia can occur [71]. Their model was built using data through the course of radiation but not during the recovery phase post-radiation. Even if enough cells circulated through the radiation field, another phenomena must be taking place to account for such prolonged recovery times after radiation [72, 73].

There are long standing hypotheses on lymphocyte recruitment post-radiation. The main one is that radiation damages the tissue, releasing damage associated molecular patterns (DAMPs) [74, 75, 76, 77]. The DAMPs initiate an immune response and recruit T-cells to the site of damage. As fractions of radiation accumulate, T-cells are killed directly by the radiation, as well as, through the immune response. This results in a prolonged recovery of lymphocytes to baseline post-radiation.

1.9 RADIOSENSITIZATION

There can be added benefits of giving both chemotherapy and radiation to treat cancer patients. Chemotherapies that impact DNA damage repair, or arrest cells in a phase of the cell cycle, create a certain level of damage [78]. With the addition of radiation, the damage can be sufficient to result in cell death. Timing of radiation and radiosensitizing chemotherapy, whether it is given before and/or concurrently, is still being studied.

Another radiosensitizer, besides chemotherapy, is oxygen. Solid tumors invade already occupied space and eventually use up all the local resources, such as oxygen carrying blood supplies. This creates a hypoxic environment that limits the efficacy of radiation [79]. Radiation and oxygen produce free radicals that are toxic to cells. In the absence of oxygen, the free radicals are reduced and the DNA can be repaired.

1.10 DISSERTATION OVERVIEW

Chemotherapy and radiation were huge advances in cancer treatment. They are both potent methods of reducing cancerous cell populations. This efficacy comes with a cost, and it is ultimately what limits how much treatment a patient undergoes. Dose limiting toxicities often are hematological, because bone marrow cells are rapidly proliferating. Moreover, radiation eliminates sensitive, circulating lymphocytes. Building biologically-motivated models, that describe hematocyte elimination and regulation, is a cost and time effective method of research that could lead to improved patient outcomes.

Chapter 2 starts with the first toxicity model of chemotherapy-induced thrombocytopenia. The model was developed using patient platelet counts after a high dose of carboplatin and incorporated two key regulators. The two regulatory molecules are thrombopoietin (TPO) and stromal cell-derived factor 1. The model was subjected to a affine parallel tempering Markov chain Monte Carlo (APT-MCMC) technique to find parameter distributions. The distributions for patients that entered grade 4 toxicity and required platelet transfusions were statistically different than for those who were less sensitive to the pharmacodynamic

effects. A test dose lower in magnitude is proposed to determine early on which patients can tolerate larger doses.

Chapter 3 takes the previously built thrombocytopenia model and expands it to include neutropenia. This is possible because platelets and neutrophils share a common myeloid progenitor state and regulation from TPO. Additional motivation for combining the two cell types is that both seem to be sensitive to chemotherapy in a locally advanced pancreatic cancer population. Granulocyte-colony stimulating factor (G-CSF), specific to neutrophil production, was also added. This combined model of platelets and neutrophils was implemented in APT-MCMC, and parameter distributions were found for two patient subpopulations. The two groups of two subgroups for this patient data set were "high delta" and "low delta" which describe the tumor histology, and poor and good overall survival. "High delta" tumors were previously associated with a poorer outcome than "low delta". While the histology is an indicator of survival, the actual survival times for patients were also used. Patients were subdivided into those that survived shorter and longer than the median overall survival of 19.1 months. This model was validated with another dataset of patients, receiving a different chemotherapy plan, with a new cutoff of 14 months overall survival.

Chapter 4 covers a model of radiation-induced lymphocytopenia. Lymphocytes play a critical role in the immune system, and low counts can result in infection. The fraction of cells that die after a given beam of radiation is predicted using an algorithm inclusive of cell death and generation. The probability of cell death is based on *in vitro* radiosensitivities, and generation is applied via a daily lymphocyte turnover. This model can be combined with a chemotherapy-induced myelosuppression model to predict toxicity in combination therapy regimens.

Chapter 5 focuses on the conclusions of all the hematological toxicity models and what impact they have made. Furthermore, it discusses future work that has the potential to translate to the clinic.

2.0 BIOLOGICALLY-MOTIVATED MODEL OF CHEMOTHERAPY-INDUCED THROMBOCYTOPENIA

Thrombocytopenia is when an individual has a below average platelet count. This can be an inherited or acquired condition, due to a decreased production such as from dehydration, sepsis, or a hereditary syndrome, or an increased destruction, such as from idiopathic thromocytopenic purpura, lupus, or dengue fever, or drugs such as heparin or chemotherapy. Carboplatin is a chemotherapy with the dose limiting toxicity of thrombocytopenia. Two previously published studies have control groups that only received carboplatin, and the patients developed severe thrombocytopenia [5, 6]. A model was built to capture the dynamics behind platelet production, regulation, and response after carboplatin.

Platelet production is critical in hemostasis, coagulation, and inflammation and is regulated by many types of feedback [15]. Blood cells start as stem cells that mature and differentiate in the bone marrow into specific end cell types, based on chemical cues in the microenvironment. For a platelet, this path starts with a colony-forming unit megakaryocyte (CFU-Mk) that turns into a megakaryoblast, matures to a promegakaryocyte and finally into a megakaryocyte. Megakaryocytes are large cells with lobulated nuclei and are the last step before becoming a platelet. Megakaryocytes migrate and localize to the endothelial border, through the help of stromal cell-derived factor 1 (SDF-1), where fragments break off into the blood stream. These fragments are the platelets, and each megakaryocyte produces 1000-3000 platelets [44, 45]. Once in circulation, one-third of the thrombocytes will sequester in the spleen while the rest are circulated as depicted in Figure 2.4 [46, 47, 48, 80]. Thrombopoietin (TPO), a ligand molecule with associated receptors on platelets and megakaryocytes, relays feedback signals to stimulate proliferation as needed.

2.1 MATERIALS AND METHODS

2.1.1 Patient Data

Individual platelet time series data was obtained from Smith *et al.* for seven patients (Figure 2.1) [5]. The data was from a study observing if interleukin-1α could be used as a toxicity rescue for thrombocytopenia. In order to study changes from baseline, a control group was only given high dose carboplatin and no interleukin-1α. Therefore, to build a model in response to only carboplatin, the control group data was used. The patients received 800 mg/m^2 intravenously over 30 minutes. Platelet transfusions were given when platelet counts were below 20,000 per cubic millimeter (Figure 2.1).

The three patients that did not receive platelet transfusions were not assigned any values, and every data point is a true measurement. The four patients that received platelet transfusions were assigned a value of 2.0 x10^7 platelets/mL during the transfusion period. Since the infusion protocol used by Smith *et al.* was not given, a 30 minute infusion was administered every other day when platelet counts were assigned.

The second set of data is also individual platelet time series data in response to carboplatin [6]. This study also was used to test the effects of a rescue, but in this case it was recombinant human thrombopoietin in gynecological cancer. Six patients were given carboplatin with a calculated area under the curve (AUC) of 11. The same patients, upon recovery from the first dose of carboplatin, received another dose with the rescue. Only the first dose data was used and is represented by the dotted line in Figure 2.2.

Five patients received at least one platelet transfusion, while one did not need any. Again no information was given on the duration or magnitude of the platelet transfusion, but the time and number of transfusions was available. Therefore, the same 30 minute infusion of 2 x10^7 platelets/mL was assumed at each time that the patient was listed to get a transfusion.

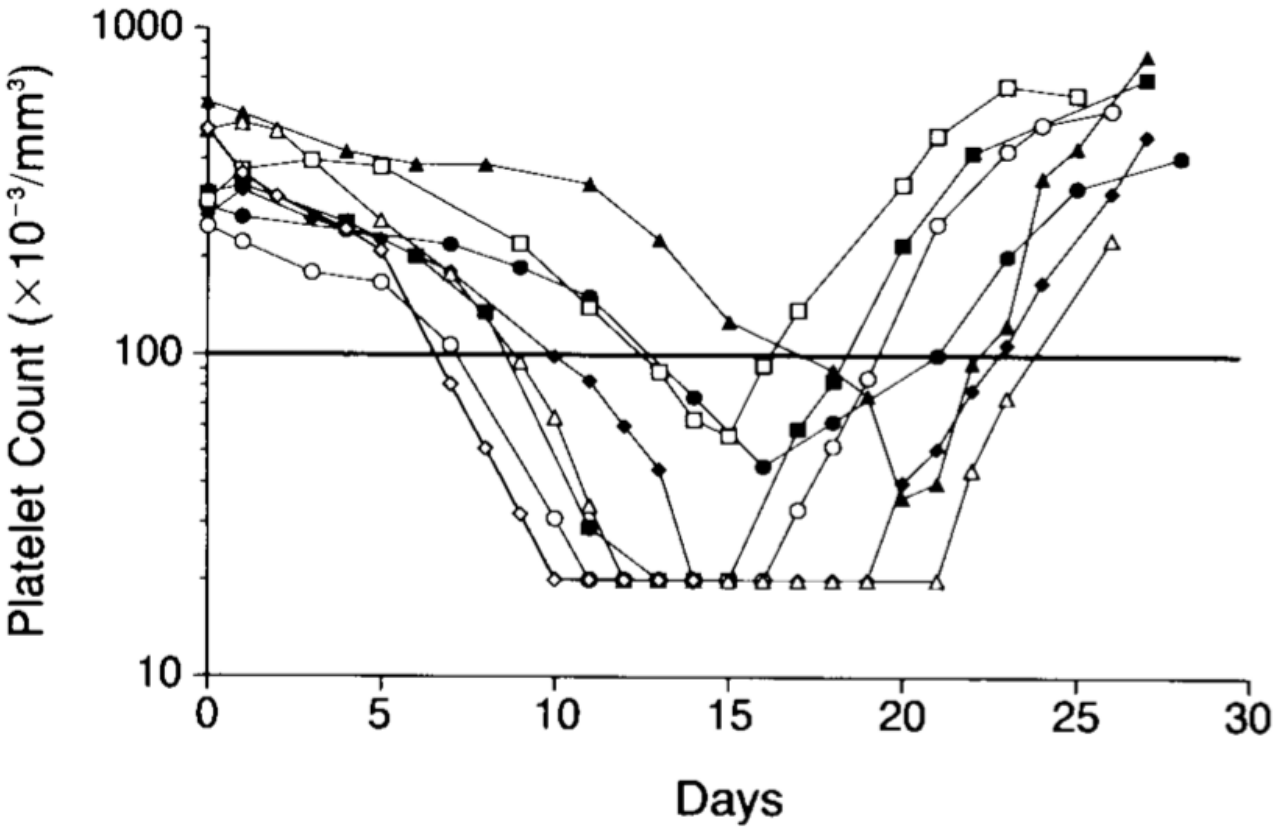

Figure 2.1: Platelet counts over time of the 7 patients used to fit the model. Patients were administered 800 mg/m^2 of carboplatin on day 0. [5].

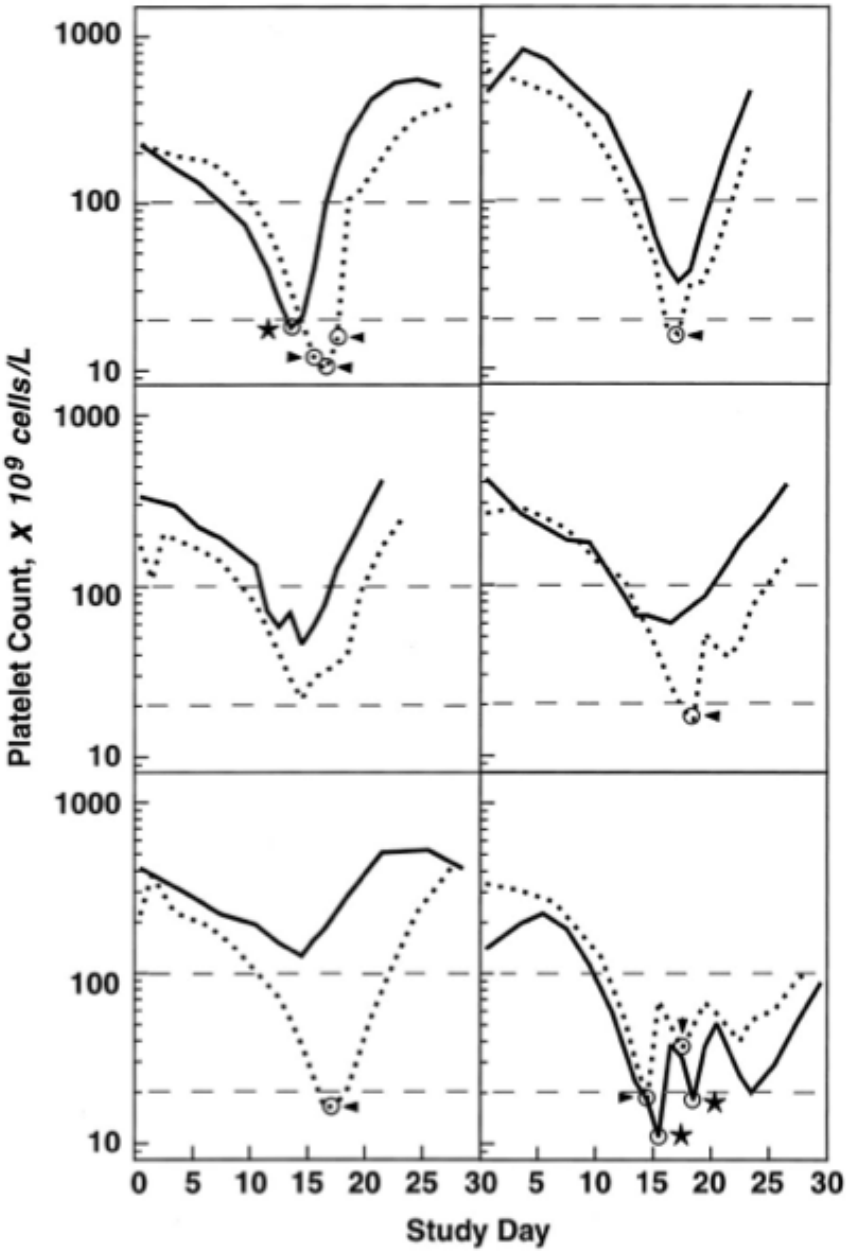

Figure 2.2: Second set of platelet counts over time for 6 patients administered carboplatin at an AUC of 11. The dotted lines represent the data used and the arrowheads are when platelet transfusions occured. [6].

2.1.2 Carboplatin

Carboplatin is an FDA approved alkylating agent in the platinum family and is cell-cycle nonspecific. It is used to treat ovarian, lung, head and neck, endometrial, and breast cancers among others. The primary route of elimination is renal excreation [81]. This is why the Calvert formula is used to dose patients. In recurrent ovarian cancer, carboplatin is dosed at 360 mg/m^2 IV every 4 weeks as a monotherapy [81]. The doses used to fit this model are very high doses and greater than what is recommended. In comparison to cisplatin, another platinum agent, carboplatin has fewer side effects such as no nephrotoxic effects. However, thrombocytopenia is a main dose limiting toxicity.

In order to capture the dynamics of carboplatin toxicity, a PK model from the literature fit to data at 450 mg/m^2 was linearly scaled up (Figure 2.3) [8, 82, 7]. This two compartment model incorporates exchange between a central and peripheral compartment as well as a clearance term [8]. The following equations represent the PK model with $Drug$, C_b, and C_p being the, dose rate of carboplatin, concentration of carboplatin in the blood, and concentration of carboplatin in the peripheral compartment respectively:

$$\frac{dC_b(t)}{dt} = \frac{Drug(t)}{V_1} - k_{12}C_b(t) - k_{10}C_b(t) + k_{21}C_p(t) \tag{2.1}$$

$$\frac{dC_p(t)}{dt} = -k_{21}C_p(t) + k_{12}C_b(t) \tag{2.2}$$

Carboplatin PK is the driving force behind the dynamics in the bone marrow. Individual PK profiles corresponding to individual PD profiles were not available, therefore, an average PK profile was used for patients.

The model can scale to accommodate different dose magnitudes. The dose for the second dataset was found using the Calvert formula, to go from an AUC to dose (dose = target AUC $\times$ glomerular filtration rate + 25). Individual glomerular filtration rates were not provided, so an average dose was given to each patient equivalent to 1650 mg/m^2.

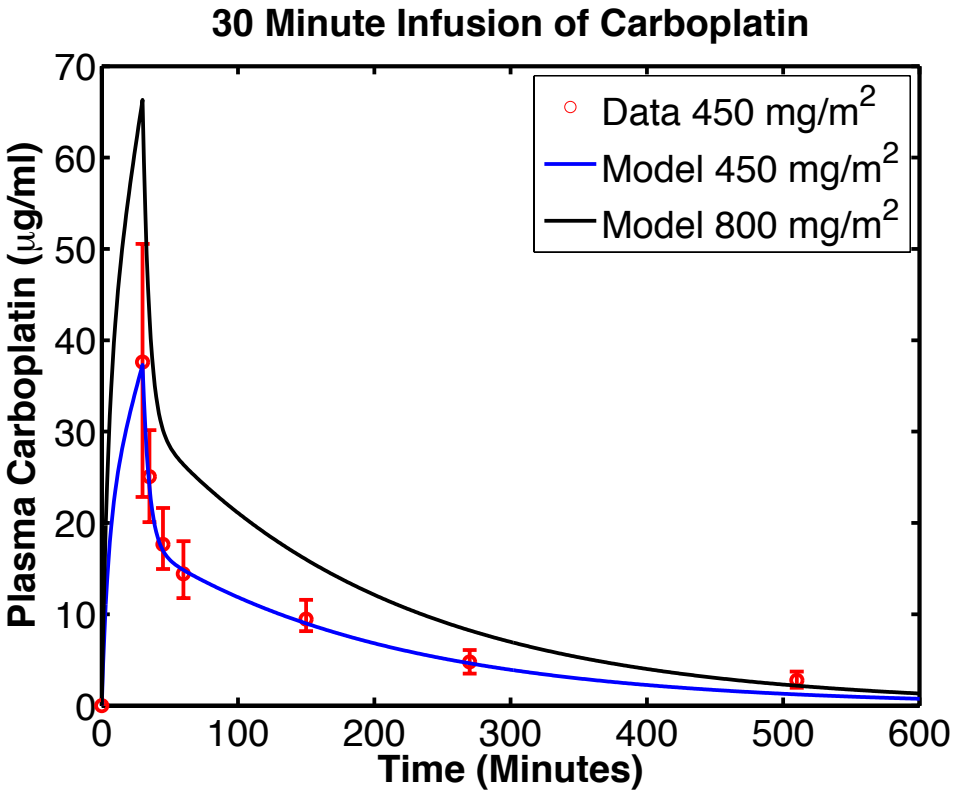

Figure 2.3: The PK model (blue curve) is fit to data (red dots) from the literature [7, 8]. The model is then scaled up (black curve) to the dose of interest.

2.1.3 Model Development

2.1.3.1 Existing Hematopoietic Models Existing models of chemotherapy-induced thrombocytopenia have a phenomenological point of view, neglecting drug pharmacokinetics (PK) [21] or incorporating biological response and regulation via a nonlinear mathematical feedback effect [54, 55, 57]. Some models incorporate the age structure of the precursors and megakaryocytes [21, 57, 83], but this is not clinically measurable. One model, while more biological and less empirical, explicitly models the ligand receptor relationship of TPO, but uses data from mice not humans [57]. That mouse model captures the effects of multiple doses of carboplatin and radiation [57]. However, the simulation presented for a single carboplatin dose does not rebound significantly above the baseline platelet count, which is an observable phenomenon in human patient data.

The highly used, more phenomenological model structure created by Friberg *et al.* will be the starting point [3] for building a biologically-motivated model with clinical measurements in humans. The Friberg *et al.* model has a proliferating compartment of cells that mature through a series of transit compartments, with mean transit times, and eventually become circulating cells. As chemotherapy is introduced, the proliferating cells are eliminated and this results in a drop in circulating cell count. Nonlinear feedback from deviations of basal circulating count to current circulating count stimulates proliferation. The delayed feedback produces a circulating cell count profile of a decrease then overshoot above baseline before returning to baseline levels.

2.1.3.2 Platelet Production and Regulation Platelet production has a transit rate of maturation, k_{tr}, as cells differentiate from stem cell to end cell type (Eq.2.3 -Eq.2.5) that is a patient specific parameter. After the stem cells mature into megakaryocytes (Eq.2.6), they can move to the endothelial border and release platelets into the bloodstream. Each megakaryocyte is assumed to produce 1000 platelets with lifespans of roughly 7-10 days. Platelets, as modeled herein, represent the circulating platelets in the vascular space (Eq.2.7). Platelets are free to move in and out of the spleen (Eq.2.9) and kidney and liver (Eq.2.8). One-third of the total platelet count is represented in the spleen state (Eq.2.9).

Table 2.1: Thrombocytopenia Model Equations and Corresponding Biological States.

State	**Biological Meaning**	**Unit**
$P_1(t)$	Progenitor 1 CFU-Mk	$\frac{10^6 cells}{\mu L}$
$P_2(t)$	Progenitor 2 Megakaryoblast	$\frac{10^6 cells}{\mu L}$
$P_3(t)$	Progenitor 3 Promegakaryocyte	$\frac{10^6 cells}{\mu L}$
$M(t)$	Megakaryoctye	$\frac{10^6 cells}{\mu L}$
$Pc(t)$	Circulating Platelets	$\frac{10^6 cells}{mL}$
$Pt(t)$	Platelets in Liver and Kidneys	$\frac{10^6 cells}{mL}$
$Ps(t)$	Platelets in Spleen	$\frac{10^6 cells}{mL}$
$S(t)$	Stromal Cell-Derived Factor-1	-
$T(t)$	Thrombopoietin	$\frac{pg}{mL}$
$T_1(t)$	Thrombopoietin Signal	-
$T_2(t)$	Thrombopoietin Signal	-
$T_3(t)$	Thrombopoietin Signal	-

$$\frac{dP_1(t)}{dt} = k_{tr}P_{1_0} - k_{tr}P_1(t) - SlopeE_2^2(t)P_1(t) + k_{tr}k_T(k_{T3}T_3^2(t) - T_0)P_1(t) \tag{2.3}$$

$$\frac{dP_2(t)}{dt} = k_{tr}P_1(t)k_{tr}P_2(t) - SlopeE_2^2(t)P_2(t) + k_{tr}k_T(k_{T3}T_3^2(t) - T_0)P_2(t) \tag{2.4}$$

$$\frac{dP_3(t)}{dt} = k_{tr}P_2(t) - k_{tr}P_3(t) \tag{2.5}$$

$$\frac{dM(t)}{dt} = k_{tr}P_3(t) - k_{tr2}M(t) \tag{2.6}$$

$$\frac{dPc(t)}{dt} = k_{tr2}M(t) - k_{tr}Pc(t) - k_{ps}Pc(t) - k_{pt}Pc(t) + k_{kp}Pt(t) + k_{sp}Ps(t) \tag{2.7}$$

$$\frac{dPt(t)}{dt} = k_{pt}Pc(t) - k_{kp}Pt(t) \tag{2.8}$$

$$\frac{dPs(t)}{dt} = k_{ps}Pc(t) - k_{sp}Ps(t) \tag{2.9}$$

$$\frac{dS(t)}{dt} = \frac{Pc_0S_0}{k_m + S_0} - \frac{Pc(t)S(t)}{k_m + S(t)} \tag{2.10}$$

$$\frac{dT(t)}{dt} = T_0(\frac{Pc_0}{M(t)})^\gamma - T(t) \tag{2.11}$$

$$\frac{dT_1(t)}{dt} = k_{ts}T(t) - k_{ts}T_1(t) \tag{2.12}$$

$$\frac{dT_2(t)}{dt} = k_{ts}T_1(t) - k_{ts}T_2(t) \tag{2.13}$$

$$\frac{dT_3(t)}{dt} = k_{ts}T_2(t) - k_{ts}T_3(t) \tag{2.14}$$

$where$

$$k_{tr2} = k_{tr}(1 + (S(t) - S_0)) \tag{2.15}$$

The first key regulator of thrombopoiesis is thrombopoietin (TPO). TPO is constitutively produced in the liver and kidneys and inducibly produced in the liver [47]. It is a ligand molecule with a corresponding receptor found on both megakaryocytes and platelets. As platelet production increases, more receptors are occupied, internalized and degraded by TPO [49]. TPO plays such a major role in feedback regulation that in TPO deficient mice, a 90% reduction in platelet count was observed [50]. The ligand/receptor relationship relays feedback to achieve homeostasis through signals to the stem and progenitor cells [48]. Many myelosuppression models rely on the power exponent of the ratio between circulating and baseline cell counts to account for rebound after a toxicity challenge but this model uses TPO explicitly.

A second regulatory feedback in platelet production is through stromal cell-derived factor 1 (SDF-1) produced by stromal cells. This chemokine is involved in the chemotaxis of the megakaryocyte to the endothelial border [51]. In response to low platelet counts, SDF-1 helps localize the megakaryocyte and increases the likelihood that it will release platelets into the bloodstream [52].

To model TPO, a series of transition states were used to represent a signal being passed from ligand to receptor to stem/progenitor cells (Eq.2.12- Eq.2.14). This signal is the regulatory feedback in response to the megakaryocyte count. TPO has a standing steady state around 200 pg/mL but can increase or decrease depending on saturation of receptors [84]. If there are more ligand molecules than receptors, then an accumulation of extracellular TPO will occur. While TPO alters the rate of cell division (Eq.2.11), SDF-1 alters the maturation transition rate (Eq.2.10), k_{tr2}, of the megakaryocyte to platelets [85, 86, 87]. Akin to TPO, a basal level of SDF-1 is present but more can be produced in response to platelet count to produce a gradient for chemotaxis. The model and parameterization above is for the healthy dynamic system. Chemotherapy challenges will kill progenitor cells, decrease platelet count, and activate TPO and SDF-1 to compensate for the chemotherapy-induced thrombocytopenia.

2.1.3.3 Toxicity Pharmacodynamics Chemotherapy is administered on the time scale of minutes to hours but has delayed and long-lasting effects ranging from days to weeks. This is biologically-motivated by a cytotoxic transition that occurs after the carboplatin-DNA adduct forms [59]. To account for this time scale issue, effect states were added (Eqs.2.16 and 2.17). The concentration of drug that makes it to the bone marrow is set by the transition rate, k_{vbm}=0.0021 day^{-1}, and drug equilibrium with the plasma compartment, k_{bmv}=0.26 day^{-1}. The accumulation and decay of the toxic signal is set by rates, k_{vm1}=2300.0 day^{-1} and k_{vm2}=0.9 day^{-1}, respectively. The effect state (Eq. 2.17) with a fit *Slope* term eliminates cells in the progenitor states (Eqs.2.3 and 2.4).

$$\frac{dE_1(t)}{dt} = k_{vbm}C_b(t) - k_{bmv}E_1(t) \tag{2.16}$$

$$\frac{dE_2(t)}{dt} = k_{vm1}E_1(t) - k_{vm2}E_2(t) \tag{2.17}$$

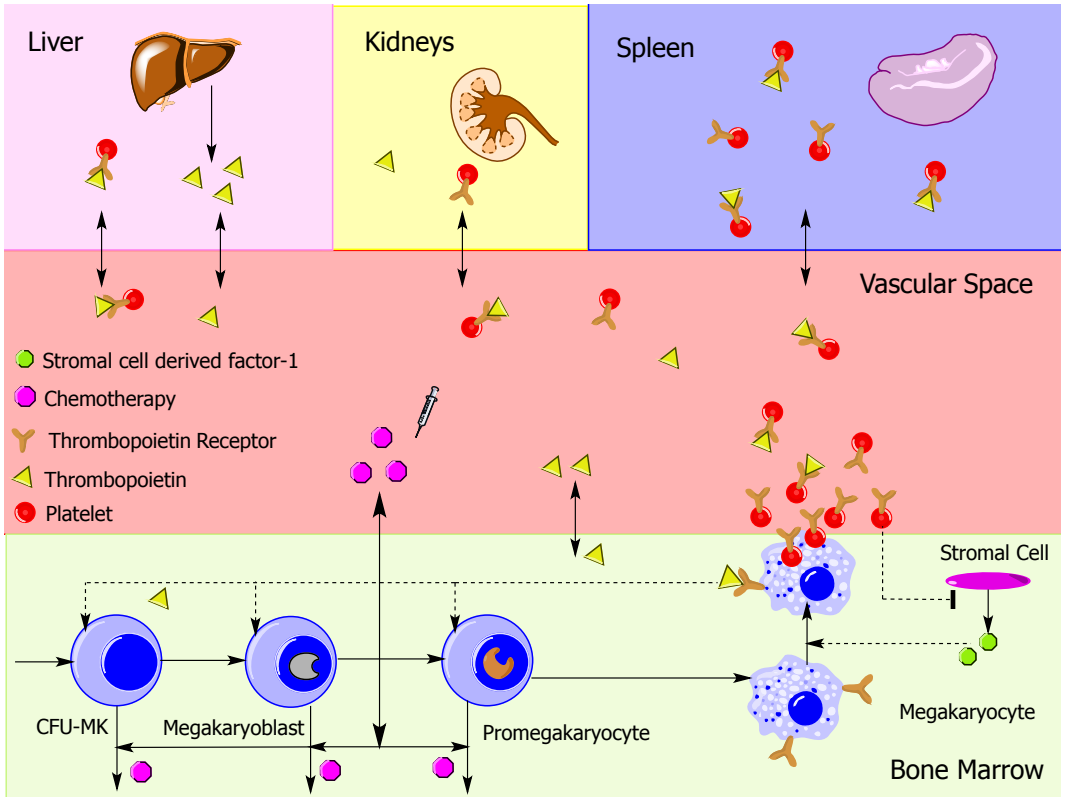

Figure 2.4: Dynamic Chemotherapy-Induced Thrombocytopenia Model. Progenitor and stem cells mature into megakaryocytes. Each megakaryocyte produces on the order of 1,000 platelets that are released into the blood stream. The progenitor cells are susceptible to cell death via chemotherapy in the bone marrow. As the circulating platelet count decreases after a dose of chemotherapy, stromal cell-derived factor 1 and thrombopoietin provide feedback regulation to regain homeostasis.

Table 2.2: Thrombocytopenia Model Parameters (P). SS fit: fit to steady state data, Dyn. fit: fit to dynamic data.

P	**Value**	**Unit**	**Source**
k_{pt}	0.288	$\frac{1}{day}$	SS fit
k_{kp}	1.44	$\frac{1}{day}$	SS fit
k_{ps}	0.864	$\frac{1}{day}$	SS fit [80]
k_{sp}	1.44	$\frac{1}{day}$	SS fit [80]
k_m	1.44×10^6	$\frac{pg}{mL}$	Dyn. fit [50]
T_0	200	$\frac{pg}{mL}$	[84]
S_0	1	-	Dyn. fit
k_{ts}	0.3	$\frac{1}{day}$	Dyn. fit
γ	0.6	-	Dyn. fit
k_{T3}	0.005	$\frac{1}{day}$	Dyn. fit

2.1.4 Parameter Estimation

Twelve ordinary differential equations were used to describe the states of the chemotherapy-induced thrombocytopenia model. The data was fit to the circulating platelet state, Pc, using Python and a affine parallel tempering Markov Chain Monte Carlo approach (APT-MCMC) [88]. The energy function, J(p), between the model, $y_{sim}(i,p)$, and data, $y(i)$, was minimized by adjusting three parameters ($Slope$, k_T, k_{tr}):

$$J(p) \quad = \quad \sum_{i=1}^{N} (y(i) - y_{sim}(i,p))^2 \tag{2.18}$$

Each time series data point is compared to the simulation output at that point in time and the difference is squared. The sum of all the squared residuals is minimized.

The fixed parameters in the model were fit to meet certain criteria. For instance, the rate constants to and from circulating platelets and the spleen were set to make the splenic concentration of platelets at steady state to be one-third of an individuals total platelet count [80]. Additionally, unlike TPO where a nominal value is found in the literature, SDF-1 basal levels were fixed at 1 to be a relative increase and decrease. However, the parameters were dynamically fit for SDF-1 feedback to account for the 10% regulation found in the literature [50]. All fixed parameters are provided in Table 3.2.

2.2 RESULTS

2.2.1 Platelet Response to Chemotherapy

In response to a chemotherapy challenge, carboplatin, the nadir for all patients fell between 12 to 25 days post treatment, and platelets rebounded reaching steady state. Figure 2.5 shows the seven patients and corresponding model fits from the Smith *et al.* data, while Figure 2.6 shows the six patients and corresponding model fits from the Vadhan-Raj *et al.* data. The grade three and grade four toxicity lines show when patients fall into thrombocytopenia and are prone to bruising and bleeding that would warrant treatment delays or reductions. The model captures individual patients well despite different nadirs, durations, grade 3 and 4

toxicities and different platelet counts. The parameter distribution histograms can be found in Figure 2.7, for the first data set, and Figure 2.8, for the second data set, and Table 3.3. The parameter distribution for *Slope* did not distinguish different patient subgroups. However, clear differences can be seen in the distributions of the TPO signal, k_T, and transit time, k_{tr}. Patients that needed platelet transfusions all had k_{tr} values greater than those that did not. This means that the drug effects the circulating platelet count at a faster rate than a smaller k_{tr}. For the patients with a smaller k_{tr} the rebound response from SDF-1 and TPO can begin to set in before they enter grade four toxicity. Additionally, the magnitude of the rebound is greater for patients that do not need platelet transfusions. This could be explained by interpatient differences in drug sensitivity. For the other data set, the same TPO statistical difference can be seen, but the *ktr* does not follow the trend and a large overlap occurs. This could be due to the fact that the carboplatin dose is so high that too many cells are eliminated at a saturable rate.

2.2.2 Thrombopoietin

The dynamic effects of TPO can be seen in Figure 2.9. On the left is the TPO output profile for a chemotherapy challenge. The peak value of TPO reaches around 4000 pg/mL and occurs before the platelets nadir [89]. The resulting platelet outcome when TPO is its nominal value of 200 pg/mL is seen on the right in Figure 2.9. A much lower platelet response occurs in the absence of TPO and the overshoot does not occur.

2.2.3 Stromal Cell-Derived Factor 1

SDF-1 is known to help localize the megakaryocyte to the endothelial barrier so platelets can be released into circulation. When platelet count drops, SDF-1 is activated and influences the rate of transition from megakaryocyte to platelets. As megakaryocytes break up into platelets, the megakaryocyte count decreases and platelet count increases (Figure 2.10). The parameters were set to regulate about 10% of platelet production [50]. This short-term compensation increases the number of platelets based on the existing pool of megakaryocytes, but TPO is needed to increase the number of megakaryocytes and aid in long-term recovery.

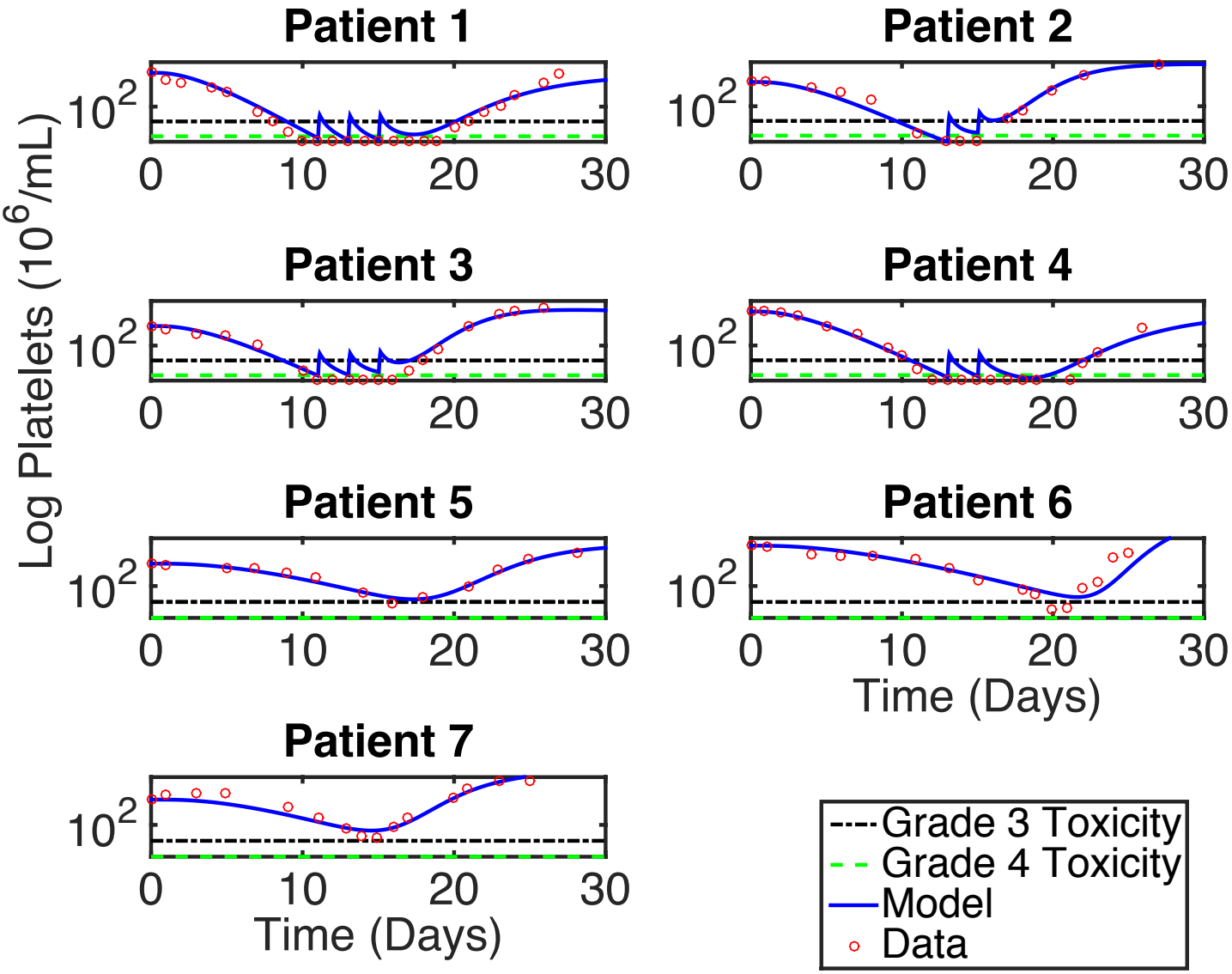

Figure 2.5: Individual thrombocyte concentration profiles over time [5]. Patients 1-4 received platelet transfusions. Patient data (red dots) and model output (blue line) with grade three (black dot dash line) and grade four (green dash line) toxicity.

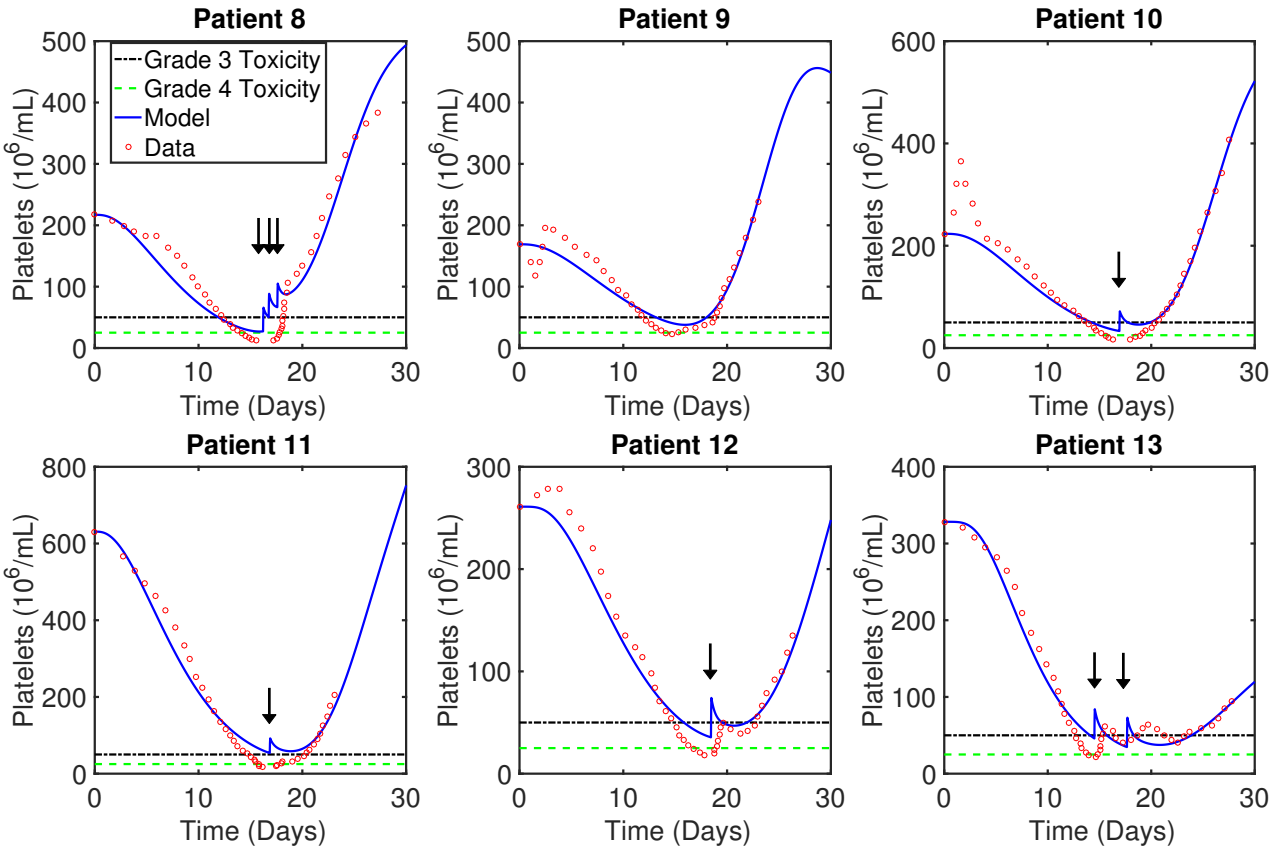

Figure 2.6: Individual thrombocyte concentration profiles over time [6]. Patients 8,10-13 received platelet infusions. Patient data (red dots) and model output (blue line) with grade three (black dot dash line) and grade four (green dash line) toxicity.

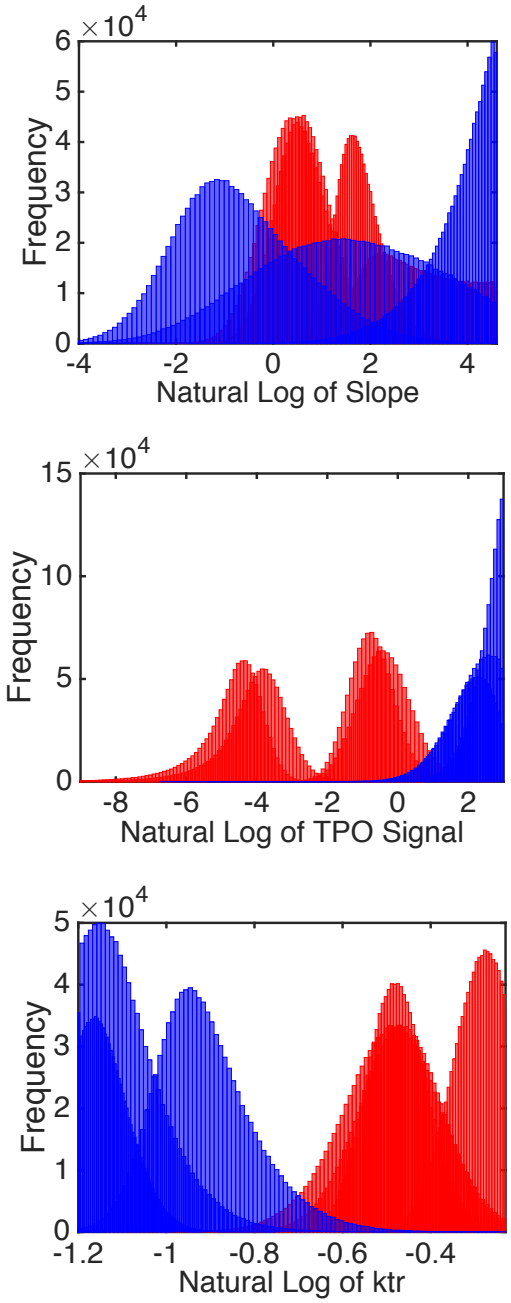

Figure 2.7: APT-MCMC histograms of the three fit parameters. Patients 1-4 are in red while patients 5-7 are in blue. The figures are all the number of simulations vs. the natural log of the parameter.

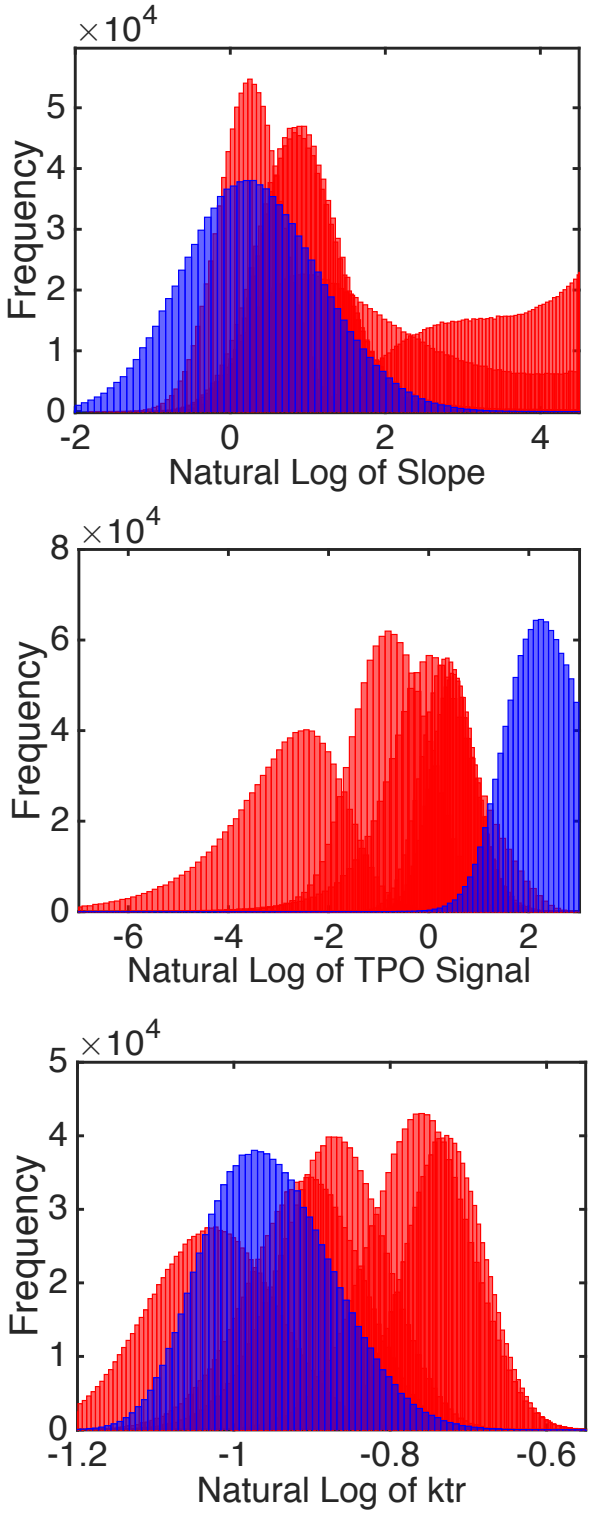

Figure 2.8: APT-MCMC histograms of fitted parameters. Patients 8,10-13 are in red while patient 9 is in blue. The figures are all the number of simulations vs. the natural log of the parameter.

Table 2.3: Individual Thrombocytopenia Fitted Model Parameters (P).

Patient	**mean Slope**	**mean** $k_T(Day^{-1})$	**mean** $k_{tr}(Day^{-1})$
1	6.9	0.012	0.74
2	2.1	0.94	0.61
3	2.53	0.6	0.63
4	27.8	0.02	0.62
5	12.7	9.4	0.34
6	52.6	8.5	0.32
7	1.29	13.0	0.405
8	1.4	1.85	0.47
9	2.0	9.2	0.39
10	2.89	1.7	0.40
11	37.0	0.61	0.48
12	12.7	1.6	0.36
13	3.6	0.09	0.41

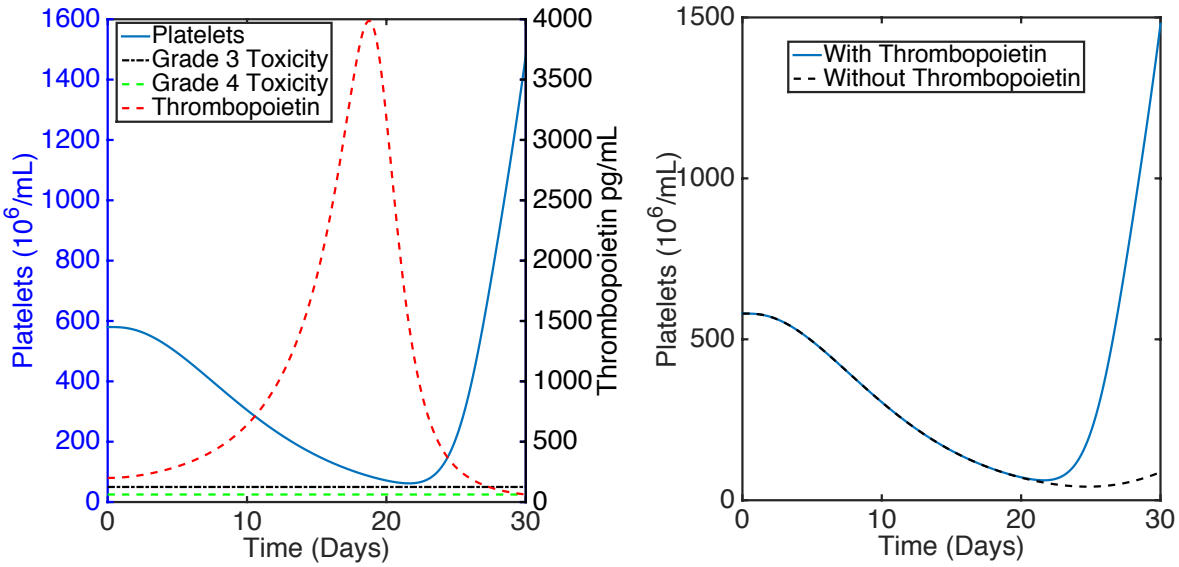

Figure 2.9: Patient 6, Left: Thrombopoietin (red dashed line, right y axis) increases with time as platelet concentration (blue line, left y axis) decreases. Right: Platelet response with (blue line) and without (black dash line) thrombopoietin regulation.

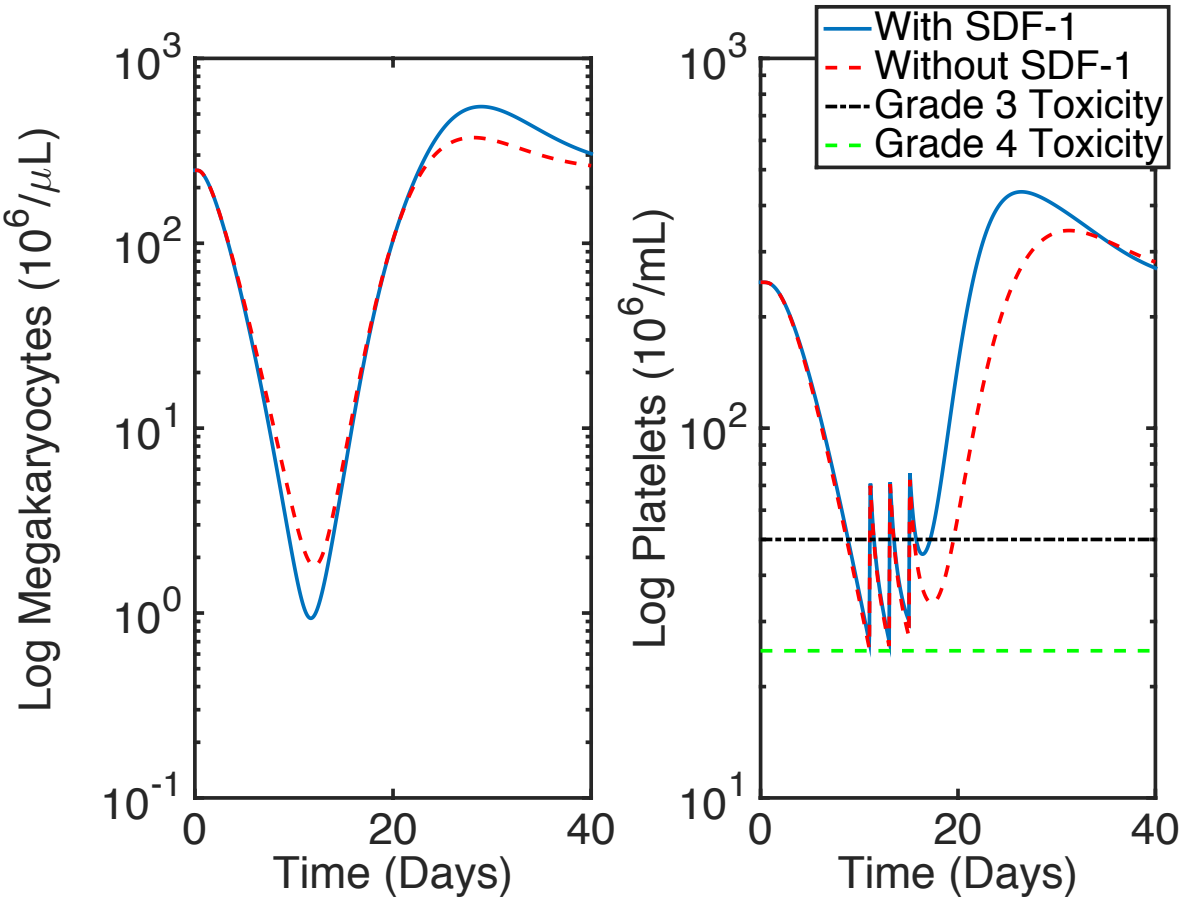

Figure 2.10: Patient 3, Stromal cell-derived factor 1, Left: Megakaryocytes, Right: Platelets, with (blue line) and without (red dash line) SDF-1 regulation.

2.3 DISCUSSION

The model presented considers, PK, thombopoiesis, and the feedback of TPO and SDF-1 both in healthy patients and those with cancer that receive chemotherapy. Additionally, it captures patients with varying drug sensitivity. Finally, the biologically driven model provides biological transition rates for progenitor maturation, transport rates, one-third of

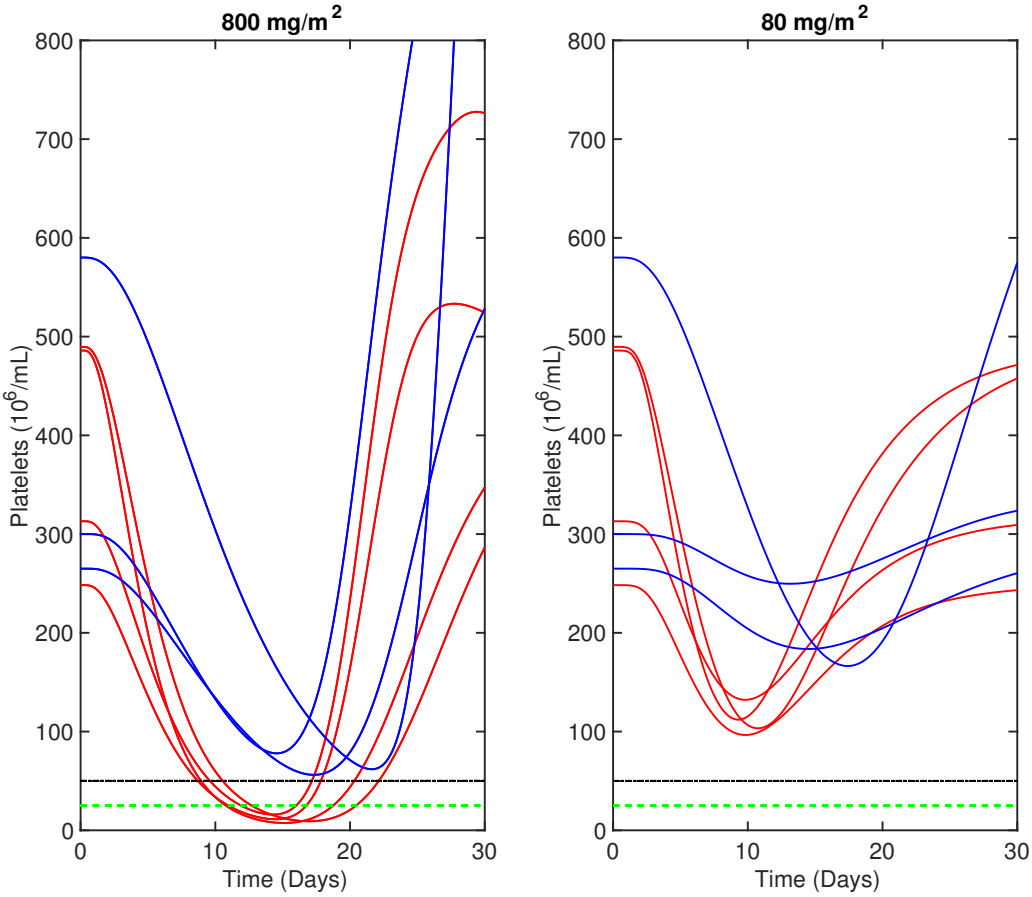

Figure 2.11: Simulated individual thrombocyte concentration profiles over time of patients receiving high dose carboplatin (right) and a low test dose (left)[5]. Patients 1-4 (red) are more sensitive to the drug while patients 5-7 (blue) are less sensitive. The grade three (black dot dash line) and grade four (green dash line) toxicity lines are provided.

the total platelet count in the spleen, circulating platelet count dynamics, and, scale and timing of TPO in response to a chemotherapeutic challenge.

The one patient that did not follow the pattern could have been an outlier, or was just at such a high dose of carboplatin, that a saturable degree of cell elimination was reached. Additionally, the initial data points, for the patient that did not need to have a platelet transfusion, was a little erratic. There was an initial dip within the first few days that does not fit the gradual decrease that is expected. The actual initial condition could be off. If the initial condition was actually a lower value, then the ktr would fall into place and be predictive. Moreover, this patient hugs the grade 4 toxicity, so the patient is too close for the model to separate this patient from the other patients. A trial with a larger sample size would make this model more robust.

Even with the help of TPO and SDF-1 regulation, interpatient variability in drug sensitivity can cause some patients to fall into grade 4 thrombocytopenia after a carboplatin dose. These patients received platelet transfusions. The underlying biology of how quickly the drug impacts circulating platelets as well as the degree of rebound due to thrombopoietin were the key parameter differences. In a similar study of neutrophils, it was concluded that patients with a faster k_{tr}, and lower EC50, in a sigmoid model of cell elimination due to drug, correlated to patients that developed febrile neutropenia [37]. Without pharmacokinetic information it is difficult to distinguish if PK, PD or a combination of both contribute to patient variability. The fact that there are data points well above baseline in the recovery phase points to the biology of PD effects.

Both severe toxicities may be able to be detected using a lower test dose. For instance, in Figure 2.11, on the left is the high dose of carboplatin, and on the right is the low dose test case. It is clear the red patients show a faster response and deeper nadir, indicating they would be more susceptible to high carboplatin doses. This could help guide dosing for patients with a high k_{tr}, including giving smaller, more frequent doses.

The model was able to capture the regulatory mechanisms behind platelet production. TPO impacts the production rate of platelets, while SDF-1 alters the localization rate of megakaryocytes. However, the response is delayed and platelets can fall drastically. When platelets fall beneath the grade three and four toxicity thresholds, the subsequent dose

of chemotherapy is often delayed until the patient recovers, which leads to lower efficacy. Additionally, as seen in some patients presented, if thrombocytopenia is too severe, platelet transfusions might be necessary. Unfortunately, platelet transfusions have a high rate of infection and short-term relief [90]. If toxicity can be predicted early on, then patients can be eligible for preventative or palliative care prior to toxic events. This model has the ability to make such estimations, or even the potential to contribute to real-time alterations of chemotherapy doses for individual patients.

3.0 A COMBINED MODEL OF THROMBOCYTOPENIA AND NEUTROPENIA

Local pancreatic cancer has a 5-year survival rate of 29% and an increase in death rate of 0.3% per year from 2005-2014 in white men [12]. By the time a patient presents with symptoms, the disease is already established and most likely has metastasized. This makes surgery an unlikely option, and clinicians turn to chemotherapy and radiation. Chemotherapy works by killing cells that rapidly divide such as cancerous cells. Toxicity arises because stem and progenitor cells in the bone marrow also rapidly divide, resulting in hematological toxicities such as thrombocytopenia and neutropenia.

One way to try to combat the low survival rates associated with pancreatic cancer is by identifying and predicting subpopulations that will respond to a given treatment schedule, using mathematical modeling and simulation. Patients predicted to underperform could be put on a different schedule or different treatment. Two subpopulations that can be used to stratify patients prior to therapy emerge via a image-defined histologic subtype, that has previously been correlated to overall survival [91]. "High delta" tumors are well defined on a CT image. The tumor is visually more distinct from normal tissue and is associated with a poor prognosis. "Low delta" tumors are poorly defined and have a better prognosis. Through modeling and simulation, distinct parameter distributions can differentiate high delta and low delta tumors. Based on the physiological meaning of the model parameters of interest, mechanistic understanding can help guide decisions regarding therapy.

Even though "high delta" and "low delta" is associated with overall survival, models can be built retrospectively by studying patients that had either good or poor overall survival, regardless of histologic subtype. Therefore, parameter distributions for both the high/low delta and poor/good overall survival cases are studied.

The mathematical model that was built is a biological extension of a seminal model describing chemotherapy-induced myelosuppression (Figure 1.4) [3]. The base model has stem and progenitor cells in the bone marrow that mature into circulating cells. As chemotherapy eliminates progenitor cells, the resulting deviation in circulating cell count from baseline drives feedback on proliferation rates. This model describes the overall time course of circulating cells but was expanded to include more biology.

The full model is a combined model describing chemotherapy-induced thrombocytopenia and neutropenia. Platelets are highly involved in the blood clotting process, and neutrophils are the main component of the innate immune response [15, 16]. If either cell type is low, then infections and bleeding can occur, compromising the patient's health. Both platelets and neutrophils start from a common myeloid progenitor population. Depending on chemical cues in the microenvironment, the myeloid progenitor cell can differentiate into a neutrophil or thrombocyte. The purpose of building this model is to find the degree of influence that parameters involving regulation and maturation have in locally advanced pancreatic cancer patients, early on during treatment.

3.1 MATERIALS AND METHODS

3.1.1 Patients Data

Individual platelet and neutrophil time series data, image-defined subtypes, and overall survival times were provided from a phase II trial at the M.D. Anderson Cancer Center [92]. Patients received gemcitabine (1,000 mg/m^2 over 100 minutes) and oxaliplatin (100 mg/m^2) every 2 weeks for four doses and cetuximab (400 mg/m2 loading dose) on day 1 of chemotherapy and then weekly (250 mg/m^2). Patients also received chemoradiation after the initial chemotherapy portion, but this model is applied to the initial chemotherapy only portion. Of the 58 patients, 13 were excluded due to not enough data or not receiving both

chemotherapy and radiation. The remaining 45 patients were grouped into "high delta", or well defined tumors on a CT image, or "low delta"/poorly defined. Additionally, the patients were grouped into those above and below the trial median survival time of 19.1 months. Due to sparse data measurements, patient data within each subgroup was pooled as a population every 1-4 then 5-7 days that make up each week, starting with the first day of chemotherapy. The cell counts that were used to fit this model are the median platelet and neutrophil counts, normalized to each individuals respective baseline count prior to therapy.

3.1.2 Gemcitabine

Gemcitabine is a nucleoside analog that is indicated for ovarian cancer with carboplatin, breast cancer with paclitaxel, non-small cell lung cancer with cisplatin, and pancreatic cancer as a single agent [93]. When given as an infusion for more than an hour or more frequently than once a week, toxicity becomes more prevalent. Some toxicites that do occur include nausea/vomiting, anemia, neutropenia, and thrombocytopenia. When gemcitabine was administered concurrently with radiation, it resulted in life-threatening mucositis.

Gemcitabine is a prodrug that must be converted to its active form through phosphorylation. The drug can also become metabolically inactive, creating complex drug pharmacokinetics. The mechanism of action of active gemcitabine involves arresting cells in the G1/S phase of the cell cycle [93]. Pharmacokinetic models of gemcitabine range from a simple two compartment model [94] to a biologically-motivated multi-compartment one [95].

3.1.3 Oxaliplatin

Oxaliplatin, like carboplatin, is a member of the platinum class of chemotherapies. Also like carboplatin, oxaliplatin comes with common adverse reactions such as peripheral sensory neuropathy, neutropenia, thrombocytopenia, anemia, fatigue, and stomatitis [96]. Oxaliplatin is often given as part of a combination therapy referred to as FOLFIRINOX for advanced pancreatic cancer. This name is a combination of many abbreviated drug names including fluorouracil, leucovorin, irinotecan, and oxaliplatin. Additionally, as is the case here, it is often given with gemcitabine for advanced pancreatic cancer. For stage III colon

cancer patients with complete resection or advanced colorectal cancer, oxaliplatin is given with fluorouracil and leucovorin.

Oxaliplatin PK is triphasic with a Cmax of 0.814 mcg/mL, and volume of distribution of 440 L at a dose of 85 mg/m^2, over 2 hours [96]. Again like carboplatin, the main route of elimination is renal excretion. A three compartment PK model which incorporates entero-hepatic recirculation was used to drive PD effects in the model [97]. Mean parameter values from the final model were used since no individual PK information was used.

3.1.4 Cetuximab

Cetuximab is a monoclonal antibody and an epidermal growth factor receptor antagonist. It is indicated for head and neck and colorectal cancers [98]. Cardiopulmonary arrest, rash, pruritus, and diarrhea are some common adverse reactions, but not myelosuppression. Since myelosuppression is not listed as a side effect of cetuximab, it will not be used in the model.

3.1.5 Model Developemnt

Oxaliplatin was the pharamcokinetic (PK) driver of this pharmacodynamic (PD) toxicity model, since gemcitabine is at a dose magnitude and frequency that does not produce significant myelosuppresion. Individual PK profiles were not available, but a previously published model of oxaliplatin was used, along with an effect state describing the concentration-time profile in the bone marrow as opposed to the plasma concentration [97].

The PD model is a combination and modification of two models, in order to mimic the hematopoietic lineage of neutrophils and thrombocytes in the bone marrow. The first model is a biologically-motivated model of thrombocytopenia that includes two regulatory molecules, including thrombopoietin (TPO) and stromal cell-derived factor 1 (SDF-1). The second is a semi-mechanistic myelosuppression model that implicitly incorporates feedback. The modified and combined model is depicted in Figure 3.1, and the unique characteristics will be explained in more detail below.

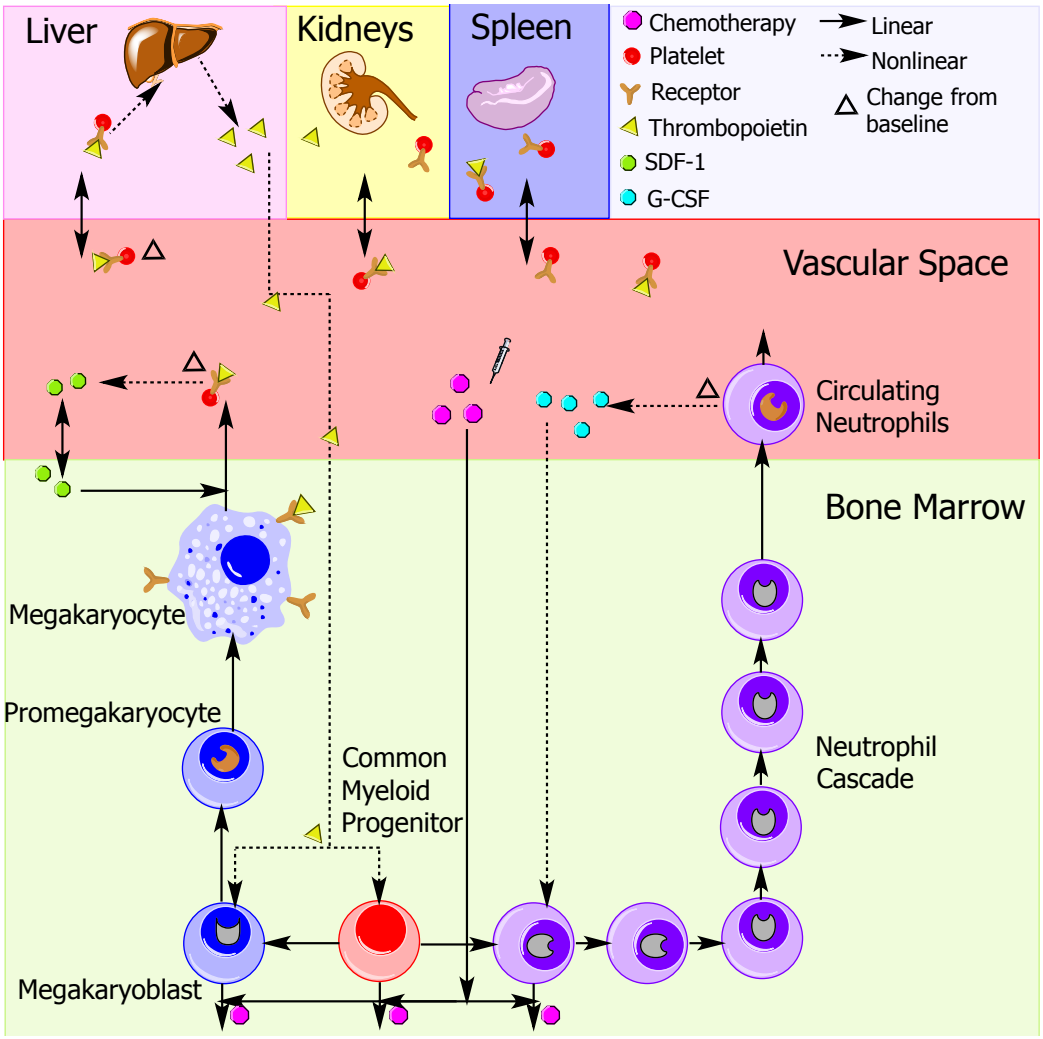

Figure 3.1: Combined model of chemotherapy-induced thrombocytopenia and neutropenia. Both branches begin at the common myeloid progenitor state. Neutrophil progenitors mature into circulating neutrophils in the blood stream and induce changes in G-CSF, thereby stimulating proliferation. Thromopoiesis is more complex and includes TPO and SDF-1. TPO stimulates proliferation in both the common myeloid progenitor and megakaryoblast state.

3.1.5.1 Combining Models: Common myeloid progenitor state

Referring back to the hematopoietic lineage tree (Figure 1.2), there are two main branches that come off the stem cell state. One branch is for lymphopoiesis, and the other branch is for myelopoiesis. The common myeloid progenitors differentiate into platelets, erythrocytes, or granulocytes, including neutrophils, and share some of the same regulatory molecules. This is the biological motivation for a single model inclusive of platelets and neutrophils. Data is provided for each individual's baseline platelet and neutrophil counts and are the initial conditions for thrombopoiesis and neutropoiesis, respectively. A fraction of the cells in the common state are fated to become platelet precursors (Eq.3.3), and the rest become neutrophil precursors (Eq.3.14).

Additionally, this state receives feedback regulation from TPO (Eq.3.10), a prominent molecule in thrombopoiesis. Therefore, even though TPO is inducibly produced through changes in platelet count, both platelets and neutrophils are subject to it's effects from their common progenitor state. Studies have compared mice with and without TPO, and it was found that neutrophil levels are significantly different [99, 100, 101]. Another study added exogenous TPO in mice and saw increased myeloproliferation [102]. These studies show that TPO is a multilineage regulator, motivating modeling both cell types jointly.

3.1.5.2 Updated TPO Signal

The thrombocyte portion of the combined model is same as in the previous chapter, with a few exceptions. Since the previous model only had one dose of chemotherapy, the function for the impact of TPO on proliferation sufficed. For this data set, the patients undergo treatment every 2 weeks for 4 cycles before radiation. The patients don't always respond uniformly after each cycle of treatment, and this warranted a new function for TPO signaling. For instance, patients may rebound well after the first cycle but not as strongly after the second.

One way to think of this function is how sensitive and strong the feedback switch is on proliferation. As TPO changes inversely to platelet count, this signal of imbalance gets transmitted back to the proliferating cells. The switch on inducing proliferation, α, describes one of the fitted parameters in the function. The parameter accounts for the patient variability seen in the recovery phase after multiple treatment cycles.The whole function is a saturating exponential of the deviations from the baseline signal. Therefore, the switch goes from 0 to 1 at a steepness of α.

$$Switch(t) = \frac{exp(\alpha(Tr3(t) - 200.0)) - 1.0}{200.0 + (exp(\alpha(Tr3(t) - 200.0)) - 1.0)} \tag{3.1}$$

3.1.5.3 G-CSF Neutrophil maturation is the same as the classic Friberg model, so a detailed explanation will not be reiterated. However, a molecule called granulocyte-colony stimulating factor (G-CSF) is the main player in granulopoiesis, and it is explicitly added to the model [103]. The same function as the TPO switch is used, except it is stimulated by deviations in circulating neutrophil count. The combination of TPO and G-CSF acting on neutrophil count was studied in myelosuppressed mice [101]. Mice with TPO alone and G-CSF alone showed improved toxicity, while mice with TPO and G-CSF showed synergistic improvement greater than TPO or G-CSF alone. Since the study was performed in mice, no patient data was provided for TPO or G-CSF, and it is unclear how the synergism occurs. TPO and G-CSF are treated separately and in an additive fashion in the model. The TPO acts on the common myeloid progenitor state (Eq.3.2), and G-CSF impacts the neutrophil specific progenitor state (Eq.3.14).

Table 3.1: Thrombocytopenia and Neutropenia Model Equations and Corresponding Biological States.

Equation Number	**State**	**Biological Meaning**
$C_{mp}(t)$	Common myeloid progenitor	$\frac{10^6 cells}{\mu L}$
$P_1(t)$	Megakaryoblast	$\frac{10^6 cells}{\mu L}$
$P_2(t)$	Promegakaryocyte	$\frac{10^6 cells}{\mu L}$
$M(t)$	Megakaryoctye	$\frac{10^6 cells}{\mu L}$
$P_c(t)$	Circulating Platelets	$\frac{10^6 cells}{mL}$
$P_t(t)$	Platelets in Liver and Kidneys	$\frac{10^6 cells}{mL}$
$P_s(t)$	Platelets in Spleen	$\frac{10^6 cells}{mL}$
$S(t)$	Stromal Cell-Derived Factor-1	-
$T(t)$	Thrombopoietin	$\frac{pg}{mL}$
$T_1(t)$	Thrombopoietin Signal	-
$T_2(t)$	Thrombopoietin Signal	-
$T_3(t)$	Thrombopoietin Signal	-
$N_1(t)$	Neutrophil progenitor 1	$\frac{10^5 cells}{mL}$
$N_2(t)$	Neutrophil progenitor 2	$\frac{10^5 cells}{mL}$
$N_3(t)$	Neutrophil progenitor 3	$\frac{10^5 cells}{mL}$
$N_4(t)$	Neutrophil progenitor 4	$\frac{10^5 cells}{mL}$
$N_5(t)$	Neutrophil progenitor 5	$\frac{10^5 cells}{mL}$
$N_6(t)$	Neutrophil progenitor 6	$\frac{10^5 cells}{mL}$
$N_c(t)$	Circulating neutrophils	$\frac{10^5 cells}{mL}$
$G(t)$	Granulocyte colony stimulating factor	-
$G_s(t)$	G-CSF signal	-

$$\frac{dC_{mp}(t)}{dt} = k_{tr}(Pc_0 + N_{c_0}) - k_{tr}C_{mp}(t) - SlopeDrug(t)C_{mp}(t) + 0.03$$
$$\frac{exp(\alpha(Tr3(t) - 200.0) - 1.0)}{200.0 + (exp(\alpha(Tr3(t) - 200.0) - 1.0)}C_{mp}(t) \tag{3.2}$$

$$\frac{dP_1(t)}{dt} = k_{tr}\frac{Pc_0}{(Pc_0 + N_{c_0})}C_{mp}(t) + 1.04\frac{exp(\alpha(Tr3(t) - 200.0) - 1.0)}{200.0 + (exp(\alpha(Tr3(t) - 200.0) - 1.0)}P_1(t)$$
$$- Drug(t)Slope_2P_1(t) - k_{tr}P_1(t) \tag{3.3}$$

$$\frac{dP_2(t)}{dt} = k_{tr}P_1(t) - k_{tr}P_2(t) \tag{3.4}$$

$$\frac{dM(t)}{dt} = k_{tr}P_2(t) - k_{tr2}M(t) \tag{3.5}$$

$$\frac{dP_c(t)}{dt} = k_{tr2}M(t) - k_{tr}P_c(t) - k_{ps}P_c(t) - k_{Pt}P_c(t) + k_{kp}P_t(t) + k_{sp}P_s(t) \tag{3.6}$$

$$\frac{dP_t(t)}{dt} = k_{P_t}P_c(t) - k_{kp}P_t(t) \tag{3.7}$$

$$\frac{dP_s(t)}{dt} = k_{ps}P_c(t) - k_{sp}P_s(t) \tag{3.8}$$

$$\frac{dS(t)}{dt} = \frac{P_{c_0}S_0}{k_m + S_0} - \frac{P_c(t)S(t)}{k_m + S(t)} \tag{3.9}$$

$$\frac{dT(t)}{dt} = T_0(\frac{P_{c_0}}{M(t)})^\gamma - T(t) \tag{3.10}$$

$$\frac{dT_1(t)}{dt} = k_{ts}T(t) - k_{ts}T_1(t) \tag{3.11}$$

$$\frac{dT_2(t)}{dt} = k_{ts}T_1(t) - k_{ts}T_2(t) \tag{3.12}$$

$$\frac{dT_3(t)}{dt} = k_{ts}T_2(t) - k_{ts}T_3(t) \tag{3.13}$$

$$\frac{dN_1(t)}{dt} = k_{trn}C_{mp}(t)\frac{N_{c_0}}{(P_{c_0}+N_{c_0})} + k_{Gs}\frac{exp(\alpha(G_s(t)-200.0)-1.0)}{200.0+(exp(\alpha(G_s(t)-200.0)-1.0)}P_1(t)$$
$$- k_{trn}N_1(t) - Slope_3 Drug(t)N_1(t) \quad (3.14)$$
$$\frac{dN_2(t)}{dt} = k_{trn}N_1(t) - k_{trn}N_2(t) \quad (3.15)$$
$$\frac{dN_3(t)}{dt} = k_{trn}N_2(t) - k_{trn}N_3(t) \quad (3.16)$$
$$\frac{dN_4(t)}{dt} = k_{trn}N_3(t) - k_{trn}N_4(t \quad (3.17)$$
$$\frac{dN_5(t)}{dt} = k_{trn}N_4(t) - k_{trn}N_5(t) \quad (3.18)$$
$$\frac{dN_6(t)}{dt} = k_{trn}N_5(t) - k_{trn}N_6(t) \quad (3.19)$$
$$\frac{dN_c(t)}{dt} = k_{trn}N_6(t) - k_{trn}N_c(t) \quad (3.20)$$
$$\frac{dG(t)}{dt} = G_0(\frac{N_{c_0}}{N_c(t)})^\gamma - G(t) \quad (3.21)$$
$$\frac{dG_s(t)}{dt} = k_{ts}G(t) - k_{ts}G_s(t) \quad (3.22)$$

where

$$k_{tr2} = k_{tr0}(1+(S(t)-S_0)\frac{500.0}{Pc_0}) \quad (3.23)$$

3.1.6 Parameter Estimation

Twenty-one ordinary differential equations were used to describe the states of the chemotherapy-induced toxicity model. Model parameters were estimated by fitting the data to the circulating platelet state, Pc, and the circulating neutrophil state, Nc, minimizing the energy function J(p) in APT-MCMC[88]. The log of the energy function results in the sum of squared residuals, between the model, $y_{sim}(i,p)$, and data, $y(i)$ with parameters, p, being *alpha*, *Slope*, and *ktr*:

$$J(p) = \sum_{i=1}^{N}(y(i) - y_{sim}(i,p))^2 \quad (3.24)$$

Table 3.2: Thrombocytopenia plus Neutropenia Model Parameters (P). SS fit: fit to steady state data, Dyn. fit: fit to dynamic data.

P	**Value**	**Unit**	**Source**
k_{pt}	0.288	$\frac{1}{day}$	SS fit
k_{kp}	1.44	$\frac{1}{day}$	SS fit
k_{ps}	0.864	$\frac{1}{day}$	SS fit [80]
k_{sp}	1.44	$\frac{1}{day}$	SS fit [80]
k_m	1.44×10^6	$\frac{pg}{mL}$	Dyn. fit [50]
T_0	200	$\frac{pg}{mL}$	[84]
G_0	200	$\frac{pg}{mL}$	[84]
S_0	1	-	Dyn. fit
k_{ts}	3.0	$\frac{1}{day}$	Dyn. fit
k_{Gs}	0.001	$\frac{1}{day}$	Dyn. fit
k_{trn}	2.2	$\frac{1}{day}$	Dyn. fit
γ	0.6	-	Dyn. fit
k_{T3}	0.005	$\frac{1}{day}$	Dyn. fit
$Slope_2$	5.0	$\frac{1}{day}$	Dyn. fit
$Slope_3$	0.008	$\frac{1}{day}$	Dyn. fit

3.2 RESULTS

3.2.1 High and Low Delta

In response to a chemotherapy challenge of oxaliplatin every 2 weeks for 4 cycles, the model captures both subpopulations of patients with high delta and low delta tumors. Figure 3.2 shows the boxplots of the neutrophil and platelet time-series normalized data scaled up to the mean baseline value for low delta patients (mean P_0=222$\times 10^9$ cells/L and N_0=66$\times 10^8$ cells/L) while Figure 3.3 shows the high delta case (mean P_0=233$\times 10^9$ cells/L and N_0=70$\times 10^8$ cells/L). The best parameter set for the model, equivalent to the APT-MCMC simulation with the lowest energy function, is shown as a solid curve (blue for low and red for high delta). The color-coordinated histograms of the parameter distribution outputs from APT-MCMC for k_{tr}, *Slope*, and α show differences between high and low delta tumors Figure 3.4.

High delta patients have a faster transit time and lower TPO signaling threshold on proliferation than low delta patients. In Figure 3.5 the switch function is plotted for each case. The proliferation is stimulated for longer periods of time for the low delta patients. The effects can be seen in the recovery phase after the patient platelet nadir. High delta patients have a steeper and deeper percent reduction in platelet count and overshoot just slightly above baseline in response to therapy (Figure 3.3). Low delta patients have a less steep and less severe percent reduction, as well as, a rapid and large overshoot (Figure 3.2). No neutrophil specific parameters were fit because the two neutrophil profile spreads were indistinguishable.

3.2.2 Good and Poor Overall Survival

High and low delta correspond to poor and good overall survival, respectively [91]. The results for survival above and below the trial median of 19.1 months align with the high and low delta cases. Figure 3.6 shows the boxplots of the neutrophil and platelet time-series normalized data, scaled up to the mean baseline value for good overall survival, while Figure 3.7 shows the poor overall survival case. The best parameter sets for the model,

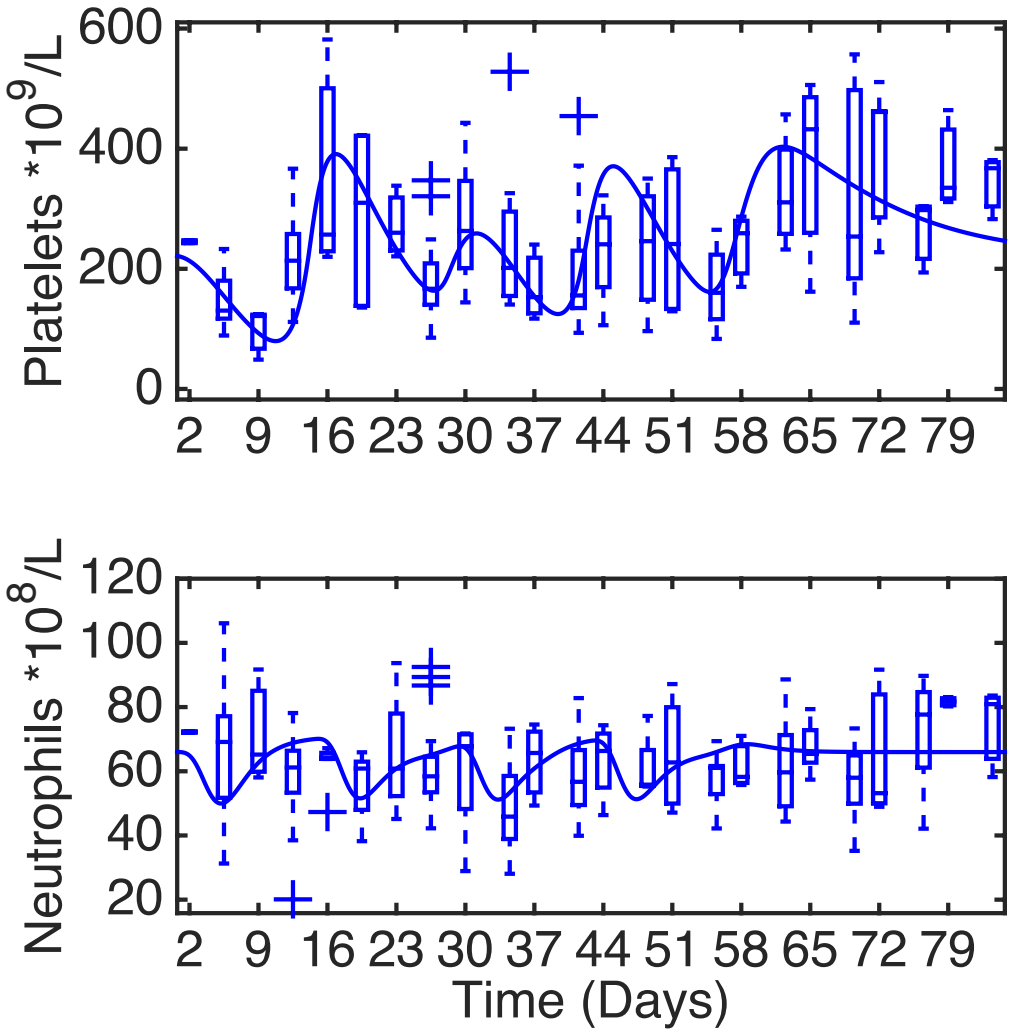

Figure 3.2: Low delta platelet and neutrophil time-series data and model fit. The top plot shows platelet count data as boxplots with the model output as the solid curve over time in days. The bottom is the same patients neutrophil profile.

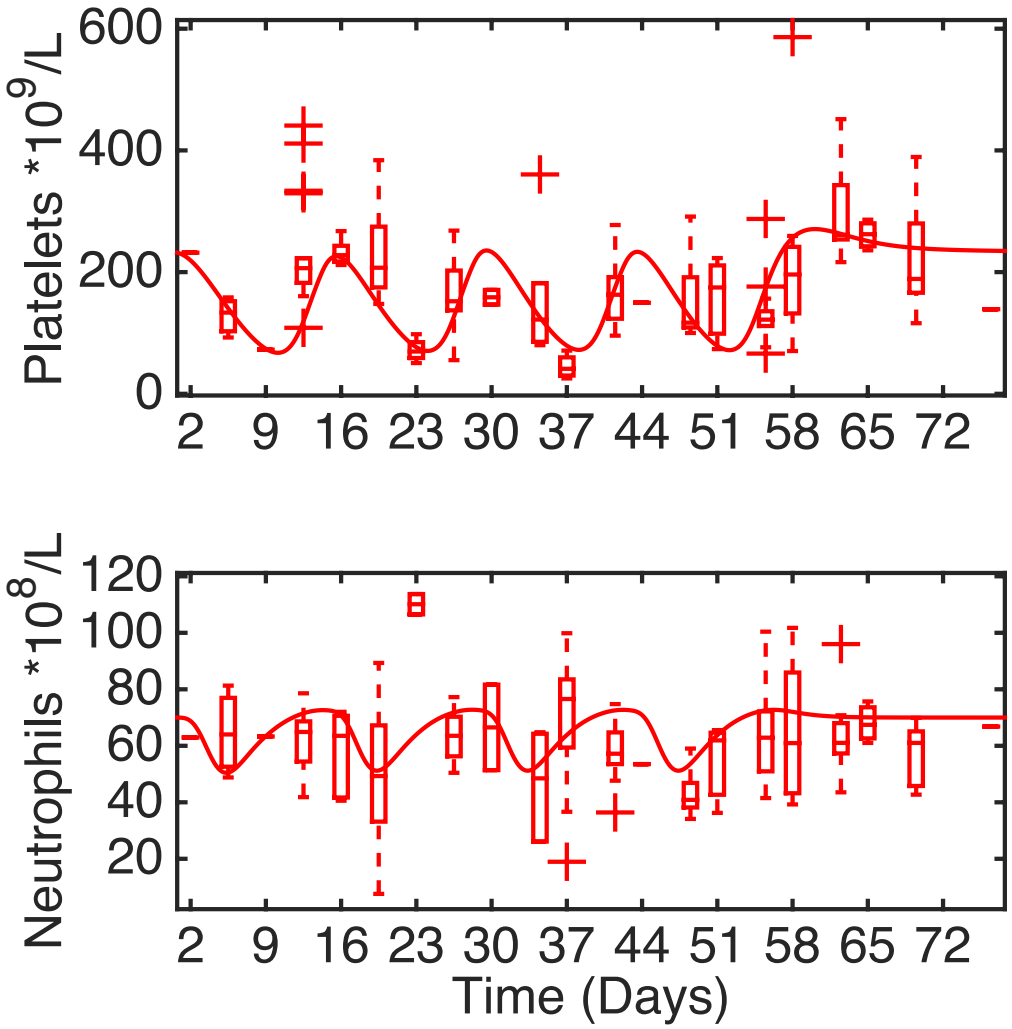

Figure 3.3: High delta platelet and neutrophil time-series data and model fit. The top plot shows platelet count data as boxplots with the model output as the solid curve over time in days. The bottom is the same patients neutrophil profile.

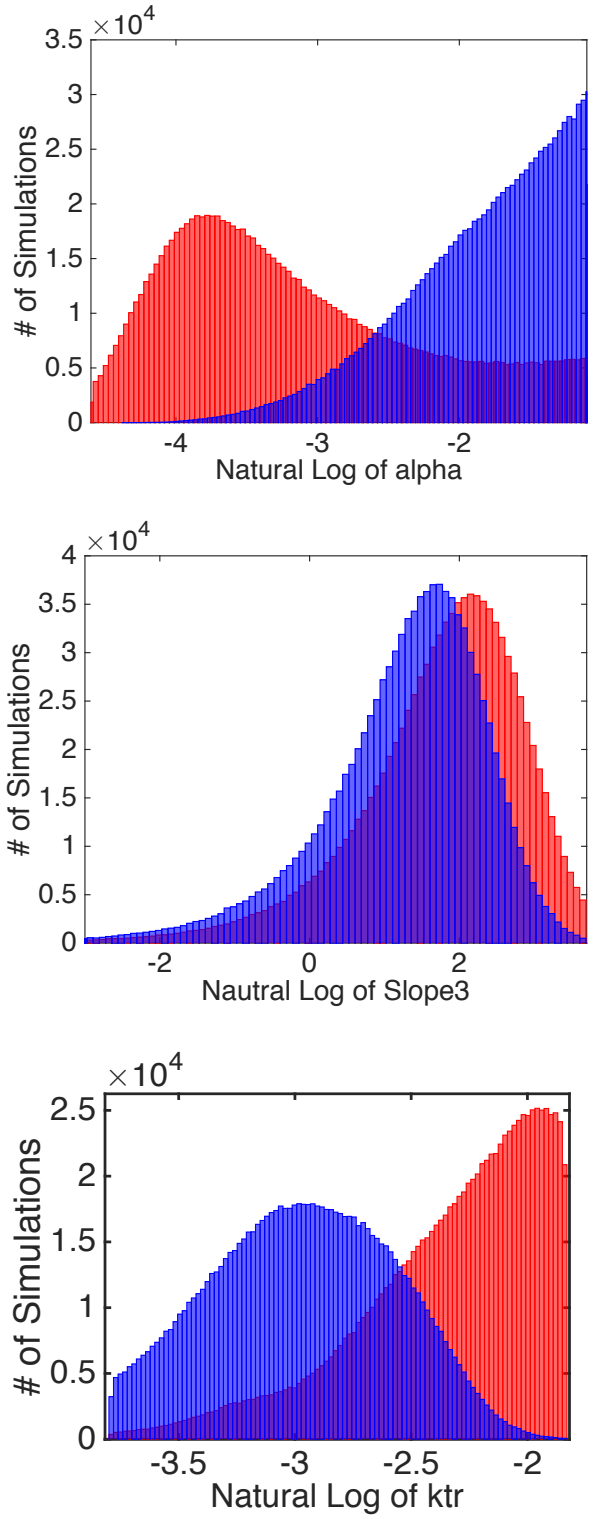

Figure 3.4: APT-MCMC histograms of fitted parameters. High delta patients are in red while low delta patients are in blue. The figures are all the number of simulations vs. the natural log of the parameter.

Table 3.3: Mean APT-MCMC Parameters (P).

Delta	$\alpha(Day^{-1})$	$Slope(Day^{-1})$	$k_{tr}(Day^{-1})$
$High$	0.068	8.8	0.61
Low	0.187	5.49	0.45

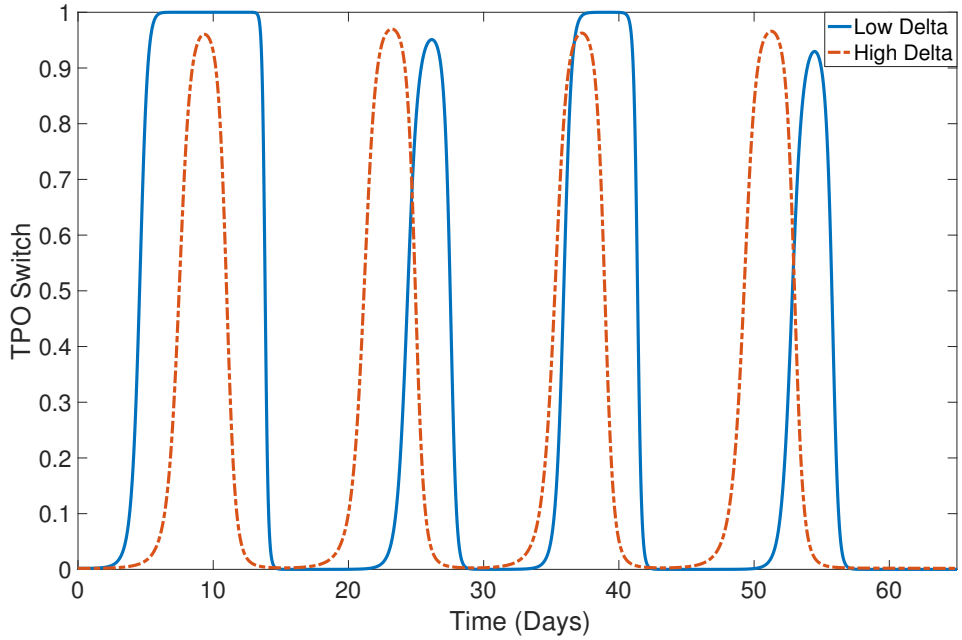

Figure 3.5: Switch function for low and high delta patients.

equivalent to the APT-MCMC simulation with the lowest energy function, is shown as a solid curve (blue for good OS and red for poor OS). The color-coordinated histograms of the parameter distribution outputs from APT-MCMC for α, *Slope*, and k_{tr} show differences between poor and good overall survival Figure 3.8.

The same trends in the parameters exist that were seen in the high and low delta case. Again, patients with low overall survival had a lower α and a higher ktr. Also, in both situations the cell elimination rate in the common myeloid progenitor state, *Slope*, did show a slight difference with more elimination occurring in the poor overall survival case; however, the difference was not significant. There is still a gaussian distribution for the *Slope* parameter, indicating patient variability.

3.2.3 Validation Data

Validation was performed by testing the model on a new dataset. 70 patients received gemcitabine (750 mg/m^2) and cisplatin (30 mg/m^2) every 2 weeks for four doses. 50 patients had an overall survival time greater than 14 months, and 20 patients had an overall survival time less than 14 months. This was how the patients were stratified, and the same model was applied to the new data. Figure 3.9 shows the histograms of overall survival times from start of therapy for both datasets.

Figure 3.10 is the histograms of the parameter sets for the validation data. The histograms, while not as distinct as the original dataset, still follow the same trends. Part of the reason the new histograms are less distinct is that the data can only be used up through day 60. This is because these patients receive radiation around that day, and this additional therapy can not be compared to the original data. This means that the recovery, after therapy ceases, is not fully observable. Another difference is the therapy itself. These patients are getting cisplatin, instead of oxaliplatin, resulting in less severe toxicity. However, clear differences are still observed between good and poor overall survival. Figure 3.11 compares both the original and validation platelet data, for both the good and poor overall survival cases. This time the top 1000 APT-MCMC fits are plotted on top of the data for each case. Around day 21 good overall survival patients are on the upward rebound after the first cycle, while the poor overall survival patients are already falling from the second cycle of therapy.

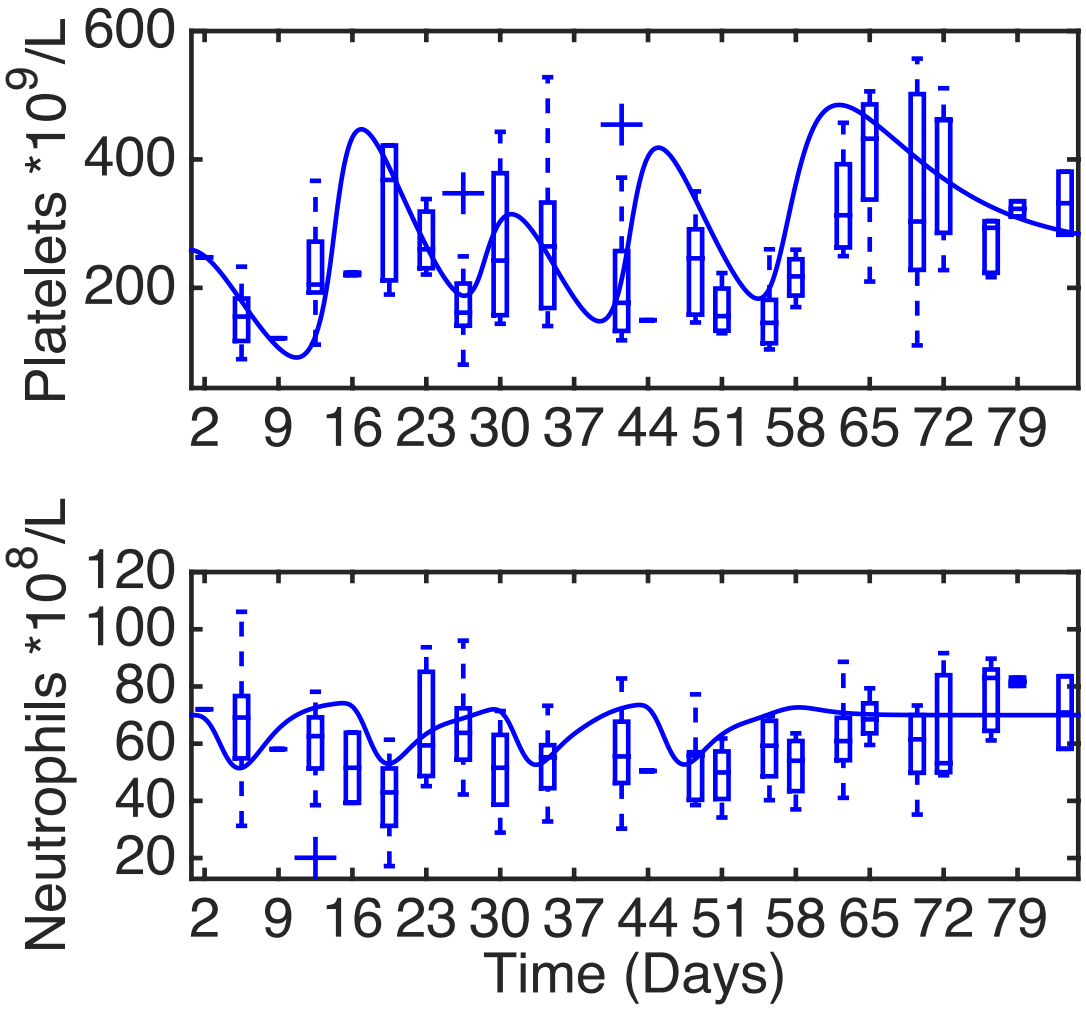

Figure 3.6: Overall survival patients above 19.1 months platelet and neutrophil time-series data and model fit. The top plot shows platelet count data as boxplots with the model output as the solid curve over time in days. The bottom is the same patients neutrophil profile.

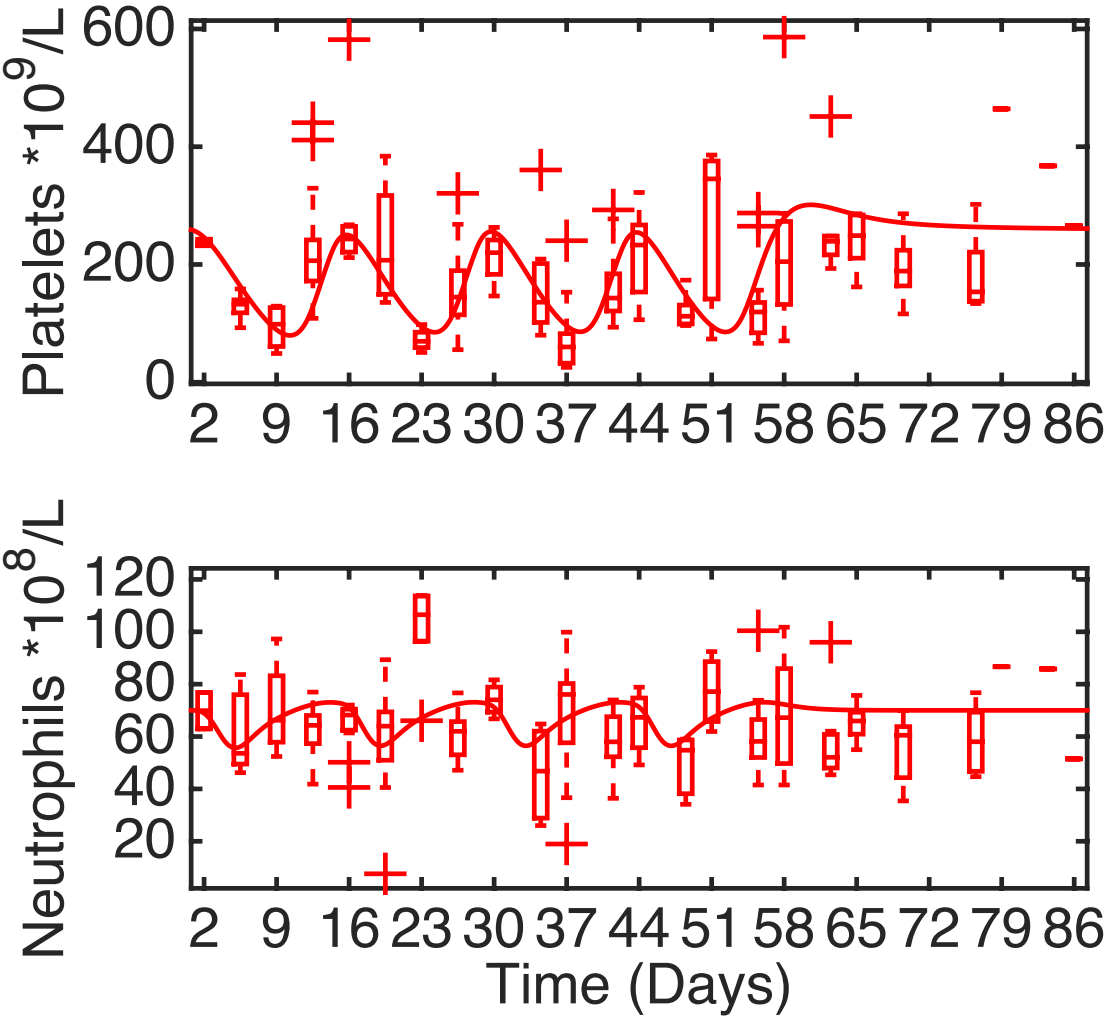

Figure 3.7: Overall survival patients below 19.1 months platelet and neutrophil time-series data and model fit. The top plot shows platelet count data as boxplots with the model output as the solid curve over time in days. The bottom is the same patients neutrophil profile.

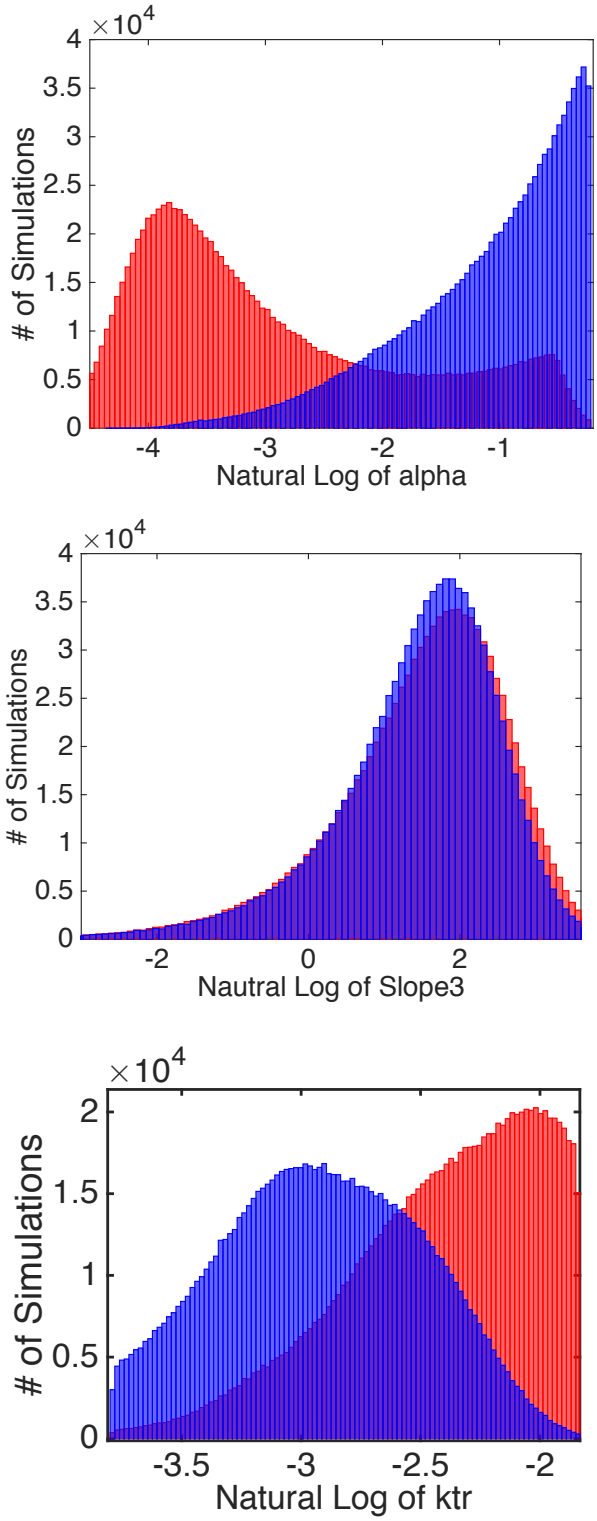

Figure 3.8: APT-MCMC histograms of fitted parameters. Poor overall survival patients are in red while good overall survival patients are in blue. The figures are all the number of simulations vs. the natural log of the parameter.

Table 3.4: Mean APT-MCMC Parameters (P).

Delta	$\alpha(Day^{-1})$	$Slope(Day^{-1})$	$k_{tr}(Day^{-1})$
Poor	0.11	7.1	0.61
Good	0.4	6.5	0.47

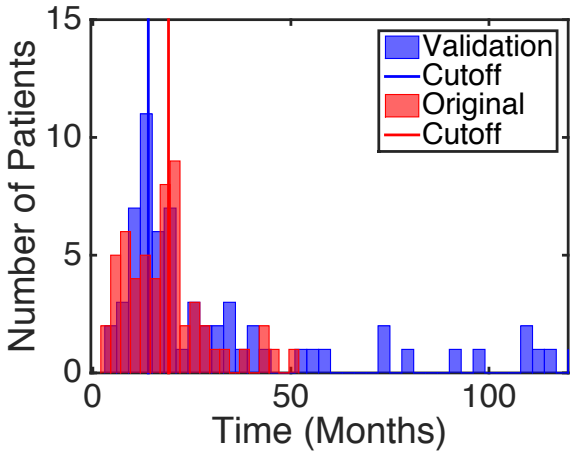

Figure 3.9: The patient overall survival time histograms for the original data (red) and validiation data (blue) are shown as well as a line for where the cutoff point for each group is.

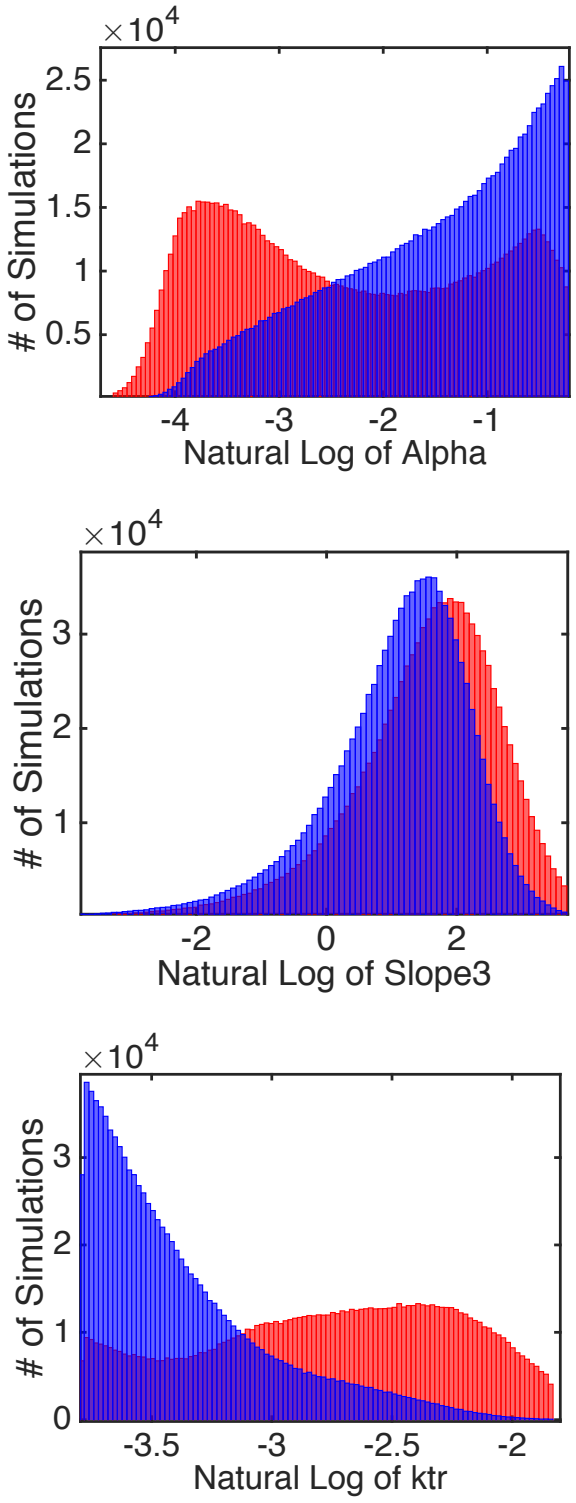

Figure 3.10: APT-MCMC histograms of fitted parameters. Poor overall survival patients are in red while good overall survival patients are in blue. The figures are all the number of simulations vs. the natural log of the parameter.

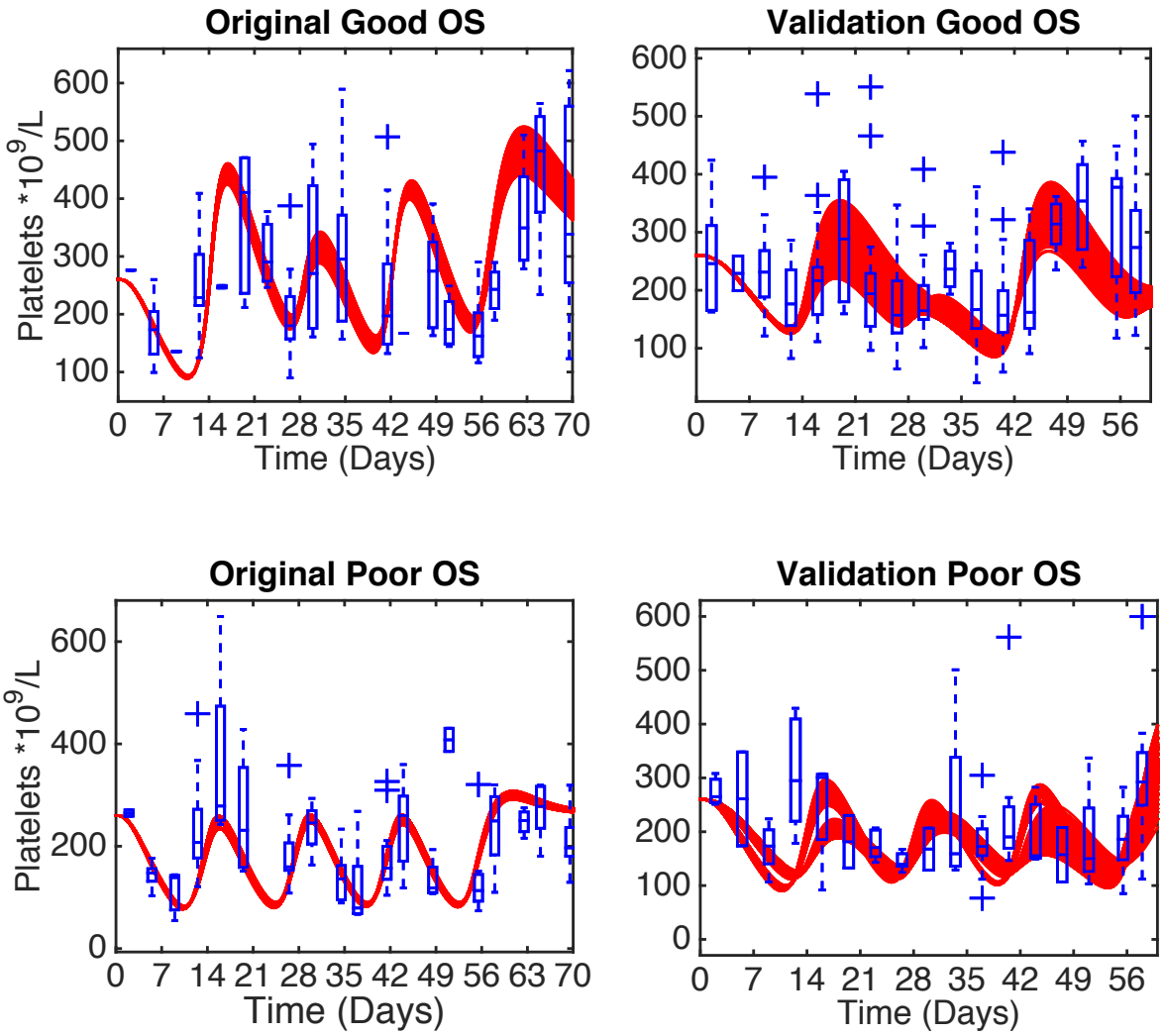

Figure 3.11: Platelet counts for the original and validation data for both the good and poor overall survival cases. The data is represented as blue boxplots and the best 1000 model simulations are the red curves.

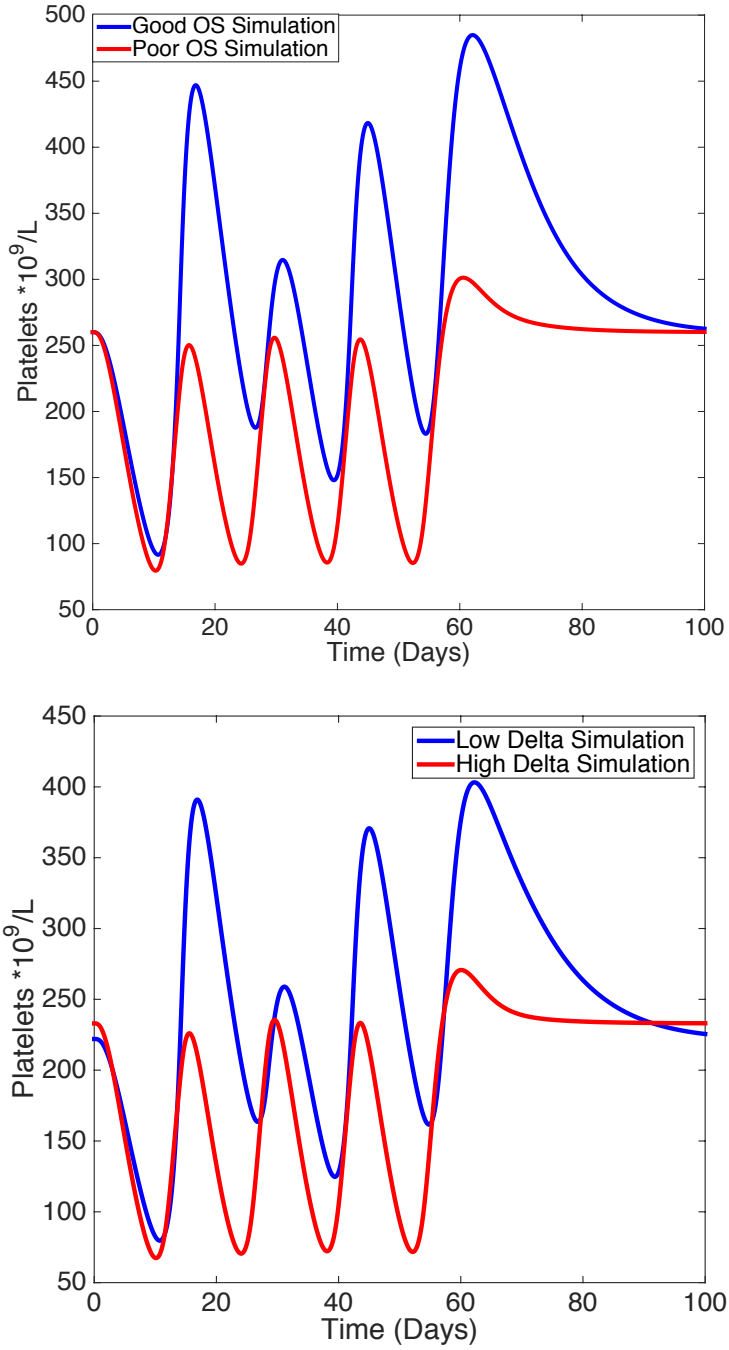

Figure 3.12: Simulations of thrombocyte count for each subgroup.

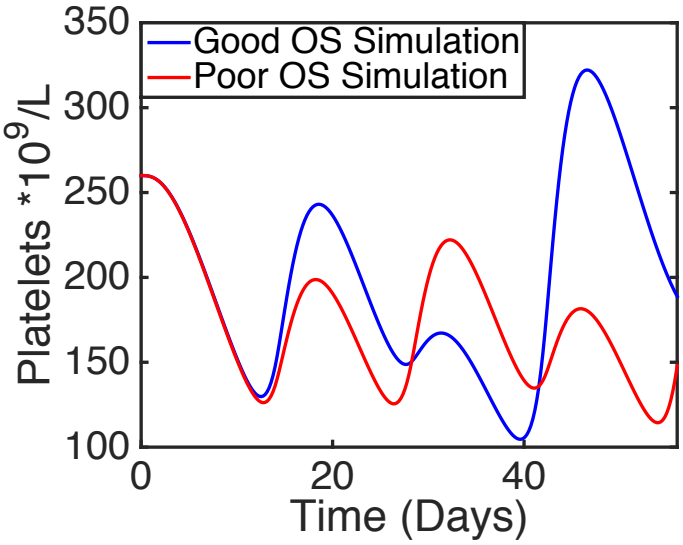

Figure 3.13: Platelet count simulations for the good and poor overall survival cases for the validation data.

Tumor subtyping is performed prior to therapy and has been correlated with overall survival [91]. This combined model of thrombocytopenia and neutropenia provides insights biologically as to why variability is seen in patient outcome. The main findings revolve around thrombopoiesis and TPO. Patients with high delta tumors and poor overall survival had a significantly faster transit time through maturation, a rapid decline in platelet count, and a lower degree of feedback from TPO on proliferation. Visually this can be seen in Figures 3.12 and 3.13. By around day 20, between the second and third rounds of chemotherapy, the subgroups begin to distinguish themselves from one another. Patients in the good OS/low delta groups would benefit from staying on the suggested course of treatment. Patients in the poor OS/high delta groups would be flagged as a subgroup that might not benefit from this treatment plan. Not only does this differentiation happen prior to radiation therapy, but it happens early on during the chemotherapy only portion of treatment.

The data for each individual was sparse and difficult to model a single patient. Once the data was pooled as subpopulations, trends that are common in the literature began to appear. For instance, a platelet nadir around 9-12 days and neutrophil nadir around day 6. The platelet toxicity was more severe than the neutrophil toxicity, likely due to oxaliplatin

being a platinum compound. Therefore, the distinctions between the two platelet subgroups was more pronounced. The neutrophil subgroups on a population level were too similar to find parameters that could stratify the groups based on a neutrophil specific parameter.

While tumor histology is correlated to overall survival, outliers on both sides are sure to be present. The outliers could be the high delta tumor patients toward the bottom of the k_{tr} and top of α parameter distributions, and the low delta tumor patients toward the top end of the k_{tr} and bottom of α parameter distributions. Even though the high/low delta correlated well with good/poor overall survival in the original dataset, the validation data did not, indicating that the correlation does not always hold true. Obtaining concentrations of TPO and G-CSF, as well as, more frequent circulating platelet and neutrophil counts during and after therapy, could help separate the patient subgroups.

Although there is not a widely used thrombocyte rescue available, unlike exogenous G-CSF for neutrophils, understanding biological differences in subgroups can open up new research regarding patient drug sensitivity. One option that can be tested in the clinic is to give high delta patients lower doses more frequently. Moreover, patients could be given the original dose the first two cycles, and the model could be used to predict what future doses could look like.

Pancreatic cancer has had few advancements in treatment options or strategies to reduce the high associated mortality rates. Modeling and simulation is a cost-effective approach to better understand why treatments are not effective for some patients. Furthermore, for patients in this trial who receive chemotherapy before radiation, flagging subpopulations early on in the trial, that will not benefit from radiation, could save the patient from radiation-induced cytotoxicity. The findings from the model indicate that sensitive patients have a faster response to the drug, with a rapid and steep decline in platelet count, and a smaller rebound in the recovery phase.

4.0 CHEMORADIATION-INDUCED LYMPHOPENIA

Radiation is a common treatment option for cancer patients, and it can be given before, after, or concurrently with chemotherapy or other treatments. While effective in killing tumor cells, radiation alone is enough to induce lymphopenia (low lymphocyte count), and the degree of lymphopenia can be indicative of outcome [104, 69]. Lymphocytes play an important role in the adaptive and innate immune responses. The innate immune response recognizes and recruits lymphocytes to defend the body against non-self invaders, infection, and damage. The adaptive immune response, used in vaccines, stores long-term memory on how to combat specific pathogens. The damage inflicted by radiation can be enough to kill the cell abruptly, in a linear fashion, but also quadratically as damage accumulates with fractionated radiation [68]. This is because DNA is double stranded and acute damage to one strand can sometimes be repaired before the next fraction of radiation [105]. With depleted lymphocyte numbers, serious infection can ensue, and damage repair may be slowed. This is one reason why radiation is often given in smaller doses spread over many weeks. The patient can rebuild their lymphocyte population and maintain a defense system throughout treatment.

The four main types of radiotherapy are 3D conformal, intensity modulated (IMRT), image-guided (IGRT), and stereotactic body (SBRT) [67]. They differ in precision of tumor margins and intensity of beam. For instance, with IMRT [106, 107, 108, 109], the clinician can control the beam angle, size, and intensity; this can be optimized using linear programming, mixed integer programming, or even a genetic algorithm with a neural network [110, 111, 112]. Also, there is a dose-volume constrained optimization of IMRT [113], and a spatiotemporal optimization to maximize tumor biologically equivalent dose with constraints for multiple organs-at-risk [114]. What these models do not address explicitly, is the radi-

ological dose affecting circulating cells, such as lymphocytes, which contribute to toxicity. While the models aim to avoid healthy tissues, their primary focus is on efficacy not toxicity.

These techniques result in energy deposition on their route to the tumor, as well as, irradiating the blood circulating through the planning volume. SBRT uses 4-dimensional imaging to build a coordinate system to deliver high doses to the tumor over fewer treatments [115]. This technique reduces the amount of healthy tissue and circulating cells that are irradiated. Therefore, different radiation techniques will irradiate different volumes of blood and impact the degree of radiation-induced lymphopenia.

Pancreatic cancer is a very challenging cancer to treat, with radiation being a common treatment and often in combination with chemotherapy. One study found that less lymphopenia is associated with better survival in pancreatic cancer patients [69]. This new algorithm aims to mathematically study the number of lymphocytes and degree of lymphopenia associated with the volume of blood in the radiation area. This can help predict the lymphotoxicity associated with different radiation therapies and how they may be linked with outcome in a quantitative method.

The model developed herein does not model the explicit beam physics, but instead uses a computationally inexpensive approach to capture the accumulation of treatment-induced damage and probability of death to the circulating cells that pass through a treatment planning volume that is being irradiated. One existing model of accumulated damage predicts that a single fraction of 2 Gy radiation yields at least 0.5 Gy to 4.6% of the circulating cells, and after 30 fractions, 99% of the blood pool has at least 0.5 Gy [71]. Dynamically, over this duration of therapy, cells will begin to die as a result of accumulated damage, and at the same time new cells are being produced. Cell death is modeled probabilistically in accordance with the *in vitro* lymphocyte radiosensitivity. A study found that the dose required to reduce the surviving lymphocyte population to 10% of their baseline values, also known as a D10, is 3 Gy, to 50%, or D50, is 2 Gy, and to 90%, or D90, is 0.5 Gy [117]. We extend the accumulated damage model to capture blood measurements throughout treatment including natural cell death and lymphocyte replenishment, with a cell turnover of 0.33% of the population per day [118].

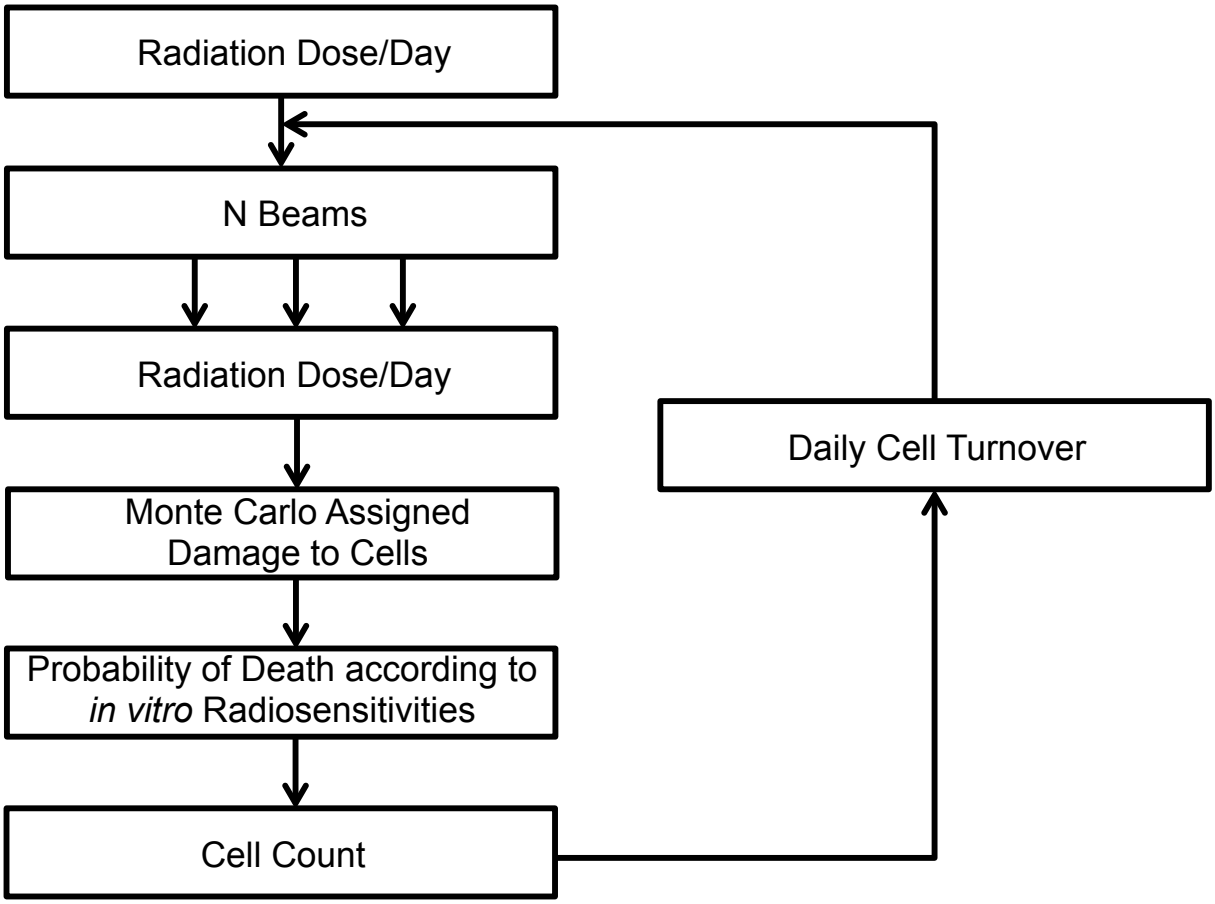

Figure 4.1: The algorithm walks through the logic behind the decisions used in the model. Radiation damage is administered randomly, and cells probabilistically die or survive and continue to have the opportunity to accumulate damage. At the same time cells are slowly generated by the body and added to the circulating population.

4.1 MATERIALS AND METHODS

4.1.1 Radiation Model Developement

The first step was to recreate the damage accumulation model in order to adapt it. A spherical planning volume of 258 cm^3, total blood volume of 5000 cm^3, and dose of 2 Gy per day for 30 fractions was used. The total damage after each fraction was totaled for each cell in the circulating pool. The damage was randomly distributed since the blood volume was able to recirculate in between each beam of radiation. The number of cells that had at least 0.5 Gy of damage was tallied up and divided by the total number of cells to get a fraction. The model captures the data from the paper (Figure 4.2) and now adaptations can be made.

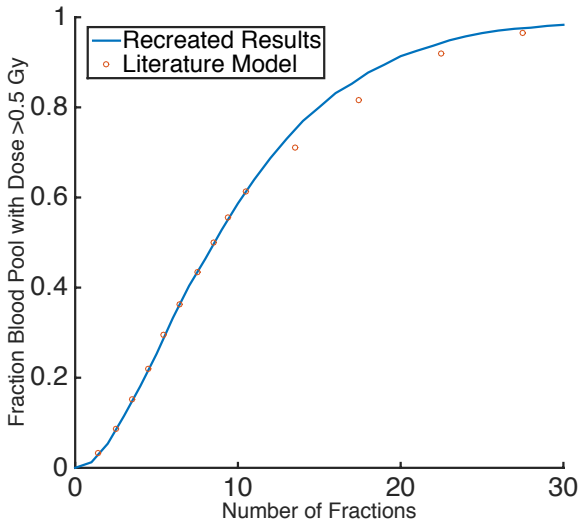

Figure 4.2: The accumulated damage model was recreated as a starting point for the new model. The blue curve is our recreation and the red dots are taken from the original papers results.

An algorithm (Figure 4.1) was developed to track the number of lymphocytes throughout radiation treatment. Radiation is given in smaller doses called fractions. These fractions can be broken up into even smaller homogenous beams. A Monte Carlo approach assigns lymphocytes to be within, or outside, the beam area, and the beams of radiation inflict

damage to cells in the beam area. As damage accumulates, the algorithm decides whether the cell dies, or lives and continues circulating. This decision is based off of *in vitro* radiosensitivities that provide cutoffs for the percentage of cells that survive a given dose. After each day of radiation a lymphocyte replenishment occurs. The algorithm tracks and updates the lymphocytes that are generated and die.

4.1.2 Radiation Treatment Details

An individual's total dose divided by the total number of days of radiation is input into the algorithm as a daily fraction. The daily fraction dose is divided by the number of beams. Radiation is assumed to be given Monday through Friday of each week and not on the weekends. The beam number can change but is set at 4 in our simulator to mimic a four-field conformal plan with equal doses. This value, the daily fraction dose divided by the number of beams, is the damage that begins to accumulate. The time each beam is on is assumed to be less than the time it takes for the blood to recirculate. For instance, 2 Gy/day is divided equally into the 4 fields of radiation to equal 0.5 Gy per beam. The time for each beam to be on is on average $0.5\ \frac{Gy}{beam}/3\frac{Gy}{min}\times 60\frac{sec}{min} = 10\ \frac{sec}{beam}$. The average time to circulate the blood is about a minute. Therefore, the randomization of cells entering the beam area occurs after, not during, each beam of radiation.

4.1.3 Lymphocytes Exposed to Radiation

A 2-dimensional cross sectional area is used to approximate how many lymphocytes are exposed to radiation. This area is found by taking the vascular volume of the organ subjected to radiation relative to the vascular volume of the entire body. When vascular volume values for organs are known [9], they are used directly; for organs like the pancreas, vascular volume values are not reported. We therefore take the liver vascular volume fraction of 11% as an upper bound, since it is one of the most well-perfused organs. The pancreas represents 0.14% of body weight. Under the assumption that body density is approximately 1 kg/L, the mass fraction and volume fraction are equivalent. The resulting fraction of the blood pool that is exposed to radiation for each beam is $11\% \times 0.14\% = 1.54\%$ [9, 119].

4.1.4 Calculating Lymphocyte Damage

Based on the assumptions explained for blood recirculation being greater than beam time, the damage can be distributed in a Monte Carlo fashion to 1.54% of the individual's unique baseline circulating lymphocyte count prior to therapy. The damage is equal to the total daily dose divided by the number of beams per fraction. For instance, a patient that receives 2 Gy/day with four fields means damage is assigned in 0.5 Gy increments per beam.

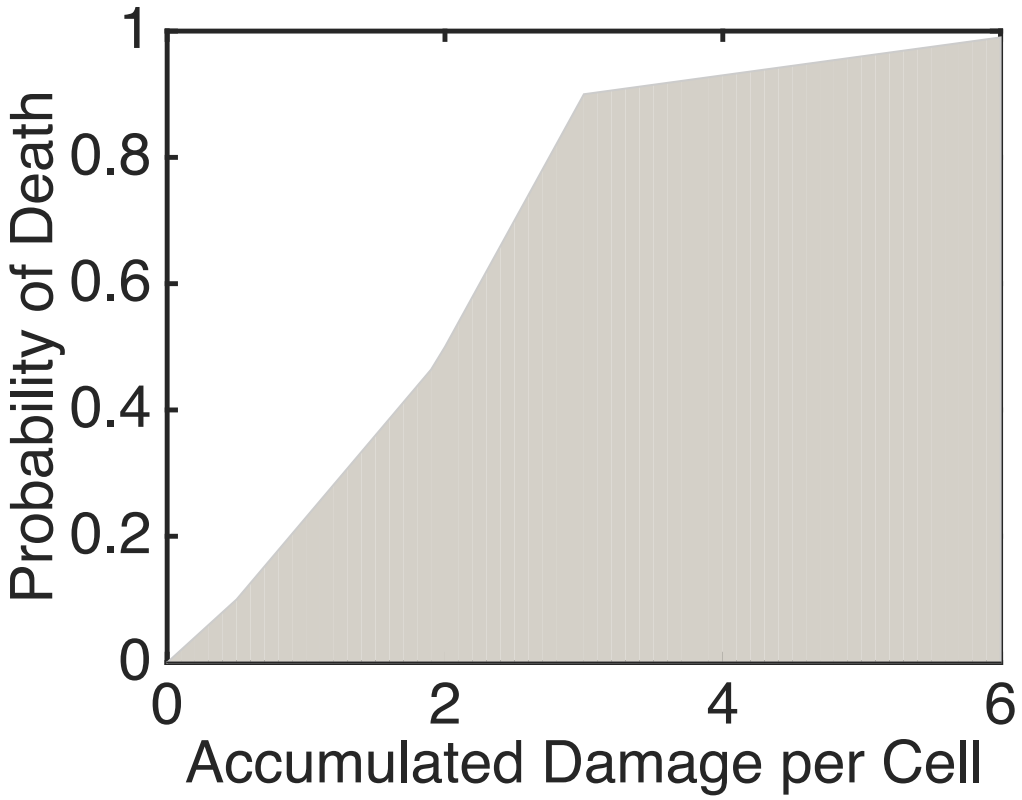

Figure 4.3: Probability of lymphocyte death as a function of total accumulated damage. Each cell has this probability evaluated daily, with death evaluated after radiation exposure on days of treatment.

4.1.5 Radiation-Induced Lymphocyte Death

The probability of lymphocyte death is a function of the total accumulated damage. Individual cells are evaluated after each beam of radiation. Since each cell is unique, and some are able to repair the damage, a probability distribution is used to determine when a cell dies. The basis for this distribution starts by taking each cell and separating them into groups of less than 0.5 Gy, between 0.5 and 2 Gy, between 2 and 3 Gy, and greater than 3 Gy. These cutoffs are established using the D10, D50 and D90 *in vitro* radiosensitivities [117]. To create a probability of survival, each cell is assigned a random value between 0 and 1. This value is compared to a function specific to the accumulated damage group the cell is in. The function for less than 0.5 Gy is [0.2×(total damage)], between 0.5 and 2 Gy is [0.1 + 0.26×(total damage - 0.5)], between 2 and 3 Gy is [0.5 + 0.4×(total damage - 2)], and greater than 3 Gy is [0.9 + 0.03×(total damage - 3)]. If the cells randomly assigned value is greater than the function output, then the cell survives. If it is less than the function output, then the cell dies (Figure 4.3). Cells that die are removed from the circulating pool. Hence, the number of circulating cells is a discrete-time dynamic variable in this model, and the number of cells affected by radiation on a particular day will vary (though the fraction, or percentage, affected is constant for a particular planning volume).

4.1.6 Cell generation

The body is always producing new lymphocytes, but the dynamics of cell generation are slow. About 0.33% of the current lymphocyte count are generated per day, which represents an average value of turnover for lymphocyte subsets in an aged population (naive B cells 0.34, memory B cells 0.69, native effector B cells 0.44, γ δ T cells 0.2, naive CD4 0.07, naive CD8 0.09, memory CD4 0.45, memory CD8 0.36) [118]. After the total number of beams of radiation are administered for a day, the model updates the current count, eliminating cells that have died and adding new cells that have been produced.

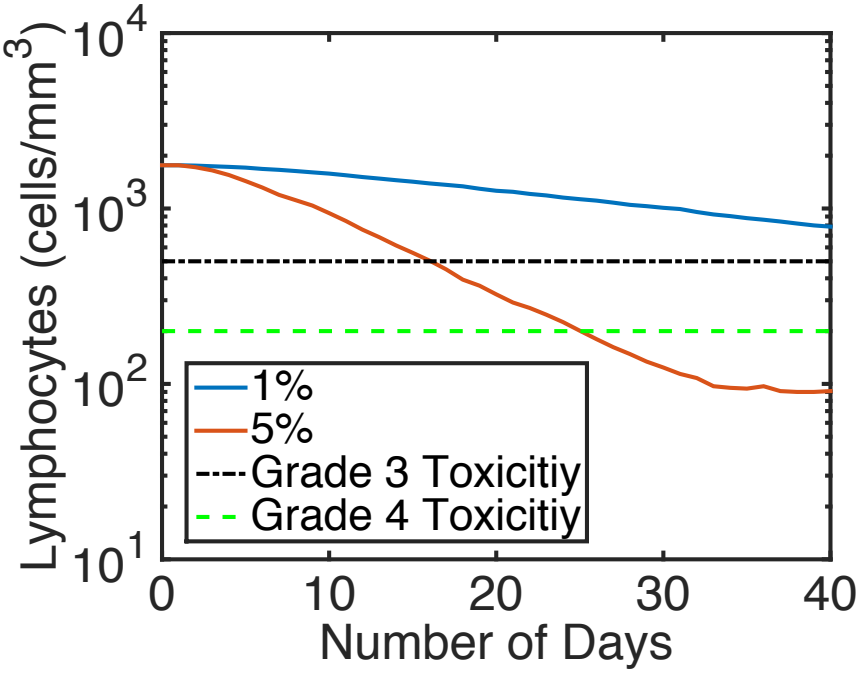

Figure 4.4: Lymphocyte count as a function of days throughout radiation. 2 Gy/day was administered for 30 fractions with a irradiated volume of 1% and daily lymphocyte turnover of 0.33% of the population.

The model captures lymphocyte death as a function of radiation exposure (Figure 4.4). Cells begin to die as the number of fractions of radiation increases. Figure 4.4 shows the lymphocyte count as a function of day with patients receiving radiation Monday through Friday of each week. After every 5 fractions there is a rest period of two days, representing the weekend. The rest period is after every 5 fractions, but can be seen more distinctly as the cell count drops. The algorithm captures expected behavior. Changes in parameters were explored including changes to the volume of blood irradiated, in organs with different relative weights, in the vascular volume of the heart, to dose per day, and to the daily lymphocyte turnover.

4.2.1 Stochastic Nature of Model

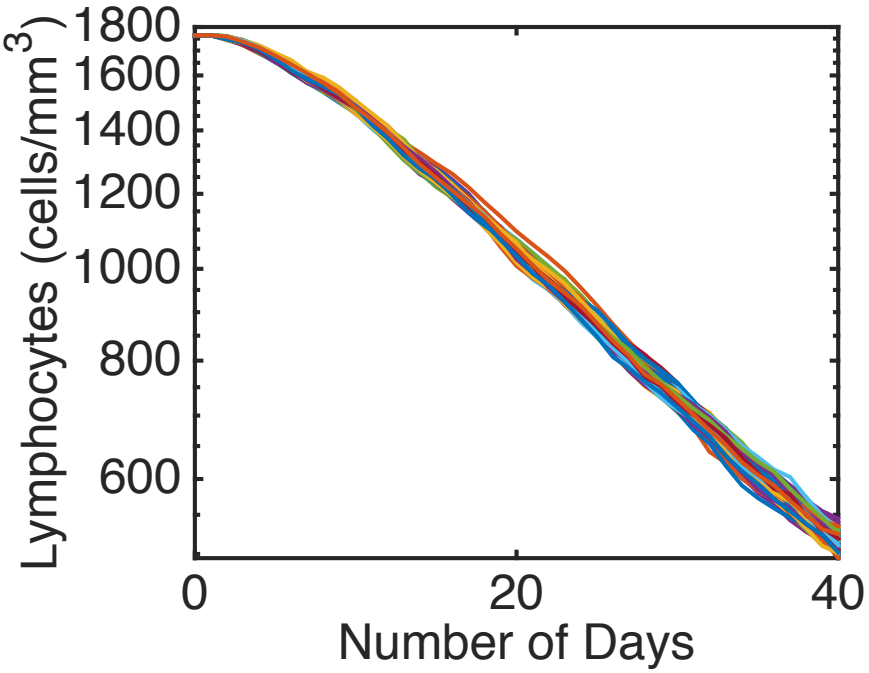

Figure 4.5: Lymphocyte count after each day at same irradiated volumes. The dose is 2 Gy/day for 30 fractions. The simulation is ran 100 times to show minor variation in probabilistic cell death.

A deterministic model will produce the same output. However, humans react stochastically to the same dose of therapy. Therefore, the cell damage is assigned in a Monte Carlo fashion, and there is a probability, not certainty, of death. The small variations can be seen in Figure 4.5. These 100 simulated patients get uniform treatment of 2 Gy per day for 30 fractions, yet there is a spread in their lymphocyte count over time.

4.2.2 Changes in Volume of Blood Irradiated to Lymphocyte Survival

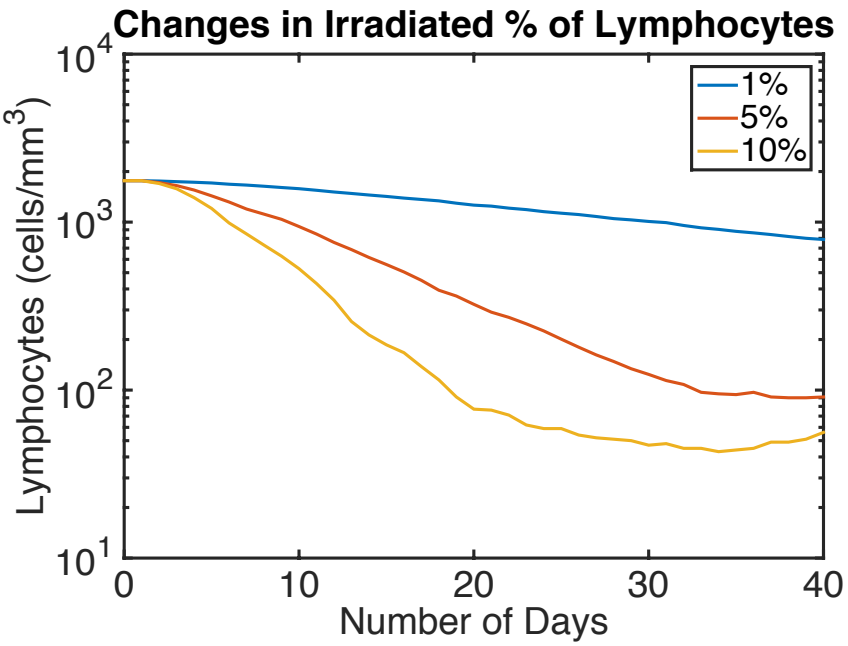

Figure 4.6: Lymphocyte count after each day at different irradiated volumes. The dose is 2 Gy/day for 30 fractions. The blue curve is a representative simulation for a patient with 1% of their cells exposed to radiation, the red is 5% and the yellow is 10%.

The same dose of radiation can produce different amounts of toxicity, depending on where it is administered to the body. The size and vascularity of the organ determine the irradiated volume, and, therefore, how many lymphocytes will pass through the beam path while it is on. The increase in toxicity can be seen in Figure 4.6. As the amount of cells in the beam path increases from 1% to 10%, the lymphoctye count decreases both overall and in their rate of death (requiring fewer and fewer radiation fractions).

4.2.3 Changes in Organ using Relative Weight

The results from the changes in irradiated volume are generalized at 1%, 5%, and 10%. These numbers are calculated from a combination of vascular volume and relative organ weight. In Figure 4.7, the relative organ weight is specified using the organs actual value [9]. The

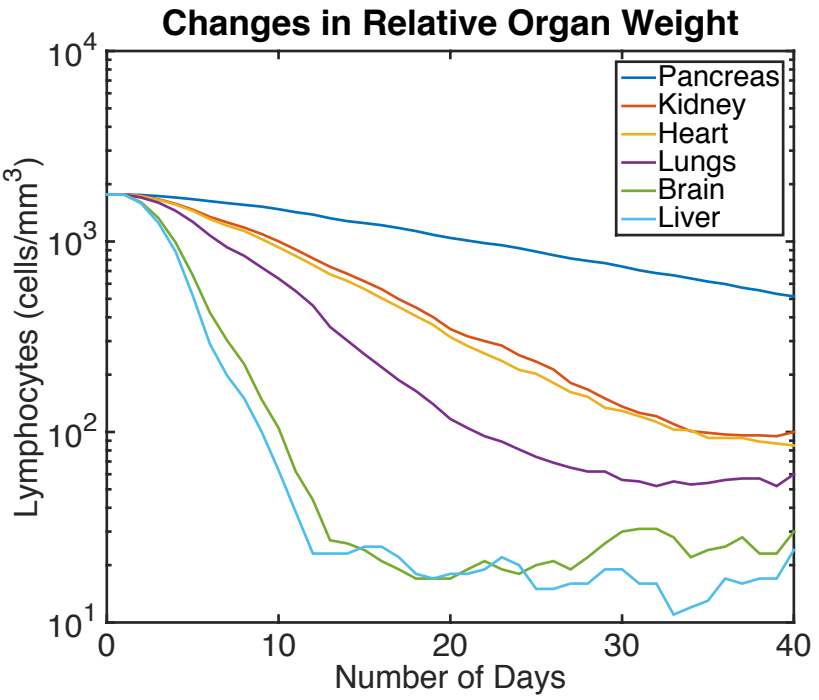

Figure 4.7: Lymphocyte count after each day for organs with different relative weights [9]. The organ vascularity is held constant at 11%, as well as the dose of 2 Gy/day.

relative organ weights as a percentage are as follows: pancreas (0.14), kidney (0.44), heart (0.47), lungs (0.76), brain (2), and liver (2.57). It must be noted that the vascular volume is set at 11% for all organs and only their relative organ weight is changed. The vascular volume will be different for different organs in but is held constant to observe changes in one variable. The greater the organ weight, the greater the decrease in lymphocyte count if the percent of vascular volume is constant.

4.2.4 Changes in the Vascular Volume of the Heart

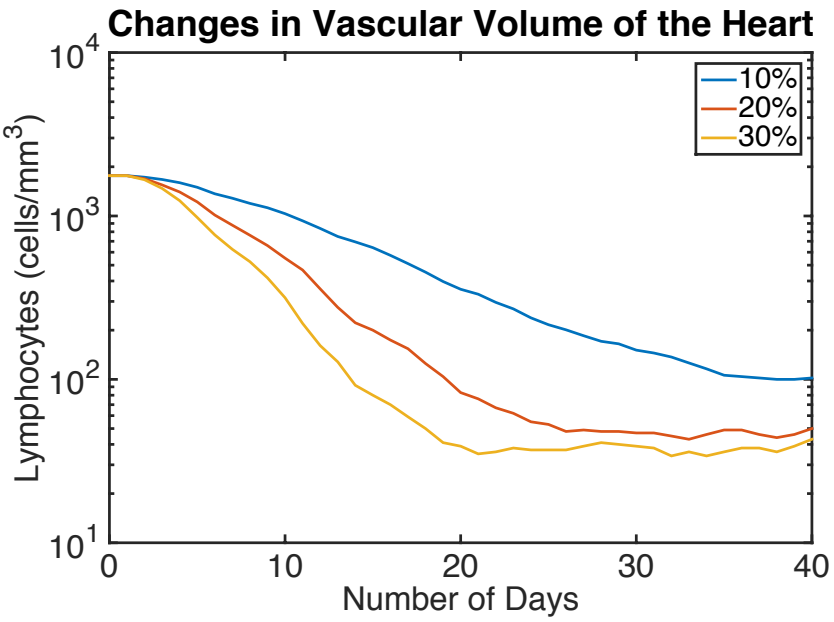

Figure 4.8: Lymphocyte count as a function of day and as a function of vascular volume in the heart. The simulations have a constant relative organ weight of 0.47% and dose of 2 Gy/day for 30 fractions. The lymphocyte curves with varying vascular volume percent are as follows: 10% (blue), 20% (red), and 30% (yellow).

The vascular volume of an organ is the other variable that determines the amount of cells that become irradiated. The heart is used to illustrate how changes in the percent of vascular volume impact lymphocyte count (Figure 4.8). The relative weight of the heart is held constant at 0.47% of the body, but the percent of blood that makes up the heart is increased from 10% to 30%.

4.2.5 Changes in Dose per Day to Lymphocyte Survival

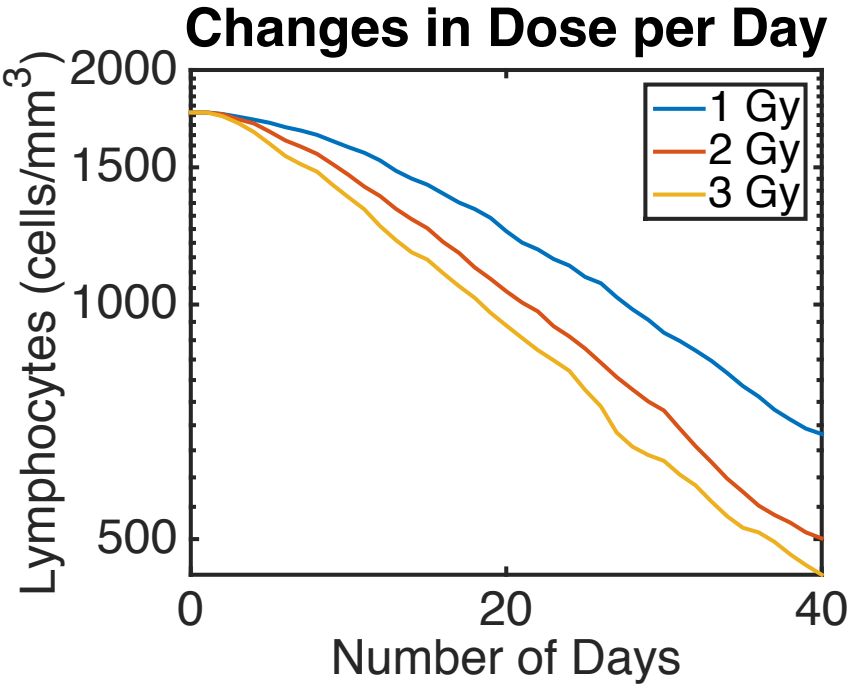

Figure 4.9: Lymphocyte count after each day at different total doses per day of radiation: 1 Gy/day (blue), 2 Gy/day (red), or 3 Gy/day (yellow). The volume irradiated is 1% for 30 total fractions.

Given a set volume of blood irradiated, but changing the dose per day, the number of lymphocytes that die increases. Figure 4.9 shows the simulation curves of 1 Gy/day, 2 Gy/day, and 3 Gy/day, with the percentage of blood being irradiated at 1% and 30 total fractions. There is a change in the lymphocyte profile, but it is not as pronounced as changing the number of irradiated lymphocytes.

4.2.6 Changes in the Daily Lymphocyte Turnover

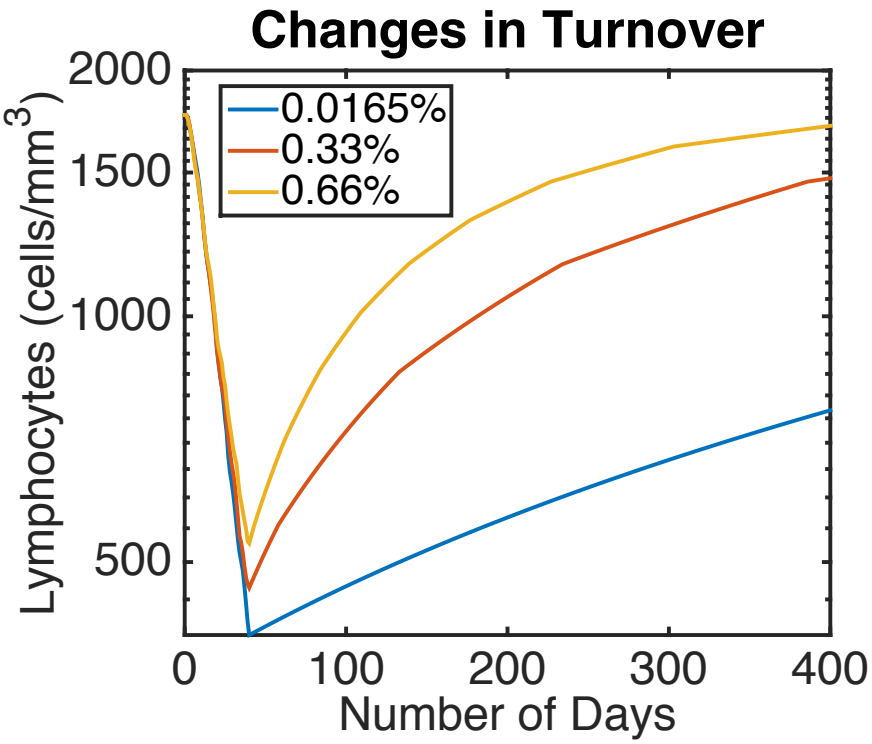

Figure 4.10: The curve of the lymphocyte count after 30 fractions of 2 Gy/day radiation with an average daily lymphocyte turnover of 0.33% of the population (red). This figure also extends a year beyond therapy to show the slow return to baseline. This value is halved (blue) and doubled (yellow).

The daily lymphocyte turnover was set by taking the average turnover value of various lymphocyte subsets. This turnover, 0.33% of the population, was allowed to vary to half and double the average value. The results are shown in Figure 4.10. In the earlier fractions, the variability is low. As lymphocyte counts drop, the turnover has a larger impact, and the curves begin to separate. As turnover increases, fewer lymphocytes die, and the lymphocyte count curve becomes less toxic. Additionally, an increase in turnover results in a faster time to recovery.

4.3 DISCUSSION

Lymphocytes are highly sensitive to radiation [120], and low lymphocyte counts after radiation have been associated with a worse overall survival in pancreatic cancer patients [69]. This algorithm is able to capture lymphocyte death and replenishment as radiation is administered, but it does not have the ability to explicitly differentiate between treatment techniques. Instead, the model takes into consideration the number of lymphocytes that are present in the beam path while radiation is on. This indirectly takes into account the treatment technique, if one technique targets less blood volume than another. IGRT, for instance, with magnetic resonance imaging (MRI) or computerized tomography (CT) scans, allows clinicians to tighten the margins and irradiate less volume [67]. The model does characterize radiation-induced lymphopenia that can be tuned to an individual. The daily lymphocyte turnover, dose, and volume of irradiation, through relative organ weights and vascular volume, can become personalized.

The volume of irradiation had the biggest impact on lymphopenia. If more lymphocytes in circulation are subjected to radiation, then more lymphocytes will die. Where the tumor is located will determine what organs receive radiation. Changing the radiation technique to minimize blood flow in the region of radiation should improve lymphotoxicity. However, in an area where that is unavoidable, this model will predict radiation-induced lymphopenia. This could aid a clinician in choosing a different dosing schedule or introducing a lymphocyte rescue if it is available.

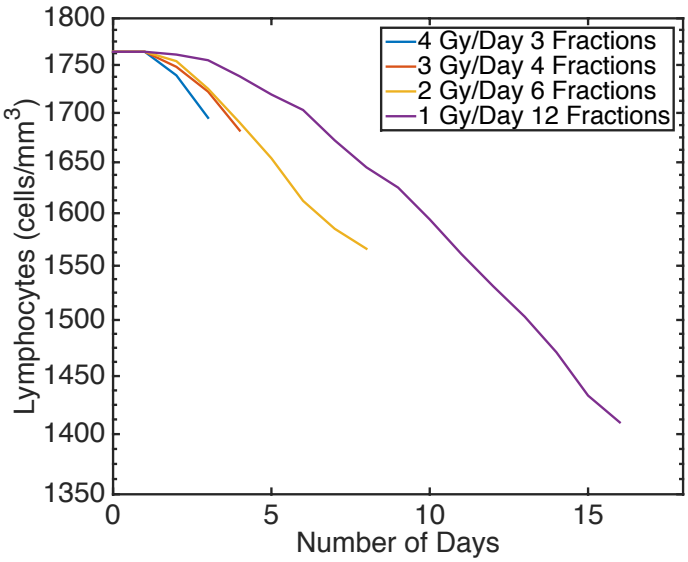

Figure 4.11: Lymphocyte count as a function of days of radiation for a total of 12 Gy divided among 3 (blue), 4 (red), 6 (yellow), and 12 (purple) fractions. The volume of irradiation and turnover were held constant at 1% and 0.33% of the population, respectively.

The model is less sensitive to changes in dose for a constant irradiated volume, consistent with the accumulated damage model [71]. The effects of dose do become more pronounced with a larger constant irradiated volume but constant fraction number. This outcome results from the probabilistic cell death functions, based off of *in vitro* lymphocyte radiosensitivity [117]. As dose increases, the damage accumulated rate increases, and the probability of death becomes greater. When dose is increased, the fraction number is often decreased. One study found that SBRT, with higher, less frequent doses, led to less lymphopenia in pancreatic cancer patients than conventional radiation [116]. This is consistent with this model as seen

in Figure 4.11. All possibilities deliver 12 Gy total to the patient. As the fractions get smaller in number, the dose gets larger, but the toxicity becomes less severe. This algorithm can help find the crossover points where increasing dose and decreasing frequency is within an acceptable toxicity burden than lower, more frequent doses.

Changes in the daily lymphocyte turnover are more prominent during later fractions of radiation. This is because turnover is constant, and these cells make up a larger subset of the total population at lower circulating counts. The model only captures what happens to lymphocytes throughout radiation therapy, and estimates recovery based on the daily turnover of cells. More research and modeling will be needed to capture how the lymphocytes recover with regulatory feedback. Radiation-induced lymphopenia can take, in some cases, years to recover from. Factors to be investigated are the impact of radiation on proliferation rates, on regulatory cytokines, and the body's immune response, among others. The long-term toxic effects are one reason to take lymphotoxicity into consideration and monitor it from the beginning.

Radiation is a critical treatment to combat cancer, especially in local pancreatic cancer, with a 5-year survival rate of only 29% [12]. The model can be used as a starting point to eventually predict patient sensitivity, prevent high grade lymphotoxicity, and improve treatment schedules to increase efficacy but control toxicity.

4.4 CHEMORADIATION-INDUCED LYMPHOPENIA

Lymphocytes, while part of the white blood cell family, follow a different generation and maturation pathway than the other subsets. Cytokines, such as IL-7, trigger lymphopoiesis in the bone marrow where stem cells commit to the common lymphoid progenitor population. From there they can differentiate into T-cells, B-cells or natural killer cells. The death from radiation is added to a chemotherapy-induced lymphosuppression model to capture a concurrent therapy plan.

The classic Friberg model works well for chemotherapy, because its mechanism of action occurs in the bone marrow. However, radiation is a localized treatment, and the planning volume often does not include the bone marrow. Therefore, the cell death directly from radiation is found using the results from the previous model.

Certain chemotherapies might not induce lymphopenia alone, but when combined with radiation can synergistically increase toxicity along with efficacy. Antimetabolites such as gemcitabine, fludarabine, and capecitabine act as radiosensitizers. Both chemotherapy and radiation can produce lethal damage, but some cells receive sublethal damage and repair themselves. When both chemotherapy and radiation are given, then the chances of repair are decreased. However, the chemotherapy only is effective for cells that are still dividing, and circulating cells are terminally differentiated. This model combines chemotherapy acting on progenitor cells in the bone marrow and radiation acting on cells located in the planning volume.

Similar behaviors even in patient groups with different chemotherapy and radiation schemes emerge in the data and model. The chemotherapy induces predictable oscillations, as cells are eliminated and subsequently recover with the help of regulatory molecules that stimulate proliferation among progenitor cells. Lymphopoiesis is less understood than myelopoiesis, and many parameters were estimated or dynamically fit. More quantitative studies need to be performed to ground the parameters.

4.4.1 Patient Data

Four sets of data were used to build this model. The first dataset comes from pancreatic cancer patients that were treated with 1000 mg/m^2 of gemcitabine over 30 minutes weekly for four weeks [121]. The absolute lymphocyte counts for 10 patients were provided and used to help decipher how much lymphopenia is associated with gemcitabine alone. Two other datasets, also of pancreatic cancer patients, have lymphocyte time-series data for patients that get gemcitabine and external-beam radiation therapy. One dataset is of patients that get seven weekly gemcitabine treatments of 400 mg/m^2 over 30 minutes and two weeks of external beam radiation (M-F) of 3 Gy/day [10]. The other is the same external beam radiation schedule but only 4 of the weekly gemcitabine treatments [11].

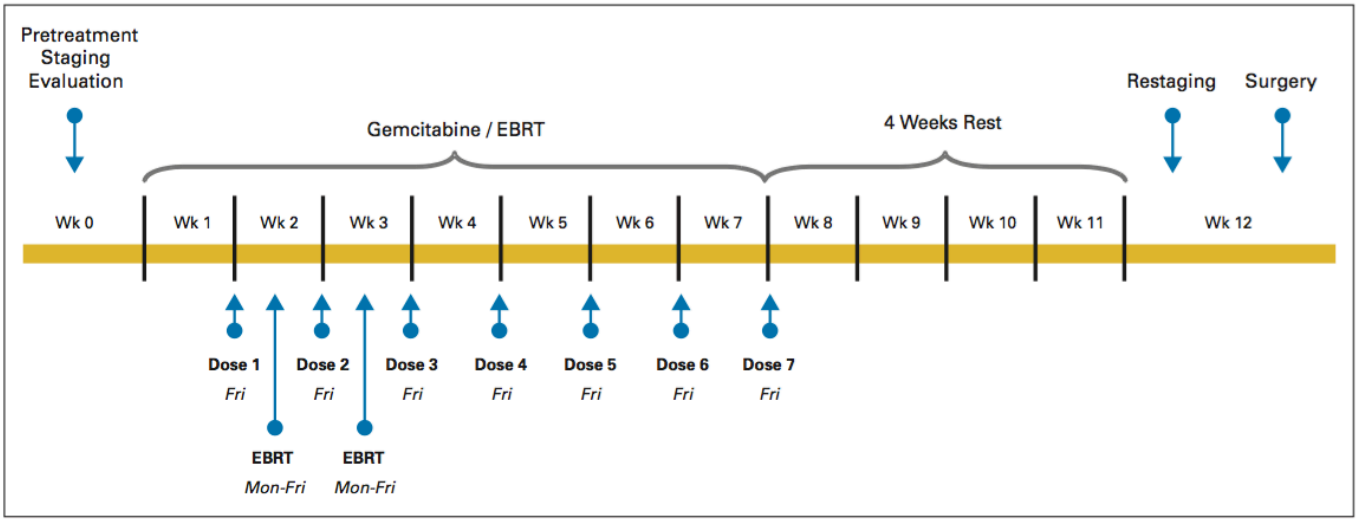

Figure 4.12: 7 weekly doses of gemcitabine with 10 days of radiation therapy schedule [10].

The final dataset is from the same group of patients that were used in the thrombocytopenia and neutropenia combined model. Patients received 50.4 Gy of radiation at 1.8 Gy per day for 28 days on weekdays. The gross primary tumor and regional lymph nodes greater than 1 cm were subjected to a three- or four-field technique with 15- or 18-MV photons. On days that radiation was administered, 825 mg/m^2 capecitabine was taken twice daily orally. Moreover, weekly cetuximab was given through the first month of chemoradiotherapy. Patient lymphocyte counts over the course of chemoradiotherapy were used to fit the model.

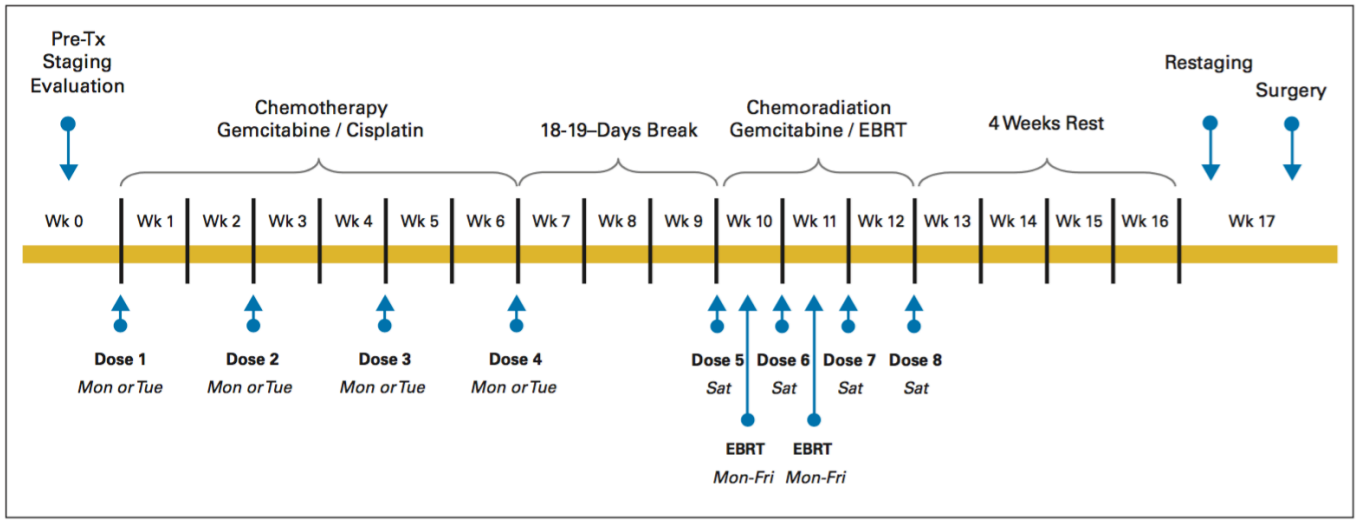

Figure 4.13: 4 weekly doses of gemcitabine with 10 days of radiation therapy schedule [11]. The starting point for this data is at Dose 5 during the chemoradiation phase.

Each patient's first day of radiation was considered day 0 for the purpose of a starting point for the model. Similarly to the previous model, all of the datasets were sparse, and therefore were combined on days 1-4 and 5-7 of each week. Unlike the last model where subgroups were established, this model includes all the patients in each treatment plan.

4.4.2 Capecitabine

Capecitabine is in the same family as gemcitabine and is a prodrug that gets converted to 5-fluorouracil (5-FU) [122]. Capecitabine is given as an adjuvant for colon cancer, as a monotherapy for metastatic colorectal cancer, and in combination with docetaxel or as a monotherapy for metastatic breast cancer. Unlike the previous intravenously infused drugs, capecitabine was a tablet that is taken orally twice daily. Common adverse events include diarrhea, hand-and-foot syndrome, nausea, vomiting, pain, fatigue, and hyperbilirubineamia. Although myelosuppression is not a main toxicity, grade 3/4 lymphopenia occured in 13% of patients in a study for capecitabine as a monotherapy for colon cancer and 44% grade 3 for stage IV breast cancer [123].

Pharmacokinetics for orally administered capecitabine show peak levels at 1.5 hours and for the active 5-FU at 2 hours. Food was shown to impact absorption and the main route of excretion is through urine. A compartmental phamacokinetic model of capecitabine has been published that accounts for oral administration and metabolism to 5-FU [124]. The other drugs were previously discussed in chapter 3.

4.4.3 Model Developement

4.4.3.1 Lymphocyte Dynamics Even though all cells start from stem cells, lymphocytes branch off into their own maturation cascade separate from neutrophils, thrombocytes, and erythrocytes. T-cells, B-cells and natural killer cells mature from the common lymphoid progenitor state (Eq.4.1) with the assistance of various cytokines (Eq.4.7). The cells mature through a series of transition states, the same rate and way the myelosuppression models of Friberg do (Eq.4.2-Eq.4.6).

Chemotherapy, in this case, capecitabine and gemcitabine, both eliminate progenitor cells, resulting in a cascade of lymphocyte reduction. The deviation of lymphocytes from baseline triggers IL-7 to stimulate the common lymphoid progenitor state to proliferate through signal feedback (Eq.4.7 and Eq.4.8). Radiation on the other hand kills cells in the beam path (Eq.4.6).

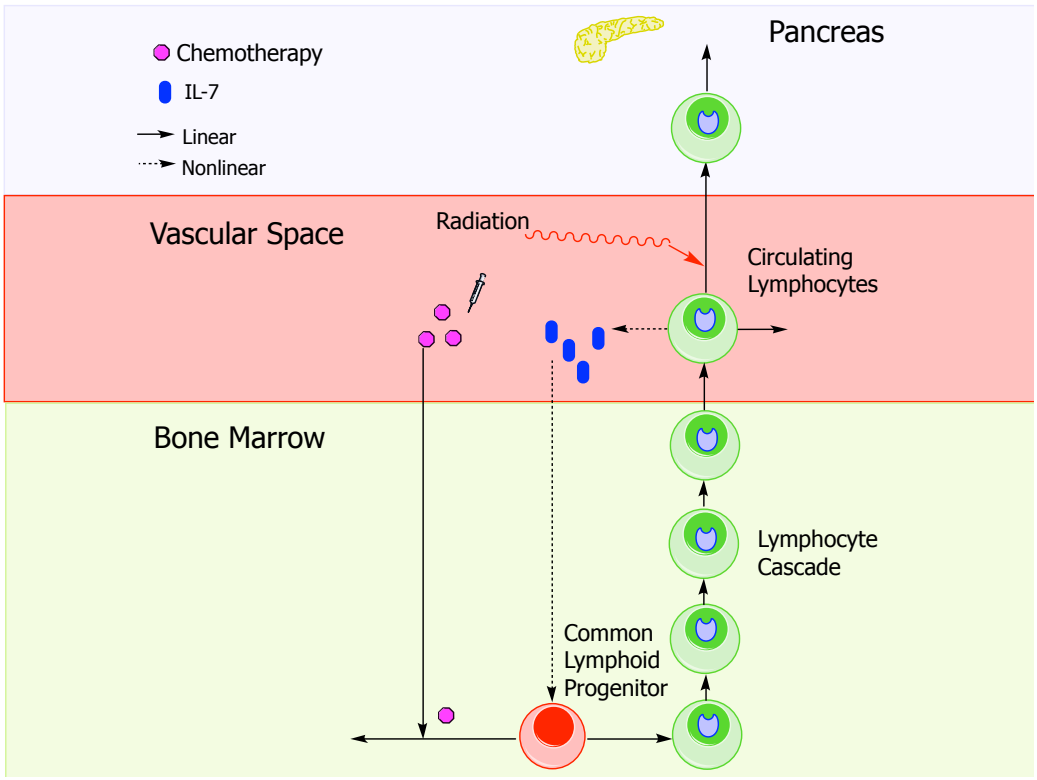

Figure 4.14: Dynamic Chemoradiotherapy-Induced Lymphocytopenia Model. Progenitor and stem cells mature into circulating lymphocytes. The progenitor cells are susceptible to cell death via chemotherapy in the bone marrow. As the circulating platelet count decreases after a dose of chemotherapy, interleukin-7 provides feedback regulation to regain homeostasis. Additionally radiation eliminates circulating lymphocytes in the beam path.

Table 4.1: Thrombocytopenia and Neutropenia Model Equations and Corresponding Biological States.

State	**Biological Meaning**	**Unit**
$C_{lp}(t)$	Common lymphoid progenitor	$\frac{10^6 cells}{\mu L}$
$L_1(t)$	Lymphocyte progenitor	$\frac{10^6 cells}{\mu L}$
$L_2(t)$	Lymphocyte maturation	$\frac{10^6 cells}{\mu L}$
$L_3(t)$	Lymphocyte maturation	$\frac{10^6 cells}{\mu L}$
$L_4(t)$	Lymphocyte maturation	$\frac{10^6 cells}{mL}$
$L_c(t)$	Circulating Lymphocytes	$\frac{10^6 cells}{mL}$
$IL(t)$	IL-7	-
$ILs(t)$	IL-7 Signal	-

$$\frac{dC_{lp}}{dt} = k_{tr}L_{c_0} - k_{tr}C_{lp}(t) - Slope_c C_{lp}(t)Drug(t) + 0.09\frac{exp(\alpha(ILs(t) - 200.0) - 1.0)}{200.0 + (exp(\alpha(ILs(t) - 200.0) - 1.0)}C_{lp} \tag{4.1}$$

$$\frac{dL_1}{dt} = k_{tr}C_{lp}(t) - k_{tr}L_1(t) \tag{4.2}$$

$$\frac{dL_2}{dt} = k_{tr}L_1(t) - k_{tr}L_2(t) \tag{4.3}$$

$$\frac{dL_3}{dt} = k_{tr}L_2(t) - k_{tr}L_3(t) \tag{4.4}$$

$$\frac{dL_4}{dt} = k_{tr}L_3(t) - k_{tr}L_4(t) \tag{4.5}$$

$$\frac{dL_c}{dt} = k_{tr}L_4(t) - k_{tr}L_c(t) - Radiation(t)L_c(t) \tag{4.6}$$

$$\frac{dIL}{dt} = IL_0(\frac{L_{c_0}}{L_c(t)})^{0.6} - IL(t) \tag{4.7}$$

$$\frac{dILs}{dt} = 0.3IL(t) - 0.3ILs(t) \tag{4.8}$$

4.4.4 Results

4.4.4.1 Gemcitabine Pancreatic cancer patients that only were administered 1000 mg/m^2 of gemcitabine, without radiation, set the basis for the contributing lymphopenia when combined with radiation. In Figure 4.15, simulations of both the higher chemotherapy only dose (blue curve) with corresponding data (box plots), and the lower dose when given with radiation (dashed black curve) are shown. Gemcitabine contributes to the elimination of some lymphocytes but not nearly as severe as seen in the chemotherapy plus radiation patients.

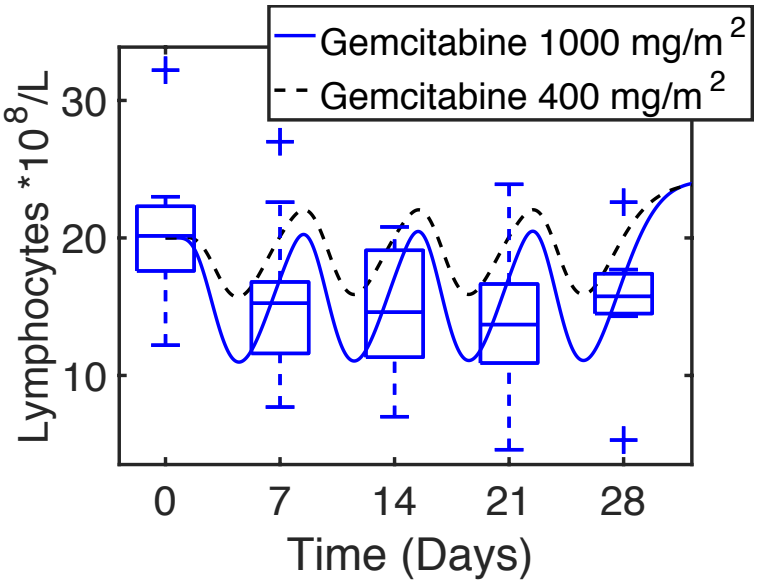

Figure 4.15: This shows the contribution of gemcitabine alone toward lymphocyte elimination. The data for chemotherapy alone is at a higher dose than the dose given with radiation. The two are shown for comparison.

4.4.4.2 Chemoradiation Gemcitabine and radiation only effects were added manually to match the degree of lymphotoxicity found from the radiation damage algorithm and gemcitabine alone data, respectively. For radiation, the dosing schedule of interest was implemented into the lymphocyte tracking algorithm using the pancreas' fraction of blood equal to 1.54% of the total blood. The effects from radiation and chemotherapy are simultaneously added to the lymphopoiesis model to capture the full dynamics.

4.4.4.3 7 weeks of Gemcitabine and 3 Gy/Day Radiation 10 Fractions This group of patients was able to get treated with 7 cycles of gemcitabine, because prior therapy was not given. However, they received the same radiation plan as the next set of patients. The model fits the decline of lymphocytes throughout the course of treatment, but patient data was not collected much further beyond that (Figure 4.16). In fact the last 4 boxplots have only 2 data points each. Therefore, the recovery phase was able to be studied better in the other data sets. For each set of results for chemoradiation, the effects of chemotherapy alone (magenta), radiation alone (black), and combined therapy (red) are plotted over the boxplot's (blue) of data.

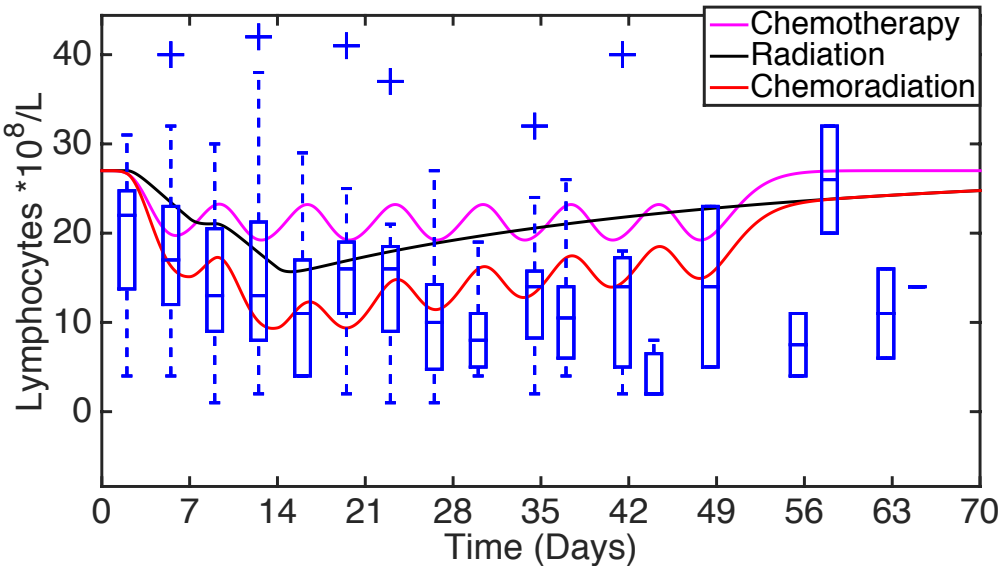

Figure 4.16: This figure is the lymphocyte count as boxplots in blue throughout therapy. Patients receive 7 weeks of gemcitabine and 10 days of radiation. The simulation of chemotherapy alone (magenta), radiation alone (black), and chemoradiation (red) are all plotted.

4.4.4.4 4 weeks of Gemcitabine and 3 Gy/Day Radiation 10 Fractions This datatset had a lot of information after therapy ceased. The last dose of any therapy was at day 21, but the data continues through day 70. The slow but steady return to baseline is seen in Figure 4.17. The oscillations and final rebound bump can be seen around day 34, from chemotherapy and proliferation stimulation from IL-7, respectively. Also, the steady decline initially and slow, long rebound from radiation are present in the data and model fit.

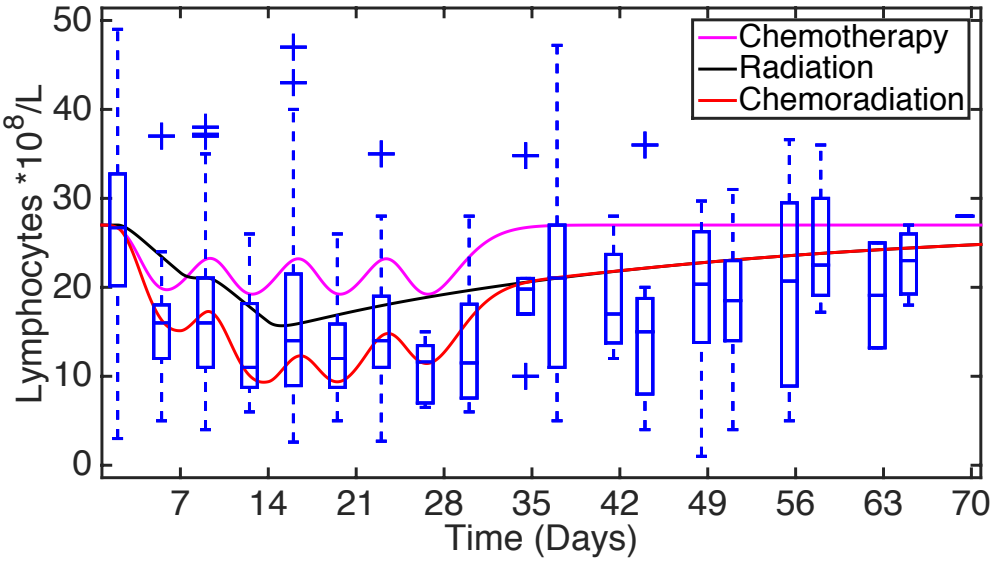

Figure 4.17: This figure is the lymphocyte count as boxplots in blue throughout therapy. Patients receive 4 weeks of gemcitabine and 10 days of radiation. The simulation of chemotherapy alone (magenta), radiation alone (black), and chemoradiation (red) are all plotted.

4.4.4.5 BID Capecitabine and 1.8 Gy/Day Radiation 28 Fractions This set of pancreatic cancer patients are given capecitabine instead of gemcitabine and a lower fraction of radiation at 1.8 Gy/Day. Since the radiation dose fraction is lower, it can be give for 5.5

weeks. Therefore, both chemotherapy and radiation are completed by day 38. Again the same initial downward slope and slow, long recovery from radiation can be seen in Figure 4.18. Additionally, the extra rebound seen after the last dose of chemotherapy, but not sustained in the long-term recovery, likely due to IL-7, is observed.

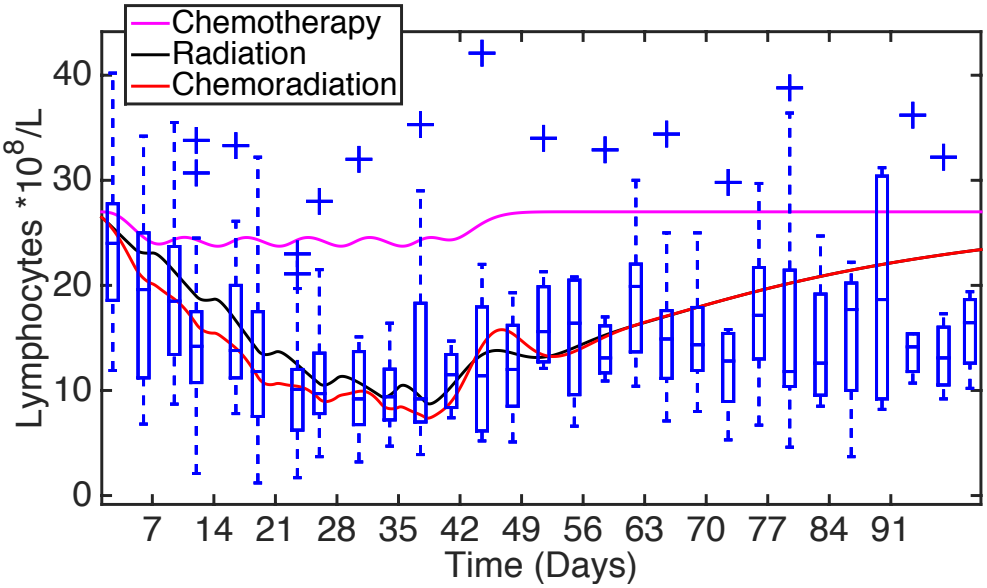

Figure 4.18: This figure is the lymphocyte count as boxplots in blue throughout therapy. Patients receive 28 days of capecitabine and radiation. The simulation of chemotherapy alone (magenta), radiation alone (black), and chemoradiation (red) are all plotted.

4.4.5 Discussion

The chemoradiation simulations are just a starting point for how the radiation damage model can be applied. The model captures the data throughout therapy fairly well. The effects of radiation are applied to match the degree of lymphopenia from the previously discussed

algorithm. However, the parameters for lymphopoiesis are dynamically fit, and the long term recovery after therapy is not always accounted for. Therefore, much more model analysis can be performed. For instance, radiation only data, chemotherapy only data, and concurrent data for the same therapy and doses could help ground parameters.

One way to account for the long, slow recovery of lymphocytes after radiation is through damage associated molecular patterns (DAMPs) [74, 75, 76, 77]. Radiation damages the tissue, and the DAMPs initiate an immune response, recruiting T-cells to the site of damage. As fractions of radiation accumulate, T-cells are killed directly by the radiation, as well as, through the immune response. This results in a prolonged recovery of lymphocytes to baseline post-radiation. Once a full model is validated, the possible impact of this model is great. The model can be used to monitor lymphopenia in combination therapy and used in therapy optimization algorithms.

5.0 CONCLUSIONS

Cancer treatments, like any drug, come with side effects. The benefits must outweigh the risks for patients to use them. Hematological toxicities such as thombocytopenia, neutropenia, and lymphopenia are common dose limiting toxicities for chemotherapy and radiation. Adjusting the magnitude and frequency of treatment schedules is one way to prevent patients from entering grades 3 and 4 toxicity. Predicting which patients need dose adjustments is the difficult part. Severe toxicities can lead to bleeding, infection and even death. The models presented were built to describe the chemotherapy and radiation induced toxicity, in order to predict why some patients are more sensitive than others to a given treatment. Moreover, they were built to predict trends early on, in order to make adjustments and improve outcome.

In the first model, thrombocytopenia was found to be more severe in patients with a faster transit rate of maturation and lower ability to rebound via thrombopoietin. When this model was biologically expanded to include neutropenia, a new dataset allowed the model to be tested in different subgroups of patients. A correlation between outcome and pretreatment histological subtyping was once again influenced by the platelet maturation transit rate and thrombopoietin.

The final model was developed to describe radiation-induced lymphocytopenia. Lymphocytes are especially sensitive to radiation. Severe radiation-induced lymphopenia during cancer treatment can lead to dose reductions and delays hindering patient overall survival. This work constructs a model that predicts lymphocyte cell count throughout the course of radiation treatment. The inputs to the model are the volume of blood in the beam area, number of radiation fractions, number of beams per fraction, total radiation dose, and a patient specific initial baseline lymphocyte count. A Monte Carlo approach assigns lympho-

cytes to be within, or outside, the beam area, and radiation damage is accumulated by blood cells in the treatment volume for each beam and fraction. Physiologically-motivated rates of natural (not treatment-induced) lymphocyte death and replenishment are also incorporated into the model. This model may be useful in predicting the severity of lymphopenia from a patient-specific radiation treatment plan. Also, the model can be combined with a chemotherapy-induced lymphosuppression model to study combination therapy.

As George Box said, "all models are wrong, but some are useful." The goal of the three toxicitiy models is to predict patient subpopulations that are sensitive to a given treatment. If sensitive patients can be detected early on in therapy, then modifications can be made to improve efficacy and/or toxicity. Future work to improve the models include obtaining individual pharmacokinetic data to drive pharamcodynamic effects, modeling how many and when progenitor cells commit to a certain lineage, using individual regulator profiles such as TPO, IL-7, and G-CSF to drive rebound effects, and a better understanding of lymphocyte dynamics at the site of radiation. Other future work would include designing prospective clinical trials that intervene as soon as the model predicts sensitive subpopulations.

5.1 PHARMACOKINETICS

For all sets of data only PD time series data was available. However, drug PK play an important role in efficacy and toxicity. Drugs can be cleared or metabolized at different rates in individuals, impacting residence times and cell elimination rates. In the models, the transit rate of maturation determines the downward slope of the cells as they are eliminated. This term could be set to a fixed parameter value for all patients, and the trend could be due to an individuals PK rates. For instance, patients that are less sensitive to the drug may actually be clearing the drug at a greater rate, so less is actually getting to the bone marrow. Simple compartmental PK might not be enough to accurately depict the toxicity in the bone marrow, because PK is measured by circulating blood concentrations. A physiologically based PK model could be needed to biologically inform the model in the bone marrow.

5.2 PROGENITOR COMMITMENT TO LINEAGE

The hematopoietic lineage tree begins with a single population of pluripotent stem cells that differentiate and mature into different cell types, based on chemical cues from cytokines and other molecules. Most models in the literature only consider one cell type at a time, so it does not matter how the commitment to lineage occurs. This works well for studying a single toxicity, but what happens when a multiple drug therapy has multiple hematological toxicity concerns? Currently, clinicians will not give that combination, but perhaps this combination is more efficacious as long as toxicity is controlled. If measurements of cytokines that enforce commitment were available, then predictions on how the patient will recover might be possible. For instance, IL-7 promotes lymphopoiesis and TPO promotes myelopoiesis. When radiation and a platinum chemotherapy are given concurrently, lymphopenia and thrombocytopenia are possible. Exogenous IL-7 and TPO could be given to patients to maximize efficacy but control toxicity.

5.3 CYTOKINES AND REGULATORS

TPO, G-CSF, and IL-7 lack individual data to ground the terms in the models. TPO does mimic the appropriate magnitude and peak time for a circulating platelet count, similar to the patients used, but no measurements were available. The time series profiles of these cytokines could be enough to explain why patients have variable drug sensitivities. The timing of

endogenous and/or exogenous TPO and G-CSF could prevent high grade hematological toxicities. For instance, if TPO accumulates from low platelet counts, and TPO acts on the common myeloid progenitor state, as well as, further into the platelet lineage, then a high concentration of common myeloid progenitors might follow. If at the same time, it was advantageous to increase neutrophil counts in anticipation of a neutropenia-inducing drug, then GM-CSF and/or G-CSF could be administered to boost circulating neutrophil counts. Additionally, exogenous TPO could be administered, although it is not as effective as exogenous G-CSF. Eventually dosing optimization routines could include toxicity rescues in complex ways.

Another area of interest in the cytokines and regulators field is DAMPs. It is not currently understood why lymphocytes take so long to recover after radiation therapy. There are theories on the immune system and DAMPs, but nothing is conclusive. This is a broad field with many avenues for further research. Improvements in experimental measurement techniques, especially dynamically throughout therapy, are needed to characterize trends.

5.4 PROSPECTIVE STUDIES FOR EARLIER SUBGROUP STRATIFICATION

Model validation is one of the most challenging aspects for transitioning models to the clinic. The data used to build these models were all from previously established trials. Therefore, the individual pharmacokinetic data, regulatory molecule time series data, and frequent blood count measurements were not present. Designing a prospective trial to obtain all of these measurements and get an accurate description of the patient's dynamics is needed to verify significant findings. Once that data is acquired and analyzed, then future prospective trials can be performed to detect subpopulations earlier in the treatment plan. Changes in therapy can then be made to improve outcome.

BIBLIOGRAPHY

[1] N. DCTD, D. NIH, Common terminology criteria for adverse events v3. 0 (ctcae), Published date: December 12.

[2] eBioscience, Hematopoiesis from multipotent stem cell. (2012).

[3] L. E. Friberg, A. Henningsson, H. Maas, L. Nguyen, M. O. Karlsson, Model of chemotherapy-induced myelosuppression with parameter consistency across drugs, Journal of clinical oncology 20 (24) (2002) 4713–4721.

[4] A. L. Quartino, L. E. Friberg, M. O. Karlsson, A simultaneous analysis of the time-course of leukocytes and neutrophils following docetaxel administration using a semi-mechanistic myelosuppression model, Investigational new drugs 30 (2) (2012) 833–845.

[5] J. W. Smith, D. L. Longo, W. G. Alvord, J. E. Janik, W. H. Sharfman, B. L. Gause, B. D. Curti, S. P. Creekmore, J. T. Holmlund, R. G. Fenton, et al., The effects of treatment with interleukin-1α on platelet recovery after high-dose carboplatin, New England Journal of Medicine 328 (11) (1993) 756–761.

[6] S. Vadhan-Raj, S. Patel, C. Bueso-Ramos, J. Folloder, N. Papadopolous, A. Burgess, L. D. Broemeling, H. E. Broxmeyer, R. S. Benjamin, Importance of predosing of recombinant human thrombopoietin to reduce chemotherapy-induced early thrombocytopenia, Journal of clinical oncology 21 (16) (2003) 3158–3167.

[7] Y. Sasaki, T. Tamura, K. Eguchi, T. Shinkai, Y. Fujiwara, M. Fukuda, Y. Ohe, M. Bungo, N. Horichi, S. Niimi, K. Minato, K. Nakagawa, N. Saijo, ancer hemotherapy and harmacology a new platinum derivative , in comparison with cisplatin and carboplatin, Cancer Chemother Pharmacol (1989) 243–246.

[8] M. Joerger, A. D. Huitema, D. J. Richel, C. Dittrich, N. Pavlidis, E. Briasoulis, J. B. Vermorken, E. Strocchi, A. Martoni, R. Sorio, et al., Population pharmacokinetics and pharmacodynamics of paclitaxel and carboplatin in ovarian cancer patients: a study by the european organization for research and treatment of cancer-pharmacology and molecular mechanisms group and new drug development group, Clinical Cancer Research 13 (21) (2007) 6410–6418.

[9] L. Birnbaum, R. Brown, K. Bischoff, J. Foran, J. Blancato, H. Clewell, R. Dedrick, Physiological parameter values for pbpk models, International Life Sciences Institute, Risk Science Institute, Washington, DC.

[10] D. B. Evans, G. R. Varadhachary, C. H. Crane, C. C. Sun, J. E. Lee, P. W. Pisters, J.-N. Vauthey, H. Wang, K. R. Cleary, G. A. Staerkel, et al., Preoperative gemcitabine-based chemoradiation for patients with resectable adenocarcinoma of the pancreatic head, Journal of Clinical Oncology 26 (21) (2008) 3496–3502.

[11] G. R. Varadhachary, R. A. Wolff, C. H. Crane, C. C. Sun, J. E. Lee, P. W. Pisters, J.-N. Vauthey, E. Abdalla, H. Wang, G. A. Staerkel, et al., Preoperative gemcitabine and cisplatin followed by gemcitabine-based chemoradiation for resectable adenocarcinoma of the pancreatic head, Journal of Clinical Oncology 26 (21) (2008) 3487–3495.

[12] American Cancer Society, Cancer Facts & Figures 2017, American Cancer Society.

[13] J. J. Huck, M. Zhang, J. Mettetal, et al., Translational exposure efficacy modeling to optimize the dose and schedule of taxanes combined with the investigational aurora a kinase inhibitor mln8237 (alisertib), Molecular cancer therapeutics 13 (9) (2014) 2170–2183.

[14] R. Martin, K. Teo, Optimal control of drug administration in cancer chemotherapy, World Scientific, 1994.

[15] E. C. Josefsson, D. L. Burnett, M. Lebois, M. A. Debrincat, M. J. White, K. J. Henley, R. M. Lane, D. Moujalled, S. P. Preston, L. A. OReilly, et al., Platelet production proceeds independently of the intrinsic and extrinsic apoptosis pathways, Nature communications 5.

[16] D. G. DeNardo, L. M. Coussens, Balancing immune response: crosstalk between adaptive and innate immune cells during breast cancer progression, Breast Cancer Res 9 (4) (2007) 212.

[17] Y. Shirai, H. Shiba, T. Sakamoto, T. Horiuchi, K. Haruki, Y. Fujiwara, Y. Futagawa, T. Ohashi, K. Yanaga, Preoperative platelet to lymphocyte ratio predicts outcome of patients with pancreatic ductal adenocarcinoma after pancreatic resection, Surgery 158 (2) (2015) 360–365.

[18] J. G. Kuhn, Chemotherapy-associated hematopoietic toxicity, American journal of health-system pharmacy 59 (suppl 4) (2002) S4–S7.

[19] J. M. Bailey, W. M. Haddad, Drug dosing control in clinical pharmacology, IEEE Control Systems 25 (2) (2005) 35–51.

[20] A. S. Zandvliet, J. H. Schellens, J. H. Beijnen, A. D. Huitema, Population pharmacokinetics and pharmacodynamics for treatment optimization in clinical oncology, Clinical pharmacokinetics 47 (8) (2008) 487–513.

[21] M. Scholz, A. Gross, M. Loeffler, A biomathematical model of human thrombopoiesis under chemotherapy, Journal of theoretical biology 264 (2) (2010) 287–300.

[22] D. E. Mager, E. Wyska, W. J. Jusko, Diversity of mechanism-based pharmacodynamic models, Drug Metabolism and Disposition 31 (5) (2003) 510–518.

[23] B. Alberts, A. Johnson, J. Lewis, M. Raff, K. Roberts, P. Walter, Renewal by multipotent stem cells: Blood cell formation, Molecular Biology of the Cell. 4th edition.

[24] H. Minami, Y. Sasaki, N. Saijo, T. Ohtsu, H. Fujii, T. Igarashi, K. Itoh, Indirect-response model for the time course of leukopenia with anticancer drugs, Clinical Pharmacology & Therapeutics 64 (5) (1998) 511–521.

[25] H. Minami, Y. Sasaki, T. Watanabe, M. Ogawa, Pharmacodynamic modeling of the entire time course of leukopenia after a 3-hour infusion of paclitaxel, Japanese journal of cancer research 92 (2) (2001) 231–238.

[26] L. E. Friberg, A. Freijs, M. Sandström, M. O. Karlsson, Semiphysiological model for the time course of leukocytes after varying schedules of 5-fluorouracil in rats, Journal of Pharmacology and Experimental Therapeutics 295 (2) (2000) 734–740.

[27] S. Kobuchi, Y. Ito, T. Hayakawa, A. Nishimura, N. Shibata, K. Takada, T. Sakaeda, Pharmacokinetic–pharmacodynamic (pk–pd) modeling and simulation of 5-fluorouracil for erythropenia in rats, Journal of pharmacological and toxicological methods 70 (2) (2014) 134–144.

[28] J. S. McCune, P. Vicini, D. H. Salinger, P. V. ODonnell, B. M. Sandmaier, C. Anasetti, D. E. Mager, Population pharmacokinetic/dynamic model of lymphosuppression after fludarabine administration, Cancer chemotherapy and pharmacology 75 (1) (2015) 67–75.

[29] N. V. De Mendizábal, I. Martínez-Forero, M. J. Garrido, E. Bandrés, J. García-Foncillas, C. Segura, I. F. Trocóniz, A semi-physiological-based pharmacokinetic/pharmacodynamic model to describe the effects of topotecan on b-lymphocyte lineage cells, Pharmaceutical research 27 (3) (2010) 431–441.

[30] A. J. Templeton, M. G. McNamara, B. Šeruga, F. E. Vera-Badillo, P. Aneja, A. Ocaña, R. Leibowitz-Amit, G. Sonpavde, J. J. Knox, B. Tran, et al., Prognostic role of neutrophil-to-lymphocyte ratio in solid tumors: a systematic review and meta-analysis, Journal of the National Cancer Institute 106 (6) (2014) dju124.

[31] H. Cho, H. W. Hur, S. W. Kim, S. H. Kim, J. H. Kim, Y. T. Kim, K. Lee, Pre-treatment neutrophil to lymphocyte ratio is elevated in epithelial ovarian cancer and predicts survival after treatment, Cancer immunology, immunotherapy 58 (1) (2009) 15–23.

[32] G. J. Guthrie, K. A. Charles, C. S. Roxburgh, P. G. Horgan, D. C. McMillan, S. J. Clarke, The systemic inflammation-based neutrophil–lymphocyte ratio: experience in patients with cancer, Critical reviews in oncology/hematology 88 (1) (2013) 218–230.

[33] M. Stotz, A. Gerger, F. Eisner, J. Szkandera, H. Loibner, A. Ress, P. Kornprat, W. Zoughbi, F. Seggewies, C. Lackner, et al., Increased neutrophil-lymphocyte ratio is a poor prognostic factor in patients with primary operable and inoperable pancreatic cancer, British journal of cancer 109 (2) (2013) 416–421.

[34] X. Wang, G. Zhang, X. Jiang, H. Zhu, Z. Lu, L. Xu, Neutrophil to lymphocyte ratio in relation to risk of all-cause mortality and cardiovascular events among patients undergoing angiography or cardiac revascularization: a meta-analysis of observational studies, Atherosclerosis 234 (1) (2014) 206–213.

[35] T. Bhat, S. Teli, J. Rijal, H. Bhat, M. Raza, G. Khoueiry, M. Meghani, M. Akhtar, T. Costantino, Neutrophil to lymphocyte ratio and cardiovascular diseases: a review, Expert Review of Cardiovascular Therapy 11 (1) (2013) 55–59.

[36] I. Bhatti, O. Peacock, G. Lloyd, M. Larvin, R. I. Hall, Preoperative hematologic markers as independent predictors of prognosis in resected pancreatic ductal adenocarcinoma: neutrophil-lymphocyte versus platelet-lymphocyte ratio, The American Journal of Surgery 200 (2) (2010) 197–203.

[37] E. K. Hansson, L. E. Friberg, The shape of the myelosuppression time profile is related to the probability of developing neutropenic fever in patients with docetaxel-induced grade iv neutropenia, Cancer chemotherapy and pharmacology 69 (4) (2012) 881–890.

[38] C. Zhuge, J. Lei, M. C. Mackey, Neutrophil dynamics in response to chemotherapy and g-csf, Journal of theoretical biology 293 (2012) 111–120.

[39] M. Craig, A. R. Humphries, F. Nekka, J. Bélair, J. Li, M. C. Mackey, Neutrophil dynamics during concurrent chemotherapy and g-csf administration: mathematical modelling guides dose optimisation to minimise neutropenia, Journal of theoretical biology 385 (2015) 77–89.

[40] T. Ho, G. Clermont, R. S. Parker, A model of neutrophil dynamics in response to inflammatory and cancer chemotherapy challenges, Computers & Chemical Engineering 51 (2013) 187–196.

[41] A. L. Quartino, M. O. Karlsson, H. Lindman, L. E. Friberg, Characterization of endogenous g-csf and the inverse correlation to chemotherapy-induced neutropenia in patients with breast cancer using population modeling, Pharmaceutical research 31 (12) (2014) 3390–3403.

[42] V. Mangas-Sanjuan, N. Buil-Bruna, M. J. Garrido, E. Soto, I. F. Trocóniz, Semimechanistic cell-cycle type–based pharmacokinetic/pharmacodynamic model of

chemotherapy-induced neutropenic effects of diflomotecan under different dosing schedules, Journal of Pharmacology and Experimental Therapeutics 354 (1) (2015) 55–64.

[43] M. L. Pastor, C. M. Laffont, L. Gladieff, E. Chatelut, D. Concordet, Model-based approach to early predict prolonged high grade neutropenia in carboplatin-treated patients and guide g-csf prophylactic treatment, Pharmaceutical research 32 (2) (2015) 654–664.

[44] K. Kaushansky, Historical review: megakaryopoiesis and thrombopoiesis, Blood 111 (3) (2008) 981–986.

[45] P. Stenberg, J. Levin, Mechanisms of platelet production., Blood cells 15 (1) (1988) 23–47.

[46] V. R. Deutsch, A. Tomer, Advances in megakaryocytopoiesis and thrombopoiesis: from bench to bedside, British journal of haematology 161 (6) (2013) 778–793.

[47] K. Kaushansky, Lineage-specific hematopoietic growth factors, New England Journal of Medicine 354 (19) (2006) 2034–2045.

[48] V. R. Deutsch, A. Tomer, Megakaryocyte development and platelet production, British journal of haematology 134 (5) (2006) 453–466.

[49] A. P. Ng, M. Kauppi, D. Metcalf, C. D. Hyland, E. C. Josefsson, M. Lebois, J.-G. Zhang, T. M. Baldwin, L. Di Rago, D. J. Hilton, et al., Mpl expression on megakaryocytes and platelets is dispensable for thrombopoiesis but essential to prevent myeloproliferation, Proceedings of the National Academy of Sciences 111 (16) (2014) 5884–5889.

[50] W. Alexander, A. Roberts, N. Nicola, R. Li, D. Metcalf, Deficiencies in progenitor cells of multiple hematopoietic lineages and defective megakaryocytopoiesis in mice lacking the thrombopoietic receptor c-mpl, Blood 87 (6) (1996) 2162–2170.

[51] A. Aiuti, I. Webb, C. Bleul, T. Springer, J. Gutierrez-Ramos, The chemokine sdf-1 is a chemoattractant for human cd34+ hematopoietic progenitor cells and provides a new mechanism to explain the mobilization of cd34+ progenitors to peripheral blood, Journal of Experimental Medicine 185 (1) (1997) 111–120.

[52] S. T. Avecilla, K. Hattori, B. Heissig, R. Tejada, F. Liao, K. Shido, D. K. Jin, S. Dias, F. Zhang, T. E. Hartman, et al., Chemokine-mediated interaction of hematopoietic progenitors with the bone marrow vascular niche is required for thrombopoiesis, Nature medicine 10 (1) (2004) 64–71.

[53] S. H. Bernstein, W. J. Jusko, W. Krzyzanski, J. Nichol, M. Wetzler, Pharmacodynamic modeling of thrombopoietin, platelet, and megakaryocyte dynamics in patients with acute myeloid leukemia undergoing dose intensive chemotherapy, The Journal of Clinical Pharmacology 42 (5) (2002) 501–511.

[54] B. C. Bender, F. Schaedeli-Stark, R. Koch, A. Joshi, Y.-W. Chu, H. Rugo, I. E. Krop, S. Girish, L. E. Friberg, M. Gupta, A population pharmacokinetic/pharmacodynamic model of thrombocytopenia characterizing the effect of trastuzumab emtansine (t-dm1) on platelet counts in patients with her2-positive metastatic breast cancer, Cancer chemotherapy and pharmacology 70 (4) (2012) 591–601.

[55] L. Friberg, C. Brindley, M. Karlsson, A. Devlin, Models of schedule dependent haematological toxicity of 2'-deoxy-2'-methylidenecytidine (dmdc), European journal of clinical pharmacology 56 (8) (2000) 567–574.

[56] C. van Kesteren, A. S. Zandvliet, M. O. Karlsson, R. A. Mathôt, C. J. Punt, J.-P. Armand, E. Raymond, A. D. Huitema, C. Dittrich, H. Dumez, et al., Semi-physiological model describing the hematological toxicity of the anti-cancer agent indisulam, Investigational new drugs 23 (3) (2005) 225–234.

[57] W. Krzyzanski, J. J. Perez-Ruixo, J. Harrold, Pharmacodynamic model for chemoradiotherapy-induced thrombocytopenia in mice, Journal of pharmacokinetics and pharmacodynamics 42 (6) (2015) 709–720.

[58] S. Hayes, P. N. Mudd Jr, D. Ouellet, B. M. Johnson, D. Williams, E. Gibiansky, Population pk/pd modeling of eltrombopag in subjects with advanced solid tumors with chemotherapy-induced thrombocytopenia, Cancer chemotherapy and pharmacology 71 (6) (2013) 1507–1520.

[59] S. Woo, W. Krzyzanski, W. J. Jusko, Pharmacodynamic model for chemotherapy-induced anemia in rats, Cancer chemotherapy and pharmacology 62 (1) (2008) 123–133.

[60] S. Schirm, C. Engel, M. Loeffler, M. Scholz, A biomathematical model of human erythropoiesis under erythropoietin and chemotherapy administration, PLoS One 8 (6) (2013) e65630.

[61] S. Schirm, C. Engel, M. Loeffler, M. Scholz, Modelling chemotherapy effects on granulopoiesis, BMC systems biology 8 (1) (2014) 1.

[62] D. Jayachandran, A. E. Rundell, R. E. Hannemann, T. A. Vik, D. Ramkrishna, Optimal chemotherapy for leukemia: a model-based strategy for individualized treatment, PloS one 9 (10) (2014) e109623.

[63] R. Ramakrishnan, W. K. Cheung, M. C. Wacholtz, N. Minton, W. J. Jusko, Pharmacokinetic and pharmacodynamic modeling of recombinant human erythropoietin after single and multiple doses in healthy volunteers, The Journal of clinical pharmacology 44 (9) (2004) 991–1002.

[64] S. Doshi, W. Krzyzanski, S. Yue, S. Elliott, A. Chow, J. J. Pérez-Ruixo, Clinical pharmacokinetics and pharmacodynamics of erythropoiesis-stimulating agents, Clinical pharmacokinetics 52 (12) (2013) 1063–1083.

[65] S. Quasthoff, H. P. Hartung, Chemotherapy-induced peripheral neuropathy, Journal of neurology 249 (1) (2002) 9–17.

[66] C. J. Dunton, Management of treatment-related toxicity in advanced ovarian cancer, The oncologist 7 (Supplement 5) (2002) 11–19.

[67] R. Baskar, K. A. Lee, R. Yeo, K.-W. Yeoh, Cancer and radiation therapy: current advances and future directions, Int J Med Sci 9 (3) (2012) 193–199.

[68] D. Lea, D. Catcheside, The mechanism of the induction by radiation of chromosome aberrations intradescantia, Journal of genetics 44 (2) (1942) 216–245.

[69] A. T. Wild, X. Ye, S. G. Ellsworth, J. A. Smith, A. K. Narang, T. Garg, J. Campian, D. A. Laheru, L. Zheng, C. L. Wolfgang, et al., The association between chemoradiation-related lymphopenia and clinical outcomes in patients with locally advanced pancreatic adenocarcinoma, American journal of clinical oncology 38 (3) (2015) 259.

[70] C. Tang, Z. Liao, D. Gomez, L. Levy, Y. Zhuang, R. A. Gebremichael, D. S. Hong, R. Komaki, J. W. Welsh, Lymphopenia association with gross tumor volume and lung v5 and its effects on non-small cell lung cancer patient outcomes, International Journal of Radiation Oncology* Biology* Physics 89 (5) (2014) 1084–1091.

[71] S. Yovino, L. Kleinberg, S. A. Grossman, M. Narayanan, E. Ford, The etiology of treatment-related lymphopenia in patients with malignant gliomas: modeling radiation dose to circulating lymphocytes explains clinical observations and suggests methods of modifying the impact of radiation on immune cells, Cancer investigation 31 (2) (2013) 140–144.

[72] A. T. Wild, J. M. Herman, A. S. Dholakia, S. Moningi, Y. Lu, L. M. Rosati, A. Hacker-Prietz, R. K. Assadi, A. M. Saeed, T. M. Pawlik, et al., Lymphocyte-sparing effect of stereotactic body radiation therapy in patients with unresectable pancreatic cancer, International Journal of Radiation Oncology* Biology* Physics 94 (3) (2016) 571–579.

[73] A. Balmanoukian, X. Ye, J. Herman, D. Laheru, S. A. Grossman, The association between treatment-related lymphopenia and survival in newly diagnosed patients with resected adenocarcinoma of the pancreas, Cancer investigation 30 (8) (2012) 571–576.

[74] P. Matzinger, The danger model: a renewed sense of self, Science 296 (5566) (2002) 301–305.

[75] A. D. Garg, A. M. Dudek, P. Agostinis, Cancer immunogenicity, danger signals, and damps: what, when, and how?, Biofactors 39 (4) (2013) 355–367.

[76] A. Garg, S. Martin, J. Golab, P. Agostinis, Danger signalling during cancer cell death: origins, plasticity and regulation, Cell Death & Differentiation 21 (1) (2014) 26–38.

[77] O. Krysko, T. L. Aaes, C. Bachert, P. Vandenabeele, D. Krysko, Many faces of damps in cancer therapy, Cell death & disease 4 (5) (2013) e631.

[78] T. M. Pawlik, K. Keyomarsi, Role of cell cycle in mediating sensitivity to radiotherapy, International Journal of Radiation Oncology* Biology* Physics 59 (4) (2004) 928–942.

[79] Y. Liu, Y. Liu, W. Bu, Q. Xiao, Y. Sun, K. Zhao, W. Fan, J. Liu, J. Shi, Radiation-/hypoxia-induced solid tumor metastasis and regrowth inhibited by hypoxia-specific upconversion nanoradiosensitizer, Biomaterials 49 (2015) 1–8.

[80] M. Freedman, N. Altszuler, S. Karpatkin, Presence of a nonsplenic platelet pool, Blood 50 (3) (1977) 419–425.

[81] B. M. Squibb, Paraplatin (carboplatin) package insert, Princeton, NJ.

[82] R. S. Go, A. A. Adjei, Review of the comparative pharmacology and clinical activity of cisplatin and carboplatin, Journal of Clinical Oncology 17 (1) (1999) 409–409.

[83] M. Santillan, J. M. Mahaffy, J. Belair, M. C. Mackey, Regulation of platelet production: The normal response to perturbation and cyclical platelet disease, Journal of Theoretical Biology 206 (4) (2000) 585–603.

[84] M. Chang, Y. Suen, G. Meng, J. Buzby, J. Bussel, V. Shen, C. Van De Ven, M. Cairo, Differential mechanisms in the regulation of endogenous levels of thrombopoietin and interleukin-11 during thrombocytopenia: insight into the regulation of platelet production, Blood 88 (9) (1996) 3354–3362.

[85] T. Hamada, R. Möhle, J. Hesselgesser, J. Hoxie, R. L. Nachman, M. A. Moore, S. Rafii, Transendothelial migration of megakaryocytes in response to stromal cell-derived factor 1 (sdf-1) enhances platelet formation, Journal of Experimental Medicine 188 (3) (1998) 539–548.

[86] K. Hattori, B. Heissig, K. Tashiro, T. Honjo, M. Tateno, J.-H. Shieh, N. R. Hackett, M. S. Quitoriano, R. G. Crystal, S. Rafii, et al., Plasma elevation of stromal cell–derived factor-1 induces mobilization of mature and immature hematopoietic progenitor and stem cells, Blood 97 (11) (2001) 3354–3360.

[87] M. Majka, A. Janowska-Wieczorek, J. Ratajczak, M. A. Kowalska, G. Vilaire, Z. K. Pan, M. Honczarenko, L. A. Marquez, M. Poncz, M. Z. Ratajczak, Stromal-derived factor 1 and thrombopoietin regulate distinct aspects of human megakaryopoiesis, Blood 96 (13) (2000) 4142–4151.

[88] L. Zhang, Apt-mcmc, a c++/python implementation of markov chain monte carlo for parameter identification.

[89] C. Engel, M. Loeffler, H. Franke, S. Schmitz, Endogenous thrombopoietin serum levels during multicycle chemotherapy, British journal of haematology 105 (3) (1999) 832–838.

[90] C. A. Schiffer, K. C. Anderson, C. L. Bennett, S. Bernstein, L. S. Elting, M. Goldsmith, M. Goldstein, H. Hume, J. J. McCullough, R. E. McIntyre, et al., Platelet transfusion for patients with cancer: clinical practice guidelines of the american society of clinical oncology, Journal of Clinical Oncology 19 (5) (2001) 1519–1538.

[91] Y. Lee, V. Cristini, G. Varadhachary, M. Katz, H. Wang, P. Bhosale, E. Tamm, J. Fleming, E. Koay, Quantitative computed tomography analysis identifies biophysical subtypes of pancreatic ductal adenocarcinoma, International Journal of Radiation Oncology Biology Physics 96 (2) (2016) E199.

[92] C. H. Crane, G. R. Varadhachary, J. S. Yordy, G. A. Staerkel, M. M. Javle, H. Safran, W. Haque, B. D. Hobbs, S. Krishnan, J. B. Fleming, et al., Phase ii trial of cetuximab, gemcitabine, and oxaliplatin followed by chemoradiation with cetuximab for locally advanced (t4) pancreatic adenocarcinoma: correlation of smad4 (dpc4) immunostaining with pattern of disease progression, Journal of Clinical Oncology 29 (22) (2011) 3037–3043.

[93] E. Lilly, Company, Gemzar (gemcitabine) package insert, Indianapolis, IN.

[94] A. P. Venook, M. J. Egorin, G. L. Rosner, D. Hollis, S. Mani, M. Hawkins, J. Byrd, R. Hohl, D. Budman, N. J. Meropol, et al., Phase i and pharmacokinetic trial of gemcitabine in patients with hepatic or renal dysfunction: Cancer and leukemia group b 9565, Journal of clinical oncology 18 (14) (2000) 2780–2787.

[95] M. Battaglia, R. Parker, Pharmacokinetic/pharmacodynamic modelling of intracellular gemcitabine triphosphate accumulation: translating in vitro to in vivo, IET systems biology 5 (1) (2011) 34–43.

[96] Sanofi-aventis, Eloxatin (oxaliplatin) package insert, Bridgewater, NJ.

[97] G. Bastian, A. Barrail, S. Urien, Population pharmacokinetics of oxaliplatin in patients with metastatic cancer, Anti-cancer drugs 14 (10) (2003) 817–824.

[98] E. L. Squibb, Bristol Myers, Company, Erbitux (cetuximab) package insert, Princeton, NJ and Indianapolis, IN.

[99] A. Köhler, K. De Filippo, M. Hasenberg, C. Van Den Brandt, E. Nye, M. P. Hosking, T. E. Lane, L. Männ, R. M. Ransohoff, A. E. Hauser, et al., G-csf–mediated thrombopoietin release triggers neutrophil motility and mobilization from bone marrow via induction of cxcr2 ligands, Blood 117 (16) (2011) 4349–4357.

[100] M. Murone, D. A. Carpenter, F. J. de Sauvage, Hematopoietic deficiencies in c-mpl and tpo knockout mice, Stem Cells 16 (1) (1998) 1–6.

[101] A. Grossmann, J. Lenox, H. P. Ren, J. Humes, J. Forstrom, K. Kaushansky, K. Sprugel, Thrombopoietin accelerates platelet, red blood cell, and neutrophil recovery in myelosuppressed mice., Experimental hematology 24 (10) (1996) 1238–1246.

[102] J.-L. Villeval, K. Cohen-Solal, M. Tulliez, S. Giraudier, J. Guichard, S. A. Burstein, E. M. Cramer, W. Vainchenker, F. Wendling, High thrombopoietin production by hematopoietic cells induces a fatal myeloproliferative syndrome in mice, Blood 90 (11) (1997) 4369–4383.

[103] A. W. Roberts, G-csf: a key regulator of neutrophil production, but that's not all!, Growth factors 23 (1) (2005) 33–41.

[104] F. Wirsdörfer, V. Jendrossek, The role of lymphocytes in radiotherapy-induced adverse late effects in the lung, Frontiers in Immunology 7.

[105] A. Manual, Cytogenetic analysis for radiation dose assessment, TECHNICAL REPORT SERIES-INTERNATIONAL ATOMIC ENERGY AGENCY.

[106] T. Bortfeld, Imrt: a review and preview, Physics in medicine and biology 51 (13) (2006) R363.

[107] M.-I. Bittner, A.-L. Grosu, T. B. Brunner, Comparison of toxicity after imrt and 3d-conformal radiotherapy for patients with pancreatic cancer–a systematic review, Radiotherapy and Oncology 114 (1) (2015) 117–121.

[108] J. Gomez-Millan, J. R. Fernández, J. A. M. Carmona, Current status of imrt in head and neck cancer, Reports of Practical Oncology & Radiotherapy 18 (6) (2013) 371–375.

[109] M. Baumann, M. Krause, J. Overgaard, J. Debus, S. M. Bentzen, J. Daartz, C. Richter, D. Zips, T. Bortfeld, Radiation oncology in the era of precision medicine, Nature Reviews Cancer 16 (4) (2016) 234–249.

[110] H. E. Romeijn, R. K. Ahuja, J. F. Dempsey, A. Kumar, J. G. Li, A novel linear programming approach to fluence map optimization for intensity modulated radiation therapy treatment planning, Physics in Medicine and Biology 48 (21) (2003) 3521.

[111] E. K. Lee, T. Fox, I. Crocker, Simultaneous beam geometry and intensity map optimization in intensity-modulated radiation therapy, International Journal of Radiation Oncology* Biology* Physics 64 (1) (2006) 301–320.

[112] J. Dias, H. Rocha, B. Ferreira, M. do Carmo Lopes, A genetic algorithm with neural network fitness function evaluation for imrt beam angle optimization, Central European Journal of Operations Research 22 (3) (2014) 431–455.

[113] Y. Tanaka, K. Fujimoto, T. Yoshinaga, Dose-volume constrained optimization in intensity-modulated radiation therapy treatment planning, Journal of Inequalities and Applications 2015 (1) (2015) 122.

[114] M. Kim, R. D. Stewart, M. H. Phillips, A feasibility study: Selection of a personalized radiotherapy fractionation schedule using spatiotemporal optimization, Medical physics 42 (11) (2015) 6671–6678.

[115] S. S. Lo, A. J. Fakiris, E. L. Chang, N. A. Mayr, J. Z. Wang, L. Papiez, B. S. Teh, R. C. McGarry, H. R. Cardenes, R. D. Timmerman, Stereotactic body radiation therapy: a novel treatment modality, Nature reviews Clinical oncology 7 (1) (2010) 44–54.

[116] A. T. Wild, J. M. Herman, A. S. Dholakia, S. Moningi, Y. Lu, L. M. Rosati, A. Hacker-Prietz, R. K. Assadi, A. M. Saeed, T. M. Pawlik, et al., Lymphocyte-sparing effect of stereotactic body radiation therapy in patients with unresectable pancreatic cancer, International Journal of Radiation Oncology* Biology* Physics 94 (3) (2016) 571–579.

[117] N. Nakamura, Y. Kusunoki, M. Akiyama, Radiosensitivity of cd4 or cd8 positive human t-lymphocytes by an in vitro colony formation assay, Radiation research 123 (2) (1990) 224–227.

[118] L. Westera, V. Hoeven, J. Drylewicz, G. Spierenburg, J. F. Velzen, R. J. Boer, K. Tesselaar, J. A. Borghans, Lymphocyte maintenance during healthy aging requires no substantial alterations in cellular turnover, Aging cell 14 (2) (2015) 219–227.

[119] C. Eipel, K. Abshagen, B. Vollmar, Regulation of hepatic blood flow: the hepatic arterial buffer response revisited, World J Gastroenterol 16 (48) (2010) 6046–6057.

[120] R. Schrek, Qualitative and quantitative reactions of lymphocytes to x rays, Annals of the New York Academy of Sciences 95 (2) (1961) 839–848.

[121] J. M. Plate, A. E. Plate, S. Shott, S. Bograd, J. E. Harris, Effect of gemcitabine on immune cells in subjects with adenocarcinoma of the pancreas, Cancer Immunology, Immunotherapy 54 (9) (2005) 915–925.

[122] K. S. Blesch, R. Gieschke, Y. Tsukamoto, B. G. Reigner, H. U. Burger, J.-L. Steimer, Clinical pharmacokinetic/pharmacodynamic and physiologically based pharmacokinetic modeling in new drug development: the capecitabine experience, Investigational new drugs 21 (2) (2003) 195–223.

[123] Xeloda [package insert], Roche Laboratories Inc, New Jersey (1999).

[124] S. Urien, K. Rezaí, F. Lokiec, Pharmacokinetic modelling of 5-fu production from capecitabine?a population study in 40 adult patients with metastatic cancer, Journal of pharmacokinetics and pharmacodynamics 32 (5-6) (2005) 817–833.